Characterization of Tumor Cell Biology and Development of Potential Treatment in Human Cholangiocarcinoma

by

Jiaqi Yang

A Thesis submitted to the Faculty of Graduate Studies of

The University of Manitoba

in partial fulfillment of the requirements of the degree of

DOCTOR OF PHILOSOPY

College of Pharmacy

University of Manitoba

Winnipeg

ABSTRACT

Cholangiocarcinoma (CCA) is an often fatal primary cancer of the liver that can be classified anatomically into intrahepatic and extrahepatic CCA (I-CCA and E-CCA subtypes). Human I-CCA and E-CCA have different growth features, responses to treatment and propensity to metastasize. In this research we hypothesized that these differences could reflect intrinsic differences in tumor cell biology; the prevalence of cancer stem cell (CSC) within the tumor; and/or expression profiles of multidrug resistance associated proteins (MRPs) and chemokine receptors (CRs) within the two cell types.

Tumor cell growth features, CSC prevalence, and stem cell surface markers (SCSMs) were documented in six CCA and one non-malignant cholangiocyte cell line *in vitro*. Cell proliferation was determined by the WST-1 assay, colony formation by soft-agar colony formation, spheroid formation by 3D sphere-forming, cell migration by wound healing and invasion by Transwell invasion chambers. CSC prevalences and SCSM expression were examined by flow cytometry. MRP inhibition was achieved by lentivirus-based shRNA knockdown and CR activity influenced by a specific pharmaceutical CR agonist and antagonist.

The results revealed that I-CCA cells had significantly increased proliferative activity, shortened doubling times, and were more invasive than E-CCA cells, but colony/spheroid formation and migration rates were similar. There were no clear differences in the prevalence of CSCs or SCSM expression within the I-CCA and E-CCA cell population. Regarding chemoresistance, following gemcitabine exposure, MRP5 and/or MRP6 expression were significantly upregulated

in CCA cells. MRP6 knockdown in I-CCA and MRP5 in E-CCA significantly increased gemcitabine-induced cytotoxicity. Finally, the CCR5 antagonist, Maraviroc significantly inhibited cell proliferation, migration and invasion in I-CCA cells, and spheroid formation and invasion in E-CCA cells. The CCR5 agonist RANTES had no effect on I-CCA cells but increased proliferation, migration and invasion of E-CCA cells.

In conclusion, certain features of I-CCA cells are intrinsically more aggressive than E-CCA cells, but the differences cannot be explained by differences in the prevalence of CSCs or SCSM expression profiles. Inhibition of MRP5 and/or MRP6 expression and inactivation of CCR5 should be explored as potential treatments for CCA.

ACKNOWLEDGEMENTS

First of all, I thank my supervisors, Drs. Gerald Y. Minuk and Yuewen Gong for their continuing support and academic guidance throughout my graduate career whilst giving me the opportunity to acquire independence in my study. They were always kind and able to find ways of keeping me positive to do my work. I would also like to thank my graduate committee, Drs. Frank J. Burczynski and Sam Kung, providing me with invaluable support. I extend many thanks to my external examiner Dr. Aziz Ghahary who took the time out of his busy schedule to review my thesis.

I wish to thank past and present colleagues within Drs. Minuk's and Gong's laboratory, Dr. David Sontag, Dr. David Miles, Daniel Froindlich Iluz, Qian Li, and Refaat Omar for their advice and friendship which have greatly influenced my approach to research. I am also indebted to Dr. Christine Zhang and Manli Zhang for their technical support on flow cytometry and lentivirus packaged shRNA analysis, as well as Shujun Huang for her kindly assistance on bioinformatics analysis. I am also grateful for the training environment and professional development provided by the Section of Hepatology and the College of Pharmacy.

I also thank my entire family, with special thanks to my parents, YANG Jianying and JIANG Yan, my husband, Cong Peng, and my furbaby, Benny, as well as all my friends wherever in Canada and China. You all encouraged me to keep going even when the going got tough.

October 18th, 2019

Last but not least I would like to thank the Canadian Liver Foundation and the University of Manitoba for monetary support of this project.

October 18th, 2019

TABLE OF CONTENT

Abstract 1

Table of Content 0

List of Tables 4

List of Figures 5

Abbreviation 8

1 Introduction 14

1.1 Cholangiocarcinoma 14

1.1.1 Etiology 14

1.1.2 Classification and Pathological Features 15

1.1.3 Pathophysiology 18

1.1.4 CCA Therapies and Treatment Strategies 29

1.2 Chemoresistance 32

1.2.1 Multidrug resistance and CSCs 36

1.2.2 ATP-Binding Cassette (ABC) Transporter Structure and Location 36

1.2.3 ABC Transporters in Cancer Cell Biology 38

1.2.4 ABC or Multidrug Resistance-Associated Protein (MRP) Subfamily 40

1.2.5 RNA Interference (RNAi) Technology 41

1.3 Chemokine and Chemokine Receptor (CR) System 46

1.3.1 Chemokines and Their Receptors in Liver 48

1.3.2 Chemokines and Their Receptors in Liver Cancer 49

1.3.3 The Chemokine Ligand CCL5 and Its CCR5 Receptor 53

1.4 Current Gap of Knowledge 55

1.5 Rational 55
1.5.1 Part I: Differences in Tumor Biology and CSCs 55
1.5.2 Part II: I-CCA and E-CCA Chemoresistance 56
1.5.3 Part III: I-CCA and E-CCA Chemotaxis 57
1.6 Hypothesis 57
1.6.1 Part I: Differences in Tumor Biology and CSCs 57
1.6.2 Part II: I-CCA and E-CCA Chemoresistance 58
1.6.3 Part III: I-CCA and E-CCA Chemotaxis 58
2 Materials and Methods 58
2.1 Materials 58
2.1.1 Cell Lines 58
2.1.2 Reagents and Facilities 60
2.1.3 Oligonucleotide Sequences 66
2.2 Methods 70
2.2.1 Cell Culture 70
2.2.2 Cell Proliferation and Doubling Times 70
2.2.3 Spheroid Formation 71
2.2.4 Soft-Agar Colony Formation 72
2.2.5 Wound Healing Assay 72
2.2.6 Transwell Chamber Assay 73
2.2.7 Flow Cytometry for SCSM staining 74
2.2.8 RNA Extraction 75
2.2.9 Reverse Transcription (RT) of RNA to Obtain cDNA 76

2.2.10 Quantitative qPCR 77
2.2.11 Agarose Gel Electrophoresis 77
2.2.12 Protein Extraction 78
2.2.13 Western Blot Analysis 78
2.2.14 Drug Effects on Proliferation and Cytotoxicity 79
2.2.15 Preparation of Lentivirus Packaged of shRNA Library 81
2.2.16 Lentivirus Transduction 82
2.2.17 Verification of Transduced shRNA Cells 84
2.2.18 Statistical Analysis 84
3 Results 86
3.1 Part I: Difference in Tumor Biology and Cscs 86
3.1.1 Cell Morphologies 86
3.1.2 Proliferation and Doubling Times 89
3.1.3 Spheroid Formation 91
3.1.4 Colony Formation on Soft-Agar 93
3.1.5 Cell migration by Wound Healing 95
3.1.6 Cell invasion with Transwell Chambers 100
3.1.7 CSC Prevalence and SCSM Expression 102
3.1.8 Association of SCSMs with Growth Features 107
3.2 Part II: I-CCA and E-CCA Chemoresistance 108
3.2.1 MRP1-6 Expression 108
3.2.2 Response to Gemcitabine 109

3.2.3 MRP Upregulation After Exposure to Gemcitabine 111
3.2.4 Preparation and Transduction of MRP5 and MRP6 ShRNA into CCA 118
3.2.5 Verification of ShRNA Knockdown 118
3.2.6 Gemcitabine Enhanced Cytotoxicity in MRPs 127
3.2.7 Gemcitabine Cytotoxicity at Different Concentrations Following ShRNA Knockdown 130
3.3 Part III: I-CCA and E-CCA Chemotaxis 134
3.3.1 CCR Expression Profile in CCA Cells 134
3.3.2 Altered CCR5 Activity and CCA Cell Proliferation 136
3.3.3 Altered CCR5 Activity and CCA Spheroid Formation 146
3.3.4 Altered CCR5 Activity and CCA Cell Migration 149
3.3.5 Altered CCR5 Activity and CCA Invasion 152
4 Discussion 155
4.1 Differences in Tumor Biology and CSCs 155
4.2 I-CCA and E-CCA Chemoresistance 161
4.3 I-CCA and E-CCA Chemotaxis 167
5 General conclusion and significance 172
5.1 Knowledge Translation 172
6 References 174

LIST OF TABLES

Table 1-1 Classification of the mechanisms of chemoresistance (MOC) in liver cancer 34

Table 2-1 List of cell lines 58

Table 2-2 List of reagents 60

Table 2-3 List of materials, facilities and applied software 64

Table 2-4 List of primers for real-time polymerase chain reaction (qPCR) 66

Table 2-5 List of shRNA sequences 68

Table 3-1 Cell morphologies of I-CCA, E-CCA and non-malignant cholangiocytes cell lines ... 86

Table 3-2 Correlations between tumor features, CSC prevalence, and SCSMs in CCA cells. .. 107

Table 4-1 Correlations between gemcitabine-induced cytotoxicity, MRP expression prior to and following exposure to gemcitabine, CSC prevalence, and SCSMs in CCA cells. 166

LIST OF FIGURES

Figure 1.1 Tumor classification and gross appearance of CCA 16

Figure 1.2 The principle structure of ATP-binding cassette (ABC) transporters. 37

Figure 1.3 The mechanism of ABC pump transporting substrates out of the cell. 38

Figure 1.4 Mechanisms RNA interference including siRNA, miRNA and shRNA. 42

Figure 1.5 Lentivirus delivery pathway. 46

Figure 1.6 Typical structures of chemokine and chemokine receptor. 48

Figure 3.1 Phase contrast images of I-CCA, E-CCA and non-malignant cholangiocytes. 87

Figure 3.2 Proliferative activity of I-CCA, E-CCA and non-malignant cholangiocytes 90

Figure 3.3 Spheroids formed by I-CCA, E-CCA and non-malignant cholangiocytes 92

Figure 3.4 Soft-agar colony formation of I-CCA, E-CCA and non-malignant cholangiocytes. .. 94

Figure 3.5 Wound healing activity of I-CCA cell lines. 96

Figure 3.6 Wound healing activity of E-CCA and non-malignant cells. 97

Figure 3.7 Summary of wound healing capacities of I-CCA, E-CCA, and non-malignant cholangiocytes 99

Figure 3.8 Transwell invasion ability of I-CCA, E-CCA and non-malignant cholangiocytes ... 101

Figure 3.9 The expression of SCSMs in I-CCA cell lines. 103

Figure 3.10 SCSMs in E-CCA and non-malignant cell lines. 104

Figure 3.11 SCSM expression in I-CCA after 30 days in culture. 105

Figure 3.12 SCSM expression in E-CCA after 30 days in culture. 106

Figure 3.13 mRNA expression of MRPs in CCA cells. 108

Figure 3.14 Cytotoxicity of concentration-dependent gemcitabine on CCA cells. 110

Figure 3.15 Fold changes in MRPs mRNA in I-CCA cells following gemcitabine exposure. .. 113

Figure 3.16 Fold changes in MPRs mRNA in E-CCA cells following gemcitabine exposure. . 115

Figure 3.17 MRP5 and MRP6 protein expression in CCA with following gemcitabine exposure. 117

Figure 3.18 MRP5 mRNA knockdown verification. 120

Figure 3.19 MRP6 mRNA knockdown verification. 121

Figure 3.20 Optimization of the lentivirus dilution for shMRP5 in HuCCT1 and KMBC cells.122

Figure 3.21 Optimization of the lentivirus dilution for shMRP5 in HuCCT1 cells. 123

Figure 3.22 Optimization of the lentivirus dilution for shMRP5 in KMBC cells. 125

Figure 3.23 Optimization of the lentivirus dilution for shMRP6 in HuCCT1 cells. 125

Figure 3.24 Optimization of the lentivirus dilution for shMRP6 in HuCCT1 cells. 126

Figure 3.25 Lentivirus shRNA of MRP5 and MRP6 dilution-dependent cytotoxicity of gemcitabine (10 nM) in HuCCT1 and KMBC cells. 128

Figure 3.26 Lentivirus shRNA of MRP6 dilution-dependent cytotoxicity of gemcitabine (10 nM) in HuCCT1 cells. 129

Figure 3.27 Gemcitabine induced cytotoxicity of HuCCT1 cells following inhibition of MRP5 expression. 131

Figure 3.28 Gemcitabine induced cytotoxicity of HuCCT1 cells following inhibition of MRP6 expression. 132

Figure 3.29 Gemcitabine induced cytotoxicity of KMBC cells following inhibition of MRP5 expression. 133

Figure 3.30 CCR and CXCR subtype mRNA expressions in HuCCT1 and KMBC cells as determined by qRT-PCR..... 135

Figure 3.31 Dose-dependent effects of a CCR5 antagonist on HuCCT1 cell proliferation. 137

Figure 3.32 Dose-dependent effects of a CCR5 agonist on HuCCT1 cell proliferation. 138

Figure 3.33 Dose-dependent effects of a CCR5 antagonist on KMBC cell proliferation. 139

Figure 3.34 Dose-dependent effects of a CCR5 agonist on KMBC cell proliferation. 140

Figure 3.35 Time-dependent effects of a CCR5 antagonist on HuCCT1 cell proliferation. 141

Figure 3.36 Time-dependent effects of a CCR5 agonist on HuCCT1 cell proliferation. 142

Figure 3.37 Time-dependent effects of a CCR5 antagonist on KMBC cell proliferation. 143

Figure 3.38 Time-dependent effects of a CCR5 agonist on KMBC cell proliferation. 144

Figure 3.39 Time-dependent effects of CCR5 antagonist and agonist combination on KMBC cell proliferation..... 145

Figure 3.40 Spheroid formation by HuCCT1 cells with altered CCR5 activity. 147

Figure 3.41 Spheroid formation by KMBC cells with altered CCR5 activity..... 148

Figure 3.42 Migration of HuCCT1 cells with altered CCR5 activity..... 150

Figure 3.43 Migration of KMBC cells with altered CCR5 activity..... 151

Figure 3.44 Cell invasion of HuCCT1 cells..... 153

Figure 3.45 Cell invasion of KMBC cells 154

ABBREVIATION

2D: two-dimensional

3D: three-dimensional

ABC: ATP-binding cassette

ADP: adenosine diphosphate

AJCC: American Joint Committee on Cancer

APC: allophycocyanin

ATP: adenosine triphosphate

BCRP: breast cancer resistance protein

bFGF: basic fibroblast growth factor

BSA: bovine serum albumin

CAF: cancer associated fibroblast

CCA: cholangiocarcinoma

CCL: CC chemokine

CCR: CC chemokine receptor

CD44v9: variant 9 of CD44

CDE: choline-deficient ethionine

cDNA: complementary DNA

CFTR: cystic fibrosis transmembrane conductance regulator

CK19: cytokeratin 19

COX-2: cyclooxygenase-2

CR: chemokine receptor

CSC: cancer stem cell

CT: cycle threshold

CX3CL: CX3C chemokine

CX3CR: CX3C chemokine receptor

CXCL: CXC chemokine

CXCR: CXC chemokine receptor

d-CCA: distal cholangiocarcinoma

DMEM/F12: Dulbecco's Modified Eagle Medium/Nutrient Mixture F-12

DMEM: Dulbecco's Modified Eagle Medium

dsRNA: double strand RNA

E-CCA: extrahepatic cholangiocarcinoma

ECM: extracellular matrix

EGF: epidermal growth factor

ELR: glutamic acid-leucine-arginine

EMT: epithelial-mesenchymal transition

EpCAM: epithelial cellular adhesion molecule

FACS: fluorescence-activated cell sorter

FBS: fetal bovine serum

FITC: fluorescein isothiocyanate

GPI: glycosylphosphatidylinositol

GSH: glutathione

HCC: hepatocellular carcinoma

HGF: hepatocyte growth factor

HIF: hypoxia-inducible transcription factor

HPC: hepatic progenitor cell

HRP: horseradish peroxidase

HSC: hepatic stellate cell

I-CCA: intrahepatic cholangiocarcinoma

IG: intraductal growth

IGF-II: paracrine insulin-like growth factor II

IL-6: interleukin 6

IL-8: interleukin 8

iNOS: inducible nitric oxide synthase

LB: Luria-Bertani broth

LCSGJ: Liver Cancer Study Group of Japan

LPI: lysophosphatidylinositol

LSEC: liver sinusoidal endothelial cell

LTC4: leukotriene C4

mAb: monoclonal antibody

MCP-1: monocyte chemoattractant protein-1

MDR: multidrug resistance

MDR1: g-glycoprotein 1

MDSC: myeloid-derived suppressor cells

MEM: Minimum Essential Media

MF: mass forming

MFG-E8: milk-fat globule EGF-8

miRNA: microRNA

MMP: matrix metalloproteinase

MOC: mechanisms of chemoresistance

MOI: multiplicity of infection

MRP: multidrug resistance-associated protein

MRP1: resistance-associated protein 1

MSC: mesenchymal stem cell

NASH: non-alcoholic steatohepatitis

NBD: nucleotide-binding domain

NCCN: National Comprehensive Cancer Network

ncRNA: non-coding RNA

NSC: normal stem cell

OLT: orthotropic liver transplantation

OPN: osteopontin

PBG: peribiliary gland

PBGC: cells within peribiliary glands

PBS: phosphate-buffered saline

p-CCA: perihilar cholangiocarcinoma

PDGF: platelet-derived growth factor

PE: phycoerythrin

PG: prostaglandin

PI: intraductal growth

PSC: primary sclerosing cholangitis

p-Smad2: phospho-Samd2

qPCR: real-time polymerase chain reaction

RISC: RNA-induced silencing complex

RNAi: RNA interference

ROS: reactive oxygen species

RT: reverse transcription

SCF: soft-agar colony formation

SDF-1: stromal-derived factor 1

SDS: sodium dodecyl sulfate

shRNA: short hairpin RNA

SIP: sphingosine-1-phosphate

siRNA: short interfering RNA

SP: side population

SUR: sulfonylurea receptor

SWHA: scratch wound healing assay

TAM: tumor-associated macrophage

TBS: tris-buffered saline

TBST: TBS-Tween

TE: Tris-EDTA

TGF-β: transforming growth factor beta

TGF-β1: transforming growth factor beta 1

Thy-1: thymocyte differentiation antigen-1

TMD: transmembrane domain

TNF-α: tumor necrosis factor alpha

TU/mL: infectious units per milliliter

UICC: Union for International Cancer Control

VEGF: vascular endothelial growth factor

WHO: World Health Organization

XCL: C chemokine

XCR: CX chemokine receptor

1. INTRODUCTION

1.1 CHOLANGIOCARCINOMA

The liver consists of two types of epithelial cells: hepatocytes and cholangiocytes (Alpini, McGill, & Larusso, 2002). The primary malignancy derived from cholangiocytes is termed cholangiocarcinoma (CCA). CCA can be classified according to their anatomical location into intrahepatic CCA (I-CCA) and extrahepatic (E-CCA) subtypes. CCA is considered an often fatal cancer. In most cases, patients with CCAs have no symptoms in the early stages. When symptoms do occur they include malaise, abdominal pain, fatigue, jaundice, and weight loss (Alvaro et al., 2011). Surgical treatments such as resection and liver transplantation are the only potentially curative approaches for CCA. However, only a minority of patients are candidates for these procedures. The mean overall survival for individuals with CCA is less than twelve months (Banales et al., 2016).

1.1.1 Etiology

In most cases, the etiology of CCA is unclear (Banales et al., 2016). One of the more common risk factors for CCA in North American and Europe is underlying primary sclerosing cholangitis (PSC), an immune-mediated cause of chronic cholangitis. Among PSC patients, the incidence of CCA is 5% to 15% with an annual risk of 0.5% to 1.5% (Burak et al., 2004). Hepatobiliary flukes are also an important predisposing condition for CCA, particularly in East Asia and Southeast Asia area where the highest prevalence of CCAs in the world has been reported (Shin et al., 1996; Sriamporn et al., 2004). Liver flukes such as *Opisthorchis viverrini* and *Clonorchis sinensis* are acquired by consuming undercooked fish. Following consumption they invade the

biliary system of the human host where they induce chronic inflammation and malignant transformation of epithelial cells (Sripa et al., 2007). Hepatolithiasis (intrahepatic gallstone disease) can also induce CCA. The overall incidence rate of CCA with hepatolithiasis is 5% to 13% (H. J. Kim et al., 2015). Additional risk factors for CCA include chronic infection with hepatitis B and C viruses, choledochal cystic diseases, cirrhosis per se (i.e. regardless of cause), obesity and diabetes (Banales et al., 2016; Ghouri, Mian, & Blechacz, 2015), and environmental factors such as exposure to nitrosamine, asbestos, dioxins, vinyl chlorides and thorotrast (Ghouri et al., 2015). All these associations suggest that chronic inflammation is involved in cholangiocellular carcinogenesis.

1.1.2 Classification and Pathological Features

According to where the malignancy originated in the biliary tree, CCA can be classified into intrahepatic CCA (I-CCA), perihilar CCA (p-CCA), and distal CCA (d-CCA). Recently, the latter two have been grouped together as E-CCA (Figure 1.1A).

As illustrated in Figure 1.1A, I-CCA are located within the peripheral bile ducts or bile ductules of the liver parenchyma; p-CCA, the biliary bifurcation; and d-CCA in the common bile duct and in close proximity to the head of pancreas (Buettner, van Vugt, JN, & Groot Koerkamp, 2017).

The morphological appearance of CCA can vary (Figure 1.1B). In general, the mass forming (MF) pattern presents as a gray or white color based nodular mass in hepatic parenchyma. The periductal infiltrating (PI) type grows along portal tracts with biliary stenosis. The intraductal

growth (IG) pattern shows a polypoid or papillary cancer within dilated bile duct or bile ductule lumen (Blechacz, Komuta, Roskams, & Gores, 2011). Based on the gross appearance, I-CCA most often presents as MF with only a minority of cases consisting of PI and IG patterns (Nakanuma et al., 2010). The PI growth pattern is a hallmark of E-CCA, although both PI and IG have also been reported in E-CCA patients. CCA with an MF appearance commonly contains a large necrotic area and/or central scarring (Blechacz et al., 2011; Nakanuma et al., 2010). The IG type of CCA presents as a radial pattern capable of invading adjacent portal venous and hepatic arteries (Nakanuma et al., 2010).

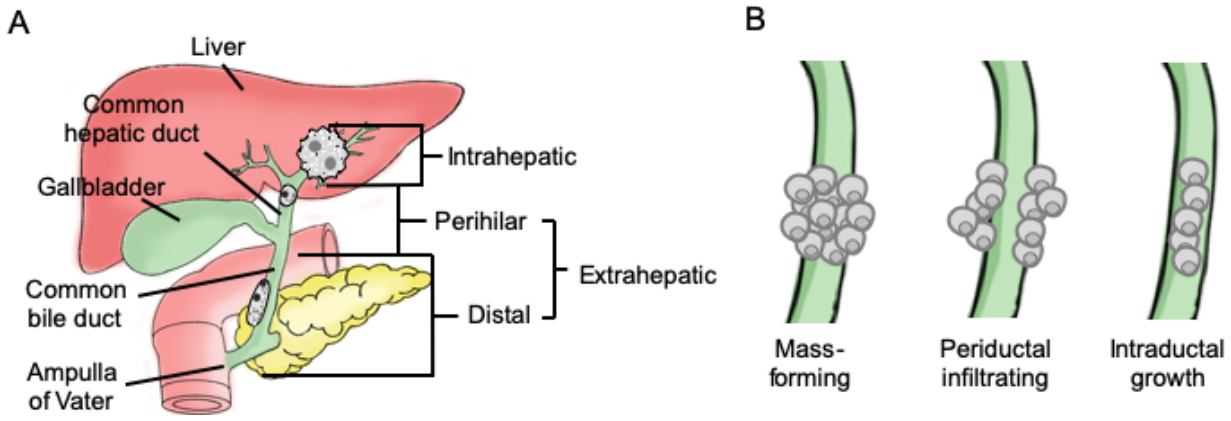

Figure 1.1 Tumor classification and gross appearance of CCA

A) The anatomic classification of CCA in intrahepatic, perihilar, and distal ductal carcinomas (Buettner et al., 2017). B) CCAs present three different growth patterns: mass formation, periductal infiltration and intraductal growth (Blechacz et al., 2011).

Regarding histological features, CCA behaves as highly heterogeneous tumors. In general, I-CCA consists of two histological subtypes, including a mixed bile ductular type that originates

from small intrahepatic bile ducts, and a mucinous bile duct type that arises from larger intrahepatic bile ducts (Nakanuma et al., 2010). E-CCA present extensively as mucinous adenocarcinoma (Komuta et al., 2012).

Different histological subtypes of I-CCA show different clinicopathological features. For instance, the mixed bile ductular type is predominantly characterized by an MF growth pattern, which is commonly derived from chronic liver diseases without intrahepatic pre-neoplastic lesions. The mixed bile ductular I-CCA presents some phenotypic similarities with the cytokeratin 19 (CK19) positive-expressed hepatocellular carcinoma (HCC). On the other hand, the mucinous bile duct I-CCA displays all three types of gross appearances. It is usually associated with chronic biliary diseases such as PSC and/or pre-neoplastic lesions. The mucinous type I-CCA shares clinical features with E-CCA or pancreatic cancers (Aishima & Oda, 2015; Cardinale, Carpino, Reid, Gaudio, & Alvaro, 2012; Nakanuma et al., 2010).

1.1.2.1 Established CCA Cell Lines

To better characterize human CCA, cancer-derived cell lines are essential tools. During the late twentieth century, several human CCA cell lines were established, including I-CCA and E-CCA cell lines, with most of them being derived from East and Southeast Asian patients. These cell lines were established and characterized by their tumor histology and morphology. Specifically, the presence and classification of tumors (I-CCA versus E-CCA) were detected by radiologic examination and blood chemistry prior to surgery. Epithelial cell features, including the presence of tight cell junctions, microvilli and microfilaments, were demonstrated by electron microscopy.

Tumor cell growth patterns were documented by xenotransplanted tumor formation, tumor-associated hormones and growth factors, cytogenetics, and cell proliferation activity (Kusaka, Tokiwa, & Sato, 1988; Miyagiwa, Ichida, Tokiwa, Sato, & Sasaki, 1989; Saijyo et al., 1995; Shimizu et al., 1992; Storto et al., 1990; Yano, Maruiwa, Iemura, Mizoguchi, & Kojiro, 1992). These cell lines could provide *in vitro* systems to characterize the tumor features, such as potential cancer driver genes, molecular expression, and functional profiles. Use of cell lines is also available in testing small molecules or biologics for developing anti-cancer therapy.

1.1.3 Pathophysiology

1.1.3.1 Hepatic Progenitor Cells (HPCs)

In hepatobiliary development, hepatic stem/progenitor cells (HPCs) are bipotential stem cells that reside in the canals of Hering. These cells are capable of differentiating into hepatocytes and cholangiocytes (Gaudio et al., 2009). In general, HPCs are quiescent with a low proliferating rate. Following relatively minor liver injury, diminished cell numbers are replenished by self-renewable hepatocytes and/or large cholangiocytes rather than by activating HPCs (Gaudio et al., 2009; L. Zhang, Theise, Chua, & Reid, 2008). Activation of HPCs only takes place following extensive injury, when the liver is continuously injured, or when the self-replication capacity of hepatic epithelial cells is inhibited. Subsequently, activated HPCs are amplified from the periportal to the pericentral zone, forming reactive ductules. In this condition, HPCs proceed into a trans-differentiation status with a variable phenotypic profile (Han et al., 2013). HPCs repair the liver damage by directly replacing dead cells and/or inducing liver repair pathways such as

fibrosis and angiogenesis. Of note, HPC-derived reactive ductules have been described in progressive fibrosis and non-alcoholic steatohepatitis (NASH) (Nobili et al., 2012).

Another reservoir of HPCs are the bile duct glands of the biliary tree. Peribiliary glands (PBGs) are tubular-alveolar glands containing serous and mucinous acini resident in large intrahepatic- and extrahepatic- bile ducts. Cells within PBGs (PBGCs) are capable of self-renewing and generating mature hepatocytes, cholangiocytes, as well as β-pancreatic cells. A histological study has shown that progenitor cells, intermediate cells, and matured epithelium cells are detected at different locations of PBGs. Specifically, undifferentiated PBGCs locate along the bottom of the glands, while cells in the transition state are observed in the middle of glands. Fully developed mature biliary cells are to be found on the surface of epithelium (Han et al., 2013; Spence et al., 2009).

1.1.3.2 Pathogenesis of CCA from HPCs

As indicated above, CCA tend to develop in the setting of chronic liver or biliary diseases. Healthy cholangiocytes undergo pathophysiological changes resulting from continuous inflammation and epithelium regeneration that can lead to CCA development. This may include various synergistic processes including amplification of HPCs, accumulated genetic and/or epigenic mutations and a modified hepatobiliary microenvironment.

HPCs are usually activated and expanded in continuous liver injury (Roskams, 2006), wherein long-term injured epithelia are replaced by HPC-differentiated cell populations instead of self-

repaired mature hepatocytes and/or cholangiocytes. The extent of HPC activation and expansion depends on the severity of inflammation: greater extents of HPC differentiation correlate with greater epithelium damage (Roskams, 2006).

The HPC or PBGC activity is tightly regulated by the microenvironment, often referred to as the stem cell niche. In the liver, the stem cell niche plays a crucial role in regulating self-renewal and division of HPCs by secreting different paracrine factors or by physical cell-to-cell contact. The niche is altered in chronic liver or biliary diseases with increased lymphocyte infiltration and activation of the fibrogenic hepatic stellate cells (HSCs). The increased lymphocyte population induces inflammation with elevated levels of reactive oxygen species (ROS), various cytokines (such as IL-6, IL-8, TGF-β, TNF-α, PDGF, EGF etc.) and chemokines. All these factors can trigger cell genetic modifications and epithelial-mesenchymal transition (EMT). Fibrogenic factors such as IL-6 and TGF-β induce HSC activation, which subsequently produces ECM and fibrosis.

1.1.3.3 Cancer Stem Cells (CSCs)

1.1.3.3.1 The Hierarchical CSC Concept

The classic stochastic hypothesis of clonal evolution as described by Nowell et al (1976), suggests normal cells undergo a series of mutations and transition into primary diploid tumor cells. Each primary tumorigenic cell is equally able of generating solid tumor tissue.

An increasing number of studies have identified tumor-initiating, stem cells in various cancers, including breast (Al-Hajj, Wicha, Benito-Hernandez, Morrison, & Clarke, 2003), prostate (Collins, Berry, Hyde, Stower, & Maitland, 2005), colon (O'Brien, Pollett, Gallinger, & Dick, 2007), and brain tumors (Singh et al., 2004). The cancer stem cell (CSC) theory was established in 2001 (Lobo, Shimono, Qian, & Clarke, 2007; Reya, Morrison, Clarke, & Weissman, 2001). Based on the CSC model, a tumor consists of various cell subpopulations that exhibit distinct phenotypes involved in carcinogenesis, tumor growth and metastasis. This property of heterogeneity suggests there is a cellular hierarchy within the developed tumor, while mature cancer cells are derived from CSCs, only the subpopulation of CSCs acquire the capacity of sustaining tumor (Lobo et al., 2007). CSC also contribute to the resistance induced by chemo- and radio- therapies. Of note, not every neoplastic formation supports the CSC hypothesis (Barabe, Kennedy, Hope, & Dick, 2007).

1.1.3.3.2 Identification of CSCs Within the Liver

Based on the CSC concept, heterogeneous CCAs are maintained at least somewhat by hepatobiliary CSCs. It has been shown that hepatobiliary CSCs display distinct biological features regarding tumorigenicity, metastasis and chemoresistance (Yamashita et al., 2013). Thus, identifying CSCs within CCA is important for diagnostic, predictive, and therapeutic purposes. Because CSCs may originate from HPCs, PBGCs and dedifferentiated non-CSC lineages, there are several approaches to identifying hepatobiliary CSCs based on their immunogenic and biological functions (Yamashita & Wang, 2013).

Certain stem cell surface markers (SCSMs) are expressed on the surface of CSC. These can be used to distinguish CSCs from non-stem cells and predict the cell's biologic properties. In the liver, these markers include CD13, CD24, CD44, CD90, CD133 and epithelial cellular adhesion molecule (EpCAM).

CD13 is a membrane glycoprotein that is often used to detect cells with CSC features. It has been suggested that CD13 plays an important role in tumor progression, cell proliferation and chemoresistance in liver cancers (Haraguchi et al., 2010). Nagano et al (2012) reported that $CD13^+$ CSC cells are closely associated with the side population (SP) phenotype in liver cancers and are related to a hypoxic marker in clinical samples. $CD13^+$ CCA cells often double stain with $CD44^+$ populations (Cardinale et al., 2015).

CD24 is a glycosylated mucin-like cell surface protein, attached to the cell membrane through a glycosylphosphatidylinositol (GPI-) anchor and localizes in lipid rafts. Overexpression of CD24 has been reported in CSCs derived from breast, colon, pancreatic and liver cancers with increased proliferative and metastatic activities (Jaggupilli & Elkord, 2012). In CCA studies, the expression of CD24 is closely related to clinical outcomes. Su et al (2006) reported that CD24 is expressed in over 50% of tumors from I-CCA patients. These $CD24^+$ patients exhibited relatively shorter survival times compared to those who were CD24 negative. Similar results were documented in another study (Agrawal et al., 2007). Leelawat et al (2013) reported that sorted $CD24^+$ CCA cells express upregulated tumor-associated genes such as cell adhesion, cell proliferation, metastasis-related as well as matrix metalloproteinases (MMPs) and MMP

inhibitor genes. In addition, increased CD24 expression in CCA highly correlates with lymph node metastasis (Keeratichamroen et al., 2011).

CD44 is a transmembrane glycoprotein that primarily serves as a receptor for hyaluronan. It mediates cell adhesion and migration as well as regulates interactions with several ligands including osteopontin (OPN), collagens, and MMPs. In CSCs, CD44 plays a critical role in cell survival, metastasis, cell-to-cell and cell-to-extracellular matrix (ECM) interactions, lymphocyte activation and CSC homing (L. Wang, Zuo, Xie, & Wei, 2017). Morine et al (2017) demonstrated that CD44 positive I-CCA patients have a worse prognosis following surgical resection than those who were CD44 negative. CD44 is also present in tissue adjacent to CCA (Kunlabut et al., 2012). The variant 9 of CD44 (CD44v9) is overexpressed in inflammation induced CCA patients with no expression in normal bile duct epithelia. These findings suggest CD44 is a candidate marker for the detection and diagnosis of CCA.

CD90 is also known as thymocyte differentiation antigen-1 (Thy-1). It is a cell adhesion glycoprotein which anchors into the cell surface through a GPI motif (Zucchini, Del Zotto, Brando, & Canonico, 2001). CD90 expression or overexpression is associated with cell proliferation, spheroid formation, metastasis, differentiation and tumorigenecity in several types of cancers (Shaikh, Kala, & Nivsarkar, 2016). It was initially considered a CSC marker in HCC, where isolated $CD90^+$ cells possessed greater tumorigenecity than $CD90^-$ cells (Z. F. Yang et al., 2008). Subsequently, there have been numerous reports that CD90 is indicative of aggressive tumor behavior and chemoresistance in HCC (Sukowati et al., 2013; Yamashita et al., 2013). In

CCA, CD90 expression associates with lymph node invasion. $CD90^+$ cells express elevated cell migration and upregulated EMT related genes (Yamaoka et al., 2018).

CD133 or AC133 is a glycoprotein in humans that was originally discovered in hematopoietic progenitor stem cells (Yin et al., 1997). CD133 displays as a membrane protrusion and regulates cell membrane topology (Miraglia et al., 1997). It has been employed for identifying CSCs in several types of tumors (Z. Li, 2013). In the adult liver, $CD133^+$ cells contribute to tissue regeneration via cell proliferation and differentiation (Suzuki et al., 2008). Leelawat et al (2011) demonstrated that $CD133^+$ CCA specimens highly correlate to the phenotype of lymph nodes metastasis, and *in vitro* studies have revealed $CD133^+$ cells display a greater extent of invasion compared to $CD133^-$ cells. Similar results were reported by Cai et al (2018) suggesting that patients with $CD133^+$, non-mucin producing I-CCA exhibit a higher incidence of metastasis and recurrence. Furthermore, significant upregulation of transforming growth factor beta 1(TGF-β1), phospho-Smad2 (p-Smad2), Vimentin and loss of E-Cadherin are detected in $CD133^+$ tumors compared to $CD133^-$. These results suggest that CD133 expression in tumors is a potential indicator of poor prognosis for patients with CCA.

EpCAM is a glycosylated membrane protein that regulates cell-to-cell interactions and transmits signaling for targeted gene transcription (Munz, Baeuerle, & Gires, 2009). In the liver, HPCs/PBGCs and hepatoblasts have increased EpCAM expression, while mature hepatocytes do not (Schmelzer & Reid, 2008). In pathological hepatic tissues, EpCAM overexpression occurs at the cirrhosis stage, suggesting EpCAM may serve as an independent diagnostic maker for early

HCC (J. W. Kim et al., 2004). Subsequent studies have shown that $EpCAM^+$ cells derived from HCC have increased tumorigenicity, cell invasion and potency of differentiation when compared to $EpCAM^-$ cells (Kimura et al., 2010; Yamashita et al., 2009; J. Yang, Gong, Sontag, Corbin, & Minuk, 2018). It is important to note that some cholangiocytes in the adult liver are $EpCAM^+$ (Tabibian et al., 2014; Tanaka, Itoh, Tanimizu, & Miyajima, 2011). Thus, results of CSC studies derived from $EpCAM^+$ cells and tissues in CCA are controversial.

1.1.3.3.3 Tumor Microenvironment and Cancer Stem Cell Niche

Similar to normal stem cell niches, there is a specialized microenvironment applied to CSC, termed the CSC niche, which interacts with CSCs to regulate tumor cell proliferation, migration, invasion, and therapeutic resistance. In hepatobiliary cancers, a range of elements including various stromal cells (i.e. cancer associated fibroblast (CAF), tumor-associated macrophage (TAM), adipocyte, vascular cells and immune stroma), hypoxia and ECM contribute to the CSC niche (Borovski, De Sousa, Vermeulen, & Medema, 2011). These factors coordinately regulate the stemness of CSCs with alteration of self-renewal signaling pathways (i.e. Wnt/β-catenin, Notch, and Hedgehog) and/or interruption of embryonic stem cell transcriptional factors (i.e. NANOG, OCT-4, and SOX-2) (Borah, Raveendran, Rochani, Maekawa, & Kumar, 2015; J. Kim & Orkin, 2011).

1.1.3.4 CSC Properties and Functional Assays *in vitro*

1.1.3.4.1 Cell Proliferation and Viability

Measuring cell proliferation, viability and cytotoxicity are commonly employed to document a cell's response to different stimuli in culture. There are several means of determining cell proliferation. The majority are based on cellular activities such as enzyme and co-enzyme metabolism, nucleotide-uptake capacity, cell membrane permeability, cell adherence and adenosine triphosphate (ATP) generation (Adan, Kiraz, & Baran, 2016). Some of the more commonly employed methods include 1) documenting active metabolism, 2) DNA synthesis, 3) ATP luminescence, 4) fluorescence dye based proliferation assays, and 5) trypan blue exclusion for viable cell counting (Stoddart, 2011).

1.1.3.4.2 Spheroid and Soft-Agar Colony Formation in Three-Dimensional (3D) Culture

Two-dimensional (2D) cell culture is a common cell growth pattern *in vitro*. However, it cannot represent the complexity and heterogeneity of the tumor cell environment *in vivo*, where tumors grow in a three-dimensional (3D) pattern with specific morphologies. Thus, relevant growth signals and cellular mechanisms might be lost in a 2D confirmation (Lee, Kenny, Lee, & Bissell, 2007). 3D cultures, on the other hand, display a number of *in vivo* properties including cell-to-cell interactions, hypoxia, and the development of ECM (Kimlin, Casagrande, & Virador, 2013). Additionally, a 3D culture is capable of mimicking the architecture of living tissue to better investigate the pathology of cancers (Weiswald, Bellet, & Dangles-Marie, 2015). To date, spheroid and soft-agar colony formation assays have been widely employed *in vitro* to bridge the gap from 2D *in vitro* cultures to *in vivo* animal models (K. M. Yamada & Cukierman, 2007)

In general, there are two types of 3D culture models relevant to cancers; scaffold-based and liquid-based systems (Thoma, Zimmermann, Agarkova, Kelm, & Krek, 2014). Scaffold-based 3D systems are usually established by synthetic or naturally derived polymers that mimic the ECM. The principle challenge of current scaffolds is there is no well-defined matrix that precisely recreates the modulating cellular progression and/or interaction of cancer *in vivo* (Cunha, Panseri, Villa, Silva, & Gelain, 2011).

Regarding liquid-based models, spheroid formation is one of the most common methods used to study stem cells and tumor cells (Cesarz & Tamama, 2016; Jung et al., 2017). With seeding in an ultra-low attachment plate, spheroids develop from either individual cell proliferation or multiple-cell-clustering (K. M. Yamada & Cukierman, 2007). Compared to tumor cells growing in a 2D plastic substrata, spheroids exhibit features similar to *in vivo* tumor growth where individual cells communicate with themselves and/or surrounding cells via autocrine and/or paracrine growth factors. In addition, large spheroids with diameters greater than 500 μm mimic the heterogeneity of *in vivo* solid tumors by consisting of external proliferation cells, internal quiescent cells exposed to hypoxia and limited nutrients, and a necrotic core, which mimic the heterogeneity of *in vivo* solid tumor (Vinci et al., 2012).

Soft-agar colony formation (SCF) is another liquid-based 3D culture system wherein cells grow in a semisolid-medium. SCF is the gold standard to test malignantly transformed cells for their ability to grow in an anchorage-independent condition. In general, CSCs can form colonies,

while neither differentiated tumor cells nor stromal cells grow or generate such colonies in semisolid agar. Human cancer cell lines, primary tumor cells isolated from patients, and cells isolated from patients derived xenograft model are feasible for SCF assays. Stem cells isolated from the bone marrow, peripheral blood or umbilical cord blood also form 3D colonies by the SCF method. They often serve as normal cell controls to examine new anticancer agents (Fiebig, Maier, & Burger, 2004; Zips, Thames, & Baumann, 2005).

1.1.3.4.3 Cell Migration and Invasion

One feature of aggressive cancers is their propensity to metastases. This phenomenon is a cumulative result of multiple alterations in tumor cells with the surrounding microenvironment resulting in tumor migration and invasion of adjacent healthy tissues (Friedl & Alexander, 2011). To document the metastatic features of tumor cells, several *in vitro* assays have been developed for whole and single cell populations.

The scratch wound healing assay (SWHA) is a commonly used 2D method for measuring whole-population migration. A brief description of the protocol involves scratching lines in a cell monolayer and capturing with photographs at the beginning and different time intervals wound closure until the entire wound has closed. Because SWHA is performed in a whole-population fashion, multiple *in vivo* effects of tumor cells such as cell-to-cell or cell-to-ECM interactions can be approximated. Moreover, the SWHA is also available for live cell imaging and tracking intracellular signals (C. C. Liang, Park, & Guan, 2007).

The Transwell assay or Boyden chamber is a widely accepted technique to study single cell invasion and chemotaxis (H. C. Chen, 2005). The assay is performed by inserting a chamber (pore size ranging from 3 to12 μm) in a well containing medium and/or a chemoattractant solution. Individual suspended cells inside the chamber are allowed to migrate through the pores of the membrane to the other side. Migrated cells are either stained or counted after a finite amount of time. In addition, ECM such as hydrogel or Matrigel can be placed on the membrane to mimic the *in vivo* microenvironment.

1.1.4 CCA Therapies and Treatment Strategies

1.1.4.1 Surgery

CCA can be successfully treated with surgical resection and/or orthotropic liver transplantation (OLT) if diagnosed at an early stage. However, since the majority of CCA patients present with advanced disease or aggressive features, less than 30% are eligible for such treatments (Khan et al., 2012).

Notwithstanding the low likelihood of success, surgical resection is often the initial consideration for CCA patients with no radiographic evidence of invasion and metastasis. When performing resection, affected segments with/without routine lymphadenectomy are undertaken for I-CCA, while pancreatoduodenctomy, lymphadenectomy, hemi-hepatectomy and/or cholecystectomy are undertaken for E-CCA (J. W. Valle et al., 2016). Survivals after resection are associated with surgical margin status, lymph node metastasis, transfusion and perineural invasion (Jang et al.,

2005; Murakami et al., 2014; Tabrizian et al., 2015). In general, the 5-year survival after resection is 22% to 44% for I-CCA versus 11% to 41% for E-CCA (Khan et al., 2012).

Among patients with unresectable CCA, OLT serves as a potential cure for both tumor and underlying liver disease. However, OLT is not appropriate for all subtypes of CCA. High tumor recurrence rates and poor overall survival are reported in I-CCA. Indeed, 60% to 90% of I-CCA patients die from recurrent CCA (Sapisochin, Fernandez de Sevilla, Echeverri, & Charco, 2015). Nevertheless, with more restricted selection criteria and neoadjuvant therapy, a 5-year survival rate of 65% can be achieved (Darwish Murad et al., 2012). E-CCA patients less often undergo OLT because their livers tend to be relatively healthy.

1.1.4.2 Chemotherapy

For patients with unresectable CCA who are not surgical or transplant candidates, chemotherapy has been attempted. However, the value of chemotherapy in CCA is limited. While guidelines have been recommended from various medical oncology groups, the regimens are primarily based on randomized trials (phase II or III) from small or disparate studies (Banales et al., 2016). A systematic review of adjuvant chemotherapy for CCA and gallbladder cancers reported no significant improvement in patient survival with adjuvant therapy (Horgan, Amir, Walter, & Knox, 2012). In general, survival benefits of single or combination drug therapy are limited and median survival time rarely exceeds one year (Morizane et al., 2018).

In the latest version of the US National Comprehensive Cancer Network (NCCN) Guidelines, capecitabine, cisplatin, fluorouracil, gemcitabine, and oxaliplatin are recommended for patients with hepatobiliary cancer. Based on findings derived from phase II studies, gemcitabine-based regimens are considered as the standard first-line chemotherapy for advanced CCA (Morizane et al., 2018). Gemcitabine plus cisplatin combinations have been reported to achieve the longest median survival time (11.7 months) (J. Valle et al., 2010). If gemcitabine-based therapy fails, a fluoropyrimidine (i.e. capecitabine, fluorouracil)- based treatment should be considered (Banales et al., 2016). Unfortunately, when both gemcitabine- and fluoropyrimidine- based regimens fail, no additional treatments beyond palliative cure are available (Morizane et al., 2018). However, several phase III trials are in progress, and various combinations of chemotherapeutic agents may provide practice-changing results (Morizane et al., 2018).

In terms of tumor subtype responses to chemotherapy, Bupathi et al (2017) reported in I-CCA patients overall response rates of 20% to 40% gemcitabine-based treatments. In a report by Babu et al (2018) gemcitabine plus cisplatin were administered to I-CCA patients, and achieved progression free survival of 5.3 months and overall survival of 10.3 months. Ishimoto et al (2018) reported I-CCA patients with gemcitabine plus cisplatin as first-line therapy, achieving median survivals of 13.8 months.

Regarding E-CCA, most E-CCA studies documented the response of chemotherapy in patients treated with fluorouracil-based agents, with response rates of 9% to 57% and median survivals of 4 to 17 months (Todoroki, 2000). Gemcitabine-based treatment for E-CCA has been mostly

combined with radiotherapy. Ben-Josef et al (2015) reported treatment with gemcitabine, capecitabine and radiotherapy achieved a median survival of 35 months for E-CCA patients. A study by Autorino et al (2016) reported that the E-CCA group treated with gemcitabine-based radiochemotherapy achieved a median survival of 14 months and local control of 25%.

There have been few studies comparing the efficacy of chemotherapy for I-CCA and/or E-CCA. Waseem and Tushar (2017) analyzed CCA patients seen at the Mayo Clinic in Florida from 1992 to 2010. They reported that 21% of I-CCA, 3.8% p-CCA and 7% d-CCA patients received chemotherapy only. There were no significant differences in response rates based on tumor subtypes. In another study by Gabriel et al (2012), the response to chemotherapy in I-CCA patients were compared to E-CCA patients in a single institution. Here again, there were no significant differences in progression-free and overall survival times within the two groups, although I-CCA patients tended to have a longer median survival times compared to E-CCA patients. To date, there have been no published reports describing and comparing responses rates in I-CCA and E-CCA patients, when the same chemotherapeutic regimen was employed.

1.2 CHEMORESISTANCE

Given the minimal response to chemotherapy, CCAs are considered highly chemoresistant tumors. The reasons for the chemoresistance are those associated with what are referred to as complexed mechanisms of chemoresistance (MOC). These mechanisms work coordinately to protect tumors from anticancer agents. They also protect adult cholangiocytes from toxic

molecules in blood and/or bile (Marin et al., 2017). In general, there are more than one hundred MOC associated genes in different cancers, including CCA (Marin et al., 2018). In CCA MOC is largely driven by the multidrug resistance (MDR) phenotype of the cell. These MOC genes are classified by their functions in chemoresistance. There have been seven major types of MOCs suggested in cancer, their roles in MDR are listed in Table 1-2.

Table 1-1 Classification of the mechanisms of chemoresistance (MOC) in liver cancer

Type of MOC	Mechanism	Genes	Role in MDR phenotype of liver cancer	Reference
MOC 1a	Reduced drug-uptake	*SLCO2A1, SLC22A3, SLC29A1, SLC28A1, SLC31A1,*	Reduced uptake of organic anion, nucleoside, copper molecules.	(Marin et al., 2017; Marin et al., 2018)
MOC 1b	Enhanced drug-export	*ABCB1, ABCC1, ABCC2, ABCC3, ABCC4, ABCC5, ABCC11*	Enhanced export of organic anion, nucleoside, copper molecules	(Banales et al., 2016; Marin et al., 2018)
MOC 2a	Reduced prodrug activation	*TYMP, UPP1, UMPS*	Reduced activation of nucleotide metabolism (i.e. gemcitabine, fluorouracil)	(Evrard, Cuq, Ciccolini, Vian, & Cano, 1999; Hahnvajanawong et al., 2012)
MOC 2b	Enhanced drug inactivation	*GSTP1*	Inactivation by conjugation with glutathione	(Nakajima et al., 2003)
MOC 3	Changes in drug target	*TYMS, ESR1, ESR2, EGFR, IGF1R,*	Enhanced or reduced expression of target	(Banales et al., 2016)
MOC 4	Enhanced DNA repair	*UNG, ERCC1, RAD51, MSH2, MSH3, MSH6, MLH1, PMS2, RRM2B, TLK1*	Enhanced ability in base-excision, nucleotide-excision, mismatch repair	(Banales et al., 2016) (Marin et al., 2017; Marin et al., 2018)

MOC 5a	Reduced Apoptosis	*NK4, MET, TNFSF10, FAS, TP53*	Reduced activity in pro-apoptotic protein, receptor interaction	(Asghar & Meyer, 2012)
MOC 5b	Enhanced survival	*BCL12, XIAP, BIRC5, AKT1*	Enhanced activity of anti-apoptotic protein and pathways.	(Cox & Weinman, 2016)
MOC 6	Alterations in microenvironment	*HIF1, HIF2*	Activation of hypoxia and promote other MOC activities	(Daskalow et al., 2010)
MOC 7	Transition in phenotype	*SNAIL1, SNAIL2, TWIST1/2, ZEB1/2, TGF-β, SMADs,*	Activation of EMT and crosstalk with TFG-β signaling pathways	(Brivio, Cadamuro, Fabris, & Strazzabosco, 2015; Fuchs et al., 2008; D. Yamada et al., 2013)

1.2.1 Multidrug resistance and CSCs

A striking feature of CSCs is enhanced resistance to conventional chemotherapy. Among the most common mechanisms regarding their MDR phenotype is the presence of high levels of ATP-binding cassette transporters (ABC). Activities of ABC transporters can be measured by side-population (SP), which is also an early method of CSC sorting. SP selection is applied in various mammalian tissue and cell lines, relying on drug efflux characteristics of ABC transporters. Most cells accumulate fluorescent dyes of Hoechst 33342 dye and Rhodamine, whereas "SP" such as stem cells possess a high capacity for effluxing drugs (Dean, 2009). To date, ABC transporters such as g-glycoprotein 1 (MDR1), multidrug resistance-associated protein 1 (MRP1) and breast cancer resistance protein (BCRP) have been reported to efflux Hoechst 33342 dye and promote the SP in CSCs (Slot, Molinski, & Cole, 2011).

1.2.2 ATP-Binding Cassette (ABC) Transporter Structure and Location

ABC transporters are one of the largest families of transmembrane proteins, with 49 members divided into seven subfamilies, from ABC-A to ABC-G. They function as primary active transporters that deliver substrates across the cellular membrane against a concentration gradient through ATP hydrolysis. ABC transporters are structurally defined by basic units of two nucleotide-binding domains (NBD) and two transmembrane domains (TMD). These four domains are linked within one polypeptide chain. There are three categories of ABC transporters according to their structures (Figure 1.2). Figure 1.3 illustrates the pathway of ABC transport during drug resistance.

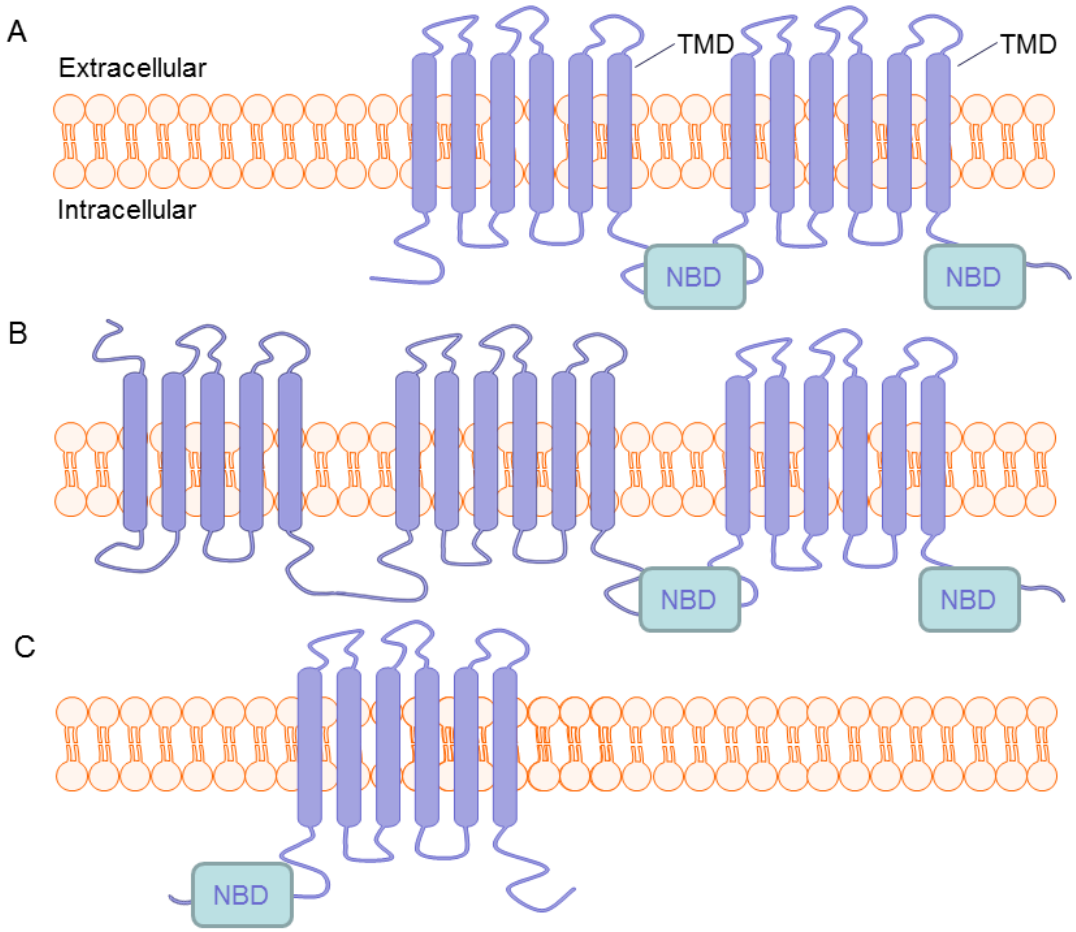

Figure 1.2 The principle structure of ATP-binding cassette (ABC) transporters.

The ABC transporter family is classified into three categories conferring drug resistance. Each ABC transporter contains one or two NBDs (ATP-biding sites) and TMDs (transmembrane domains). A) ABC transporters including ABCB1, ABCC4, ABCC5, ABCC1 and ABCB11 comprise two TMDs and two NBDs. B) ABCC subfamily membranes: ABCC1, ABCC2, ABCC3, and ABCC6 have an additional NH2-terminal TMD that is composed of five transmembrane segments. C) The half transporters (ABCG2) have one pair of TMD and NBD such that they only contain six transmembrane domains and one ATP-binding region. Thus, these half transporters need homo- or hetero-dimerization to generate a functional unit.

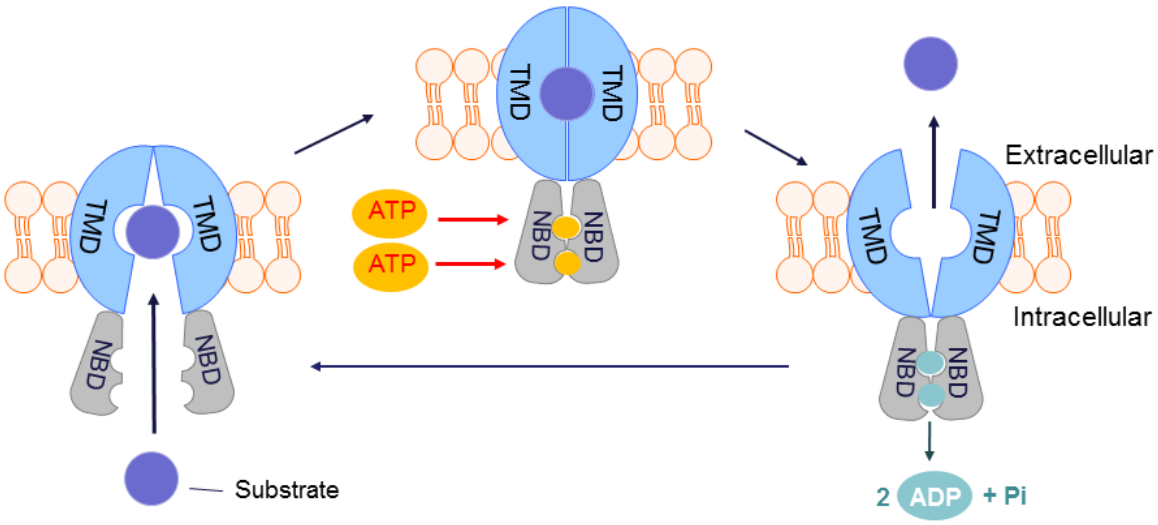

Figure 1.3 The mechanism of ABC pump transporting substrates out of the cell. The transporter remains in a closed transmembrane structure until a substrate is present. Transport activity is initiated when a substrate docks into TMDs. ATPs bind to two NBD domains to induce ATP hydrolysis. ATP is then hydrolyzed to adenosine diphosphate (ADP) which results in a conformational change of TMD and the substrate is transported out of the cell (Dean, 2009).

1.2.3 ABC Transporters in Cancer Cell Biology

To date, most studies of ABC transporters have focused on their roles in chemoresistance by effluxing cytotoxic anticancer agents out of cells. Indeed, ABC transporters can accommodate and direct a range of substrates through the cell membrane, including peptides, inorganic anions, amino acids, polysaccharides, proteins, vitamins and metallic ions (Begicevic & Falasca, 2017).

ABC transporters also enable the transport of different signaling molecules (e.g. prostaglandins, leukotriene C4, etc.) that may support cell survival (Slot et al., 2011).

There are many subtypes of ABC transporters involved in drug-efflux activities that contribute to the MDR phenotype in several types of tumors, including CCA (Begicevic & Falasca, 2017). Wee et al (2016) reported ABC-G2 to be associated with increased cell-renewal and tumorigenic capacity as well as high CSC surface marker expression in glioma cells. Overexpressed ABC-G2 in right-sided colon cancer specimens induced lymphovascular invasion, tumor recurrence and poor prognosis (Hu et al., 2017). ABC-B5 was also documented to contribute to fluorouracil-induced chemoresistance and cell invasion in colorectal cancer (Wilson et al., 2011). Compared to mature cancer cells, CSCs exhibit overexpressed membrane pumps, coupled with upregulated mitochondrial ATP generation, consequently promoting enhanced drug efflux. In addition, upregulated ABC pumps in CSCs maintain stem cell features by supporting cells escaped from naturally generated xenobiotics (Begicevic & Falasca, 2017).

In hepatobiliary cancers, ABC transporters are predominantly active in CSCs (or SP cells). CSCs efflux Hoechst 33342 dyes, leading to a diminished Hoechst 33342 stained profile (Hirschmann-Jax et al., 2004). It has been reported that human HCC cell lines (HCCLM3, MHCC97-H, MHCC97-L HepG2, HuH7 and PLC/PRF/5) are characterized by exhibiting SP and non-SP cells (Chiba et al., 2006; Haraguchi et al., 2006; Shi et al., 2008). Unlike non-SP cells, isolated SP cells show enhanced cell proliferative and anti-apoptotic features (Chiba et al., 2006). Moreover, liver SP contain a strong metastatic potential of cancer cells (Shi et al., 2008).

1.2.4 ABC or Multidrug Resistance-Associated Protein (MRP) Subfamily

In mammals, the ABCC family consists of 13 members and is classified into three groups, including MRPs, sulfonylurea receptors (SURs), and cystic fibrosis transmembrane conductance regulator (CFTR). Among the largest subgroup of ABCC pumps is MRP comprising ten members: ABCC1/MRP1, ABCC2/MRP2, ABCC3/MRP3, ABCC4/MRP4, ABCC5/MRP5, ABCC6/MRP6, ABCC10/MRP7, ABCC11/MRP8, ABCC12/MRP9 and ABCC13/MRP10. The other ABCC members include a CFTR (ABCC7) and two SURs (ABCC8 and ABCC9).

Expression profiles of MRP transporters are distributed diversely in different tissues, such as liver, kidney, intestine and brain. Given their various locations in the apical and/or basolateral membrane of cells, MRPs may have different functions in terms of ion transport, surface receptor interaction and toxin-efflux activities. In general, MRPs primarily transport a variety of critical exogenous and endogenous substances as well as their metabolites with different specificities and transport kinetics. As one of the major family of ABC transporters, most MRPs demonstrate their roles in exporting organic anions, such as glutathione, sulphate, and glucoronide (Borst, Evers, Kool, & Wijnholds, 2000). Moreover, several MRP transporters have been reported to transport endogenous substrates, such as leukotriene C4 (LTC_4) with MRP1, sphingosine-1-phosphate (SIP) with MRP1, lysophosphatidylinositol (LPI) with MRP1, glutathione (GSH) and its conjugates with MRP1-6, bilirubin glucuronides with MRP2- 3 and prostaglandins (PGs) with MRP3-5 (Mitra et al., 2006; Reid et al., 2003; Ruban, Ferro, Arifin, & Falasca, 2014; X. Wang et al., 2014; Wijnholds et al., 1997).

MRPs contribute to resistances acquired by anticancer agents and their metabolites, including platinum compounds, cyclic nucleotides, steroid conjugates and folate, arsenical and antimonial oxyanions, peptide, and alkylating agents (Borst et al., 2000; Reid et al., 2003). Although research on MRPs in CCA is limited, some studies have reported MRP1-5 expression in I-CCA (Martinez-Becerra et al., 2012; Srimunta et al., 2012), and higher MRP expression in tumor compared to surrounding normal tissues (Martinez-Becerra et al., 2012). Similar results have been described in HCC, where it has also been revealed that alterations of MRP1 correlate with tumor differentiation and invasion (Vander Borght et al., 2008), suggesting MRP1 might serve as an independent clinicopathological indicator in liver cancers. Although the finding of MRP2 expression is controversial in I-CCA, MRP3 has been detected in CCA cells resistant to etoposide, doxorubicin and pararubicin (Kang et al., 2014). MRP5 and its role in chemoresistance have been described for fluorouracil in CCAs (Pratt et al., 2005). By contrast, MRP detection is low in the HepG2 HCC cell line, but upregulates after exposure to 2-acetylaminofluorene, cisplatin, and rifampicin (Schrenk et al., 2001).

1.2.5 RNA Interference (RNAi) Technology

RNAi refers to a member of non-coding RNA (ncRNA) that is employed to interrupt mRNA molecules or inhibit their translation. Short interfering RNA (siRNA), short hairpin RNA (shRNA) and microRNA (miRNA) are major components of small regulatory ncRNAs that participate in RNAi blockade (Khvorova, Reynolds, & Jayasena, 2003). Since the first case of delivering RNAi through human systemic injection was reported in 2010 (Davis et al., 2010),

RNAi has captured much interest and widely applied in gene silencing and therapeutic development (Tatiparti, Sau, Kashaw, & Iyer, 2017). A general mechanism of RNAi in a cell is illustrated in Figure 1.4.

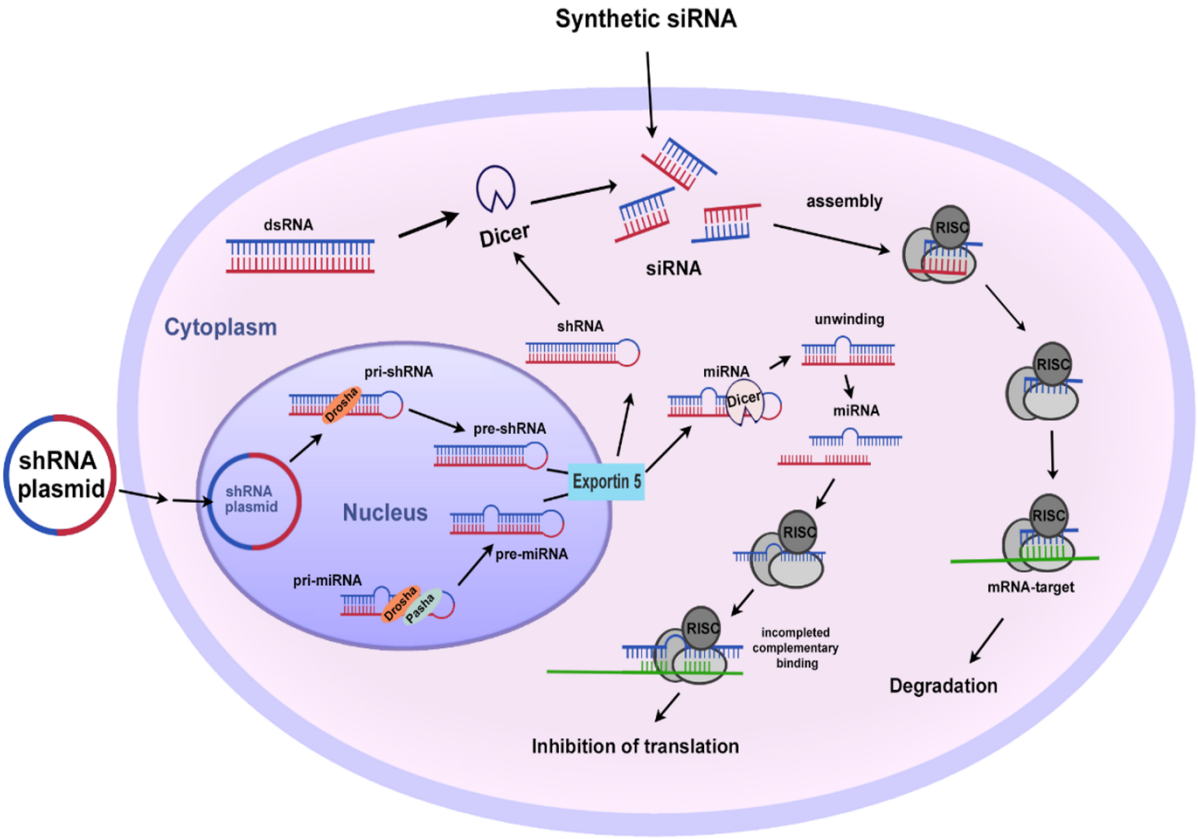

Figure 1.4 Mechanisms RNA interference including siRNA, miRNA and shRNA.

In general, a sequence of siRNA is cleaved from double stranded RNAs (dsRNAs). These dsRNAs are transcribed from either cellular genes, viruses, or artificially sequenced being introduced into the cytoplasm. Once a dsRNA is present within the cell, it is processed into a siRNA by the RNase III-like enzyme (Dicer). The siRNA is then loaded into an RNA-induced silencing complex (RISC). The RISC cleaves the passenger stand of siRNA, which is then degraded and released.

The guide strand of siRNA remains incorporated with the RISC. Subsequently, the complex of guide strand and activated RISC moves towards to the targeted mRNA for cleavage. Because siRNAs only bind to mRNA in a fully complementary pattern, the siRNA mediated process achieves specific gene blockade (Costa, 2007). Compared to siRNA, shRNAs are mostly delivered by viral vectors. The RNA sequence of shRNA is synthesized in the nucleus, which is transcribed by RNA polymerase II or III. Once the sequence is synthesized, shRNA moves into the cytoplasm for down-streaming processing. Within the cytoplasm, the shRNA interacts with the RISC for specific gene silencing in the same mechanisms as synthetic siRNA (Rao, Vorhies, Senzer, & Nemunaitis, 2009). The miRNA that is transcribed from human micro RNA gene also triggers a silencing gene in a post-transcriptional pattern. It shares a similar processing manner with that of siRNA and shRNA, including present and functions of common enzymes (e.g. Dicer and RISC). However, the miRNA matches to its targeted mRNA in an imperfect complementary pattern. Therefore, a single miRNA regulates numerous mRNA sequences instead of a specific gene target (Wahid, Shehzad, Khan, & Kim, 2010).

1.2.5.1 RNAi Therapy in Cancer

There have been a number of RNAi-based studies reported in human cancers. For example, the miR-2000 family, functions as an essential inhibitor of EMT and/or metastasis (Humphries & Yang, 2015). In addition to the role miR-2000 miRNA plays in tumorigenesis, this type of miRNA is employed to diagnose and treat many different types of malignancies including liver, stomach, lung and breast cancers (Bracken et al., 2014; Dykxhoorn et al., 2009; W. Zhu et al., 2012).

To enhance the sensitivity of cancer cells to chemotherapy, RNAi targeting of multidrug resistance proteins such as MDR1 has been investigated (Lage, 2009). It has been demonstrated that the delivery of siRNA targeting MDR1 leads to MDR1 knockdown and consequently enhances the efficacy of delivering chemotherapeutic drugs to cancer cells (X. P. Chen et al., 2006; Nieth, Priebsch, Stege, & Lage, 2003; Shao et al., 2014) .

Other targets of RNAi for attacking cancers could be carcinogenic factors, including oncogenes, tumor suppressor genes and other regulatory factors. One such factor is c-Met, which is the receptor of HGF and plays a critical role in cell proliferation and invasion. The RNAi specific to c-Met significantly inhibits tumor growth, migration and invasion (Salvi et al., 2007; B. Xie et al., 2010; S. Z. Zhang et al., 2005). Moreover, RNAi targeting p53 has been used in a triple negative breast cancer cell model to correct p53 mutation-induced metastasis (Braicu et al., 2015).

1.2.5.2 Lentivirus Delivery System of RNAi

By taking advantages of the natural features of viruses in terms of life-long gene silencing and multiple RNAi replications from one transcript, viral vectors have been identified as effective delivery carriers. After an RNAi oligonucleotide is cloned into a virus genome, the RNAi is expressed as shRNA by virus infected cells, and subsequently processed into siRNA in the host cytoplasm (Figure 1.4). There are several *in vivo* studies employing viral vectors to deliver RNAi

and achieve effective treatments for various diseases (Couto & High, 2010; Manjunath, Wu, Subramanya, & Shankar, 2009).

Lentivirus contains two clones of single strand RNA genome with an enveloped capsid. The lentivirus delivered system is characterized by its life-long expressed transgene of interest after being integrated into the host cell genome. The vector-based lentivirus has been modified being non-replicated for transgene expression. The principle behind the lentivirus delivery system is developing a virus after a single round of transduction to have stable integration of transgene with minimized viral genome, resulting in a continually expressed transgene without viral infection (Figure 1.5). Lentivirus is able to infect both dividing and non-diving cells so that lentivirus delivered RNAi could maintain long-term RNAi effects. Other advantages are that lentivirus enables the delivery of larger sequences of transgenes and expresses relatively low immunogenic activity.

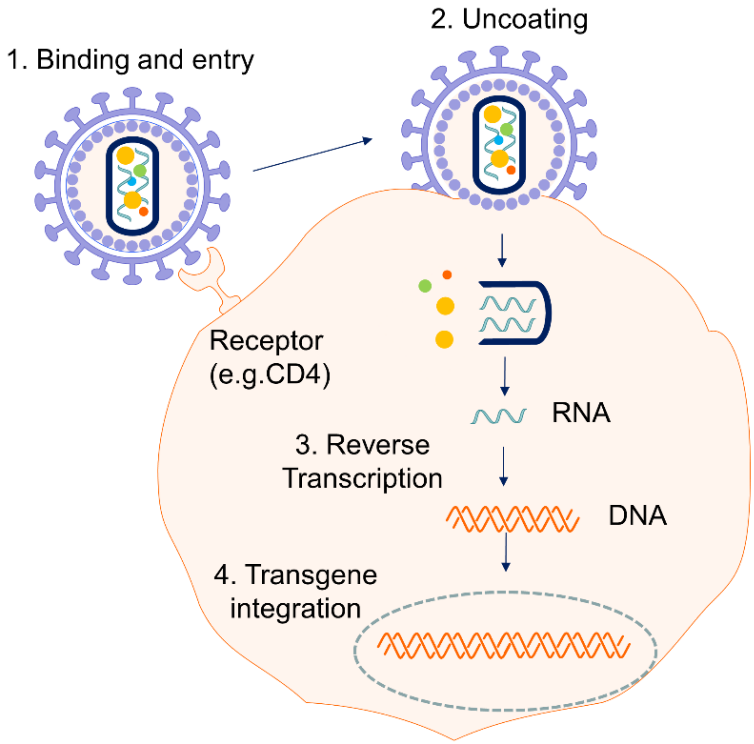

Figure 1.5 Lentivirus delivery pathway.

Transduction begins when the lentivirus envelope binds to the cellular receptor and then enters the cell. Uncoating of the virus release genetic materials from lentivirus into the cytoplasm. The RNA genome is reverse-transcribed into double strand complementary DNA (cDNA) and then enters the nucleus. The cDNA is integrated into the host genome by the enzymatic activity of IN.

1.3 CHEMOKINE AND CHEMOKINE RECEPTOR (CR) SYSTEM

In humans, chemokines consist of greater than 50 small secreted proteins. They function as immune regulators, chemoattractants and lymphocyte activators, usually accumulating in damaged tissues in order to respond to proinflammatory signals. Chemokines are classified into

four main groups, including CXC-, CC-, C (or XC) - and CX_3C-chemokine families according to the specific position of conserved cysteine residues near N-terminals (Figure 1.6A) (Charo & Ransohoff, 2006). There have been 17 different CXC- chemokines (CXCL) described in mammals and are further subgrouped based on the presence of a glutamic acid-leucine-arginine (ELR) sequence/motif. In general, ELR^+CXC chemokines regulate migration for neutrophils, while ELR^-CXC chemokines serve as chemoattractants for lymphocytes. Regarding CC-chemokines (CCL), there have been more than 27 members discovered to date. They tend to be activators, chemoattractants, and immunomodulators for monocytes and lymphocytes (Laing & Secombes, 2004). The group of C- chemokines (XCL), contains two members (XCL and XCL2) and functions as lymphotactin. Finally, the CX_3C- chemokine (CX_3CL) consists of only one member termed CX_3CL1/fractalkine, which serves as a chemoattractant and an adhesion molecule.

CRs expressed on a cell surface bind to chemokines (Figure 1.6B). To date, there have been 20 different CRs discovered in humans (Chow & Luster, 2014). They are classified into different families corresponding to the four subgroups of chemokines, including CXC chemokine receptors (CXCRs), CC chemokine receptors (CCRs), XC chemokine receptors (XCRs) and CX_3C chemokine receptors (CX_3CRs). As a G protein-coupled receptor, CRs are characterized by a seven-transmembrane domain and a second intracellular domain with a specific "DRY" sequence linked to a G-protein for signal transduction. After chemokines bind to their specific CRs on the cell surface, intracellular calcium signaling is triggered which subsequently activates

cell responses. One of the often described processes of chemokine and CR interactions is chemotaxis, which traffics cell migration and homing (Balkwill, 2004a).

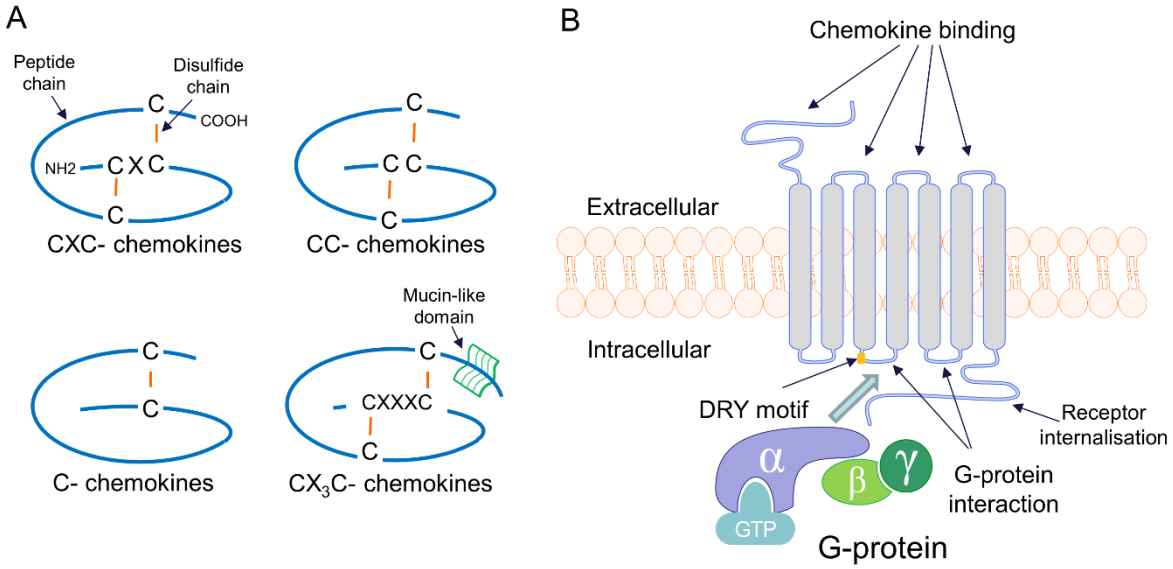

Figure 1.6 Typical structures of chemokine and chemokine receptor.

(A) Chemokine families are distinguished from each other by their schematic structure, as relationships between conserved cysteine residues C with disulfide chain (de Munnik, Smit, Leurs, & Vischer, 2015). (B) Each CR contains seven transmembrane domains, with a DRY motif in the second intracellular segments. CRs are usually linked to a G-protein through which they signal.

1.3.1 Chemokines and Their Receptors in Liver

In the liver, chemokines and their receptors are involved in initiating an inflammatory process. In response to invading pathogens or injured hepatocytes and cholangiocytes, both parenchymal and non-parenchymal cells including resident hepatic macrophages, Kupffer cells, hepatocytes,

liver sinusoidal endothelial cells (LSECs), hepatic stellate cells (HSCs) or pit cells (local immune cells) release an array of proinflammatory cytokines and chemokines (CXCL1, CXCL2, CXCL8, CXCL16 and CCL2) (Liaskou, Wilson, & Oo, 2012). Neutrophils attracted by CXCL1, CXCL2 and CXCL8 via CXCR1 and CXCR2 produce ROSs and proteases to induce epithelium injury (Zimmermann & Tacke, 2011). The interaction of CXCL16 and CXCR6 promotes recruitment of natural killer T cell and subsequently expands inflammatory signals. CCR2 expressed monocytes are recruited and accumulated in the liver in response to CCL2, where they differentiate into proinflammatory macrophages and attract more inflammatory monocytes (Marra & Tacke, 2014; Wehr et al., 2013).

1.3.2 Chemokines and Their Receptors in Liver Cancer

Beyond the functions of chemokines in modulating immune trafficking and foci of inflammation, CRs also regulate the biological functions of non-immune cells, such as cell growth and migration (Charo & Ransohoff, 2006; Miyazaki, Takabe, & Yeudall, 2013). During carcinogenesis, chemokines promote the tumor microenvironment by generating chemokine gradients that are essential for cancer cell survival and metastasis (Balkwill, 2004a). Tumor cells express specific CRs, which guide circulating tumor cells to particular anatomic locations where they produce specific chemokines to develop metastasis (Zlotnik, Burkhardt, & Homey, 2011).

1.3.2.1 Clinical Findings

From clinical studies, chemokines or CRs such as CXCL5, CXCL8, CCR1, CXCR2, CXCR4 and CXCR7 have been shown to correlate with the grade of liver cancer and prognosis. In terms

of CXCL5, this chemokine is highly expressed in HCC tissue and its overexpression is associated with intra-tumoral neutrophil infiltration, metastasis, tumor recurrence, and poor patient survival (Zhou et al., 2012). Similar findings have been reported in I-CCA patients (Zhou et al., 2014). Regarding CXCL8, Ren et al (2003) reported that serum CXCL8 levels are high in HCC patients compared to healthy individuals and levels correlate with cancer invasion and metastasis. It has also been suggested that CXCL8 is a useful prognostic factor for disease-free and overall survival. A study of CXCR2 in HCC patients suggested mRNA and protein expression are associated with intrahepatic metastases, portal venous emboli, differentiation and TNM staging (Z. Liu, Yang, Xu, Zhang, & Wang, 2011). Lu et al (2003) reported that CCR1 is detectable in both HCC specimens and HCC cell lines, but not normal liver tissues.

CXCR4 is a prognostic marker for more than 23 distinct types of cancers, and has been reported as a CSC associated protein in cancers (Balkwill, 2004b). CXCR4 with its chemokine CXCL12 participate in tumor growth and metastasis (Ribatti, Mangialardi, & Vacca, 2006). Overexpression of CXCR4 in HCC patients is associated with aggressive proliferation, metastasis and poor prognosis (Ghanem et al., 2014). Interestingly, CXCL12, the ligand of CXCR4, has been observed in malignant ascites and HCC that had metastasized to lymph nodes but not in tumor or normal tissues (H. Liu et al., 2008). In CCA, CXCR4 was detected in tumor specimens, especially tumor vessels and was associated with a poor prognosis (Ghanem et al., 2014; Kaemmerer et al., 2017). CXCL12 is only expressed in CAFs, and not in tumor cells. Finally, CXCR7 has been discovered as another receptor interacting with CXCL12. Its

expression is upregulated in HCC specimens and associated with metastasis (Monnier et al., 2012; Xue et al., 2012).

1.3.2.2 Chemokines and CR signaling

Chemokines and CRs induce tumor progression via different pathways. For instance, chemotaxis activation of CXCL5 in HCC cell lines triggers the stimulation of PI3K and ERK1/2 signaling pathway. Downregulation of CXCL5 via shRNA reduces cell proliferation *in vitro* and tumor growth *in vivo* for HCC, and inhibits I-CCA growth *in vivo* (Zhou et al., 2014; Zhou et al., 2012). In addition, enhanced secretion of CCL20 in HuH7 cells promotes cell growth by mediating the p44/42 MARK pathway (Fujii et al., 2004). Inhibition of CXCR2 in intrahepatic CCAs significantly suppresses tumor growth (Sueoka et al., 2014). Regarding the importance of CXCL12/CXCR4 axis in HCC and CCA, a number of approaches to altering CXCR4 expression have been employed such as by pharmaceutical agonists/antagonists and RNAi techniques (Duda et al., 2011; R. Zhang, Pan, Huang, Weber, & Zhang, 2011; S. Zhao, Wang, & Qin, 2014). The findings indicate CXCR4 is involved in cell growth and/or tumor progression. Suggested mechanisms include Wnt/β-catenin, Erk2 and JNK/SAPK kinase signals (Sutton et al., 2007; S. Zhao et al., 2014). However, whether other CRs are expressed in CCAs and their relative potency in influencing tumor growth features have yet to be determined.

1.3.2.3 Angiogenesis

Tumor progression depends on adequate blood perfusion to provide oxygen and nutrients. Given the rapid proliferation of tumor mass, adequate angiogenesis is required. Like other tumors, it

has been reported that chemokines and CRs are involved in liver tumor angiogenesis. Tang et al (2012) reported that CXCL8 is overexpressed in $CD133^+$ CSCs from HCC tissues and cell lines. Enhanced CXCL8 secretion from these CSCs was associated with a greater ability to induce tumor angiogenesis through the MAPK pathway. High expression of CXCR4 on HCC tumor endothelial cells results in sinusoidal vasculature development in tumors. Biological experimentation suggests CXCR4 directly promotes vessel generation both *in vitro* and *in vivo* (Xu et al., 2017). Yang et al (2006) reported CCL3- and CCR1- deficient mice form HCC tumors less frequently and with lower growth compared to wild type, these findings were associated with diminished angiogenesis in CCL3- and CCR1- deficient individuals.

1.3.2.4 Metastasis

Given the functions of chemotaxis in trafficking and homing, a number of studies have documented that chemokines and CRs are involved in metastasis. Zhou et al (2014; 2012) demonstrated the role of CXCL5 in HCC and I-CCA metastasis. By inhibiting CXCL5 both *in vitro* and *in vivo*, it was revealed that CXCL5 regulates cancer cell invasion via recruiting intratumoral neutrophils through the stimulation of PI3K and ERK1/2 signaling pathways. The important role of CXCL12/CXCR4 system in metastasis has been documented in several types of cancers, including HCC and CCA. Inhibition of CXCR4 can successfully inhibit HCC and CCA tumor cell metastasis and neural invasion (Ohira et al., 2006; Sutton et al., 2007; Tan, Chang, Liu, & Tang, 2014; Y. Xie et al., 2016; S. Zhao et al., 2014). Overexpression of CXCR4 increases the capacity of CCA cells to invade (Leelawat et al., 2013). MEK1/2, AKT, Erk2, JNK/SAPK kinase, and Wnt signaling pathways have been linked to CXCL12/CXCR4

metastasis (Leelawat, Leelawat, Narong, & Hongeng, 2007; Sutton et al., 2007; S. Zhao et al., 2014). These findings suggest the CXCL12/CXCR4 axis is highly involved in CCA metastasis. Furthermore, a recent study has demonstrated that $CD24^+$ CCA cells have upregulated CXCR4 expression, resulting in a high potency of invasion compared to $CD24^-$ CCA cells (Leelawat et al., 2013).

1.3.3 The Chemokine Ligand CCL5 and Its CCR5 Receptor

Among the subfamily of CCRs, the CCL5 chemokine (or RANTES) and its CCR5 receptor have been most extensively investigated. CCL5 is expressed in T cells, platelets, macrophages, fibroblast, tubular epithelium, and some cancer cells. CCL5 interacts with CRs including CCR1, CCR3, CCR4, CCR5, and GPR75 in different types of cells (Soria & Ben-Baruch, 2008). CCR5 is predominately expressed in immune (T cells, macrophages, dendritic cells, etc.) and selected tumor cells (Gao, Rahbar, & Fish, 2016; Singh et al., 2018; Y. Zhang et al., 2013).

CCR5 is best known for its role in the pathogenesis of human immunodeficiency virus (HIV) infections, mediating cellular entry of virus (Murphy, 2001). In terms of cancers, there have been an increasing number of studies revealing that the expression and/or regulation of CCL5 and/or CCR5 are considered as poor prognosis markers and associated with breast, prostate, ovarian, gastric and pancreatic cancer development (Cao et al., 2011; Makinoshima & Dezawa, 2009; Tsukishiro, Suzumori, Nishikawa, Arakawa, & Suzumori, 2006; Vaday, Peehl, Kadam, & Lawrence, 2006; Yaal-Hahoshen et al., 2006). In breast cancers, overexpression of CCL5 and CCR5 are detected in metastatic lymph node disease rather than primary tumors, and

intratumoral CCL5 expression associates with advanced disease (Gao et al., 2016; Yaal-Hahoshen et al., 2006; Y. Zhang et al., 2009). In gastric cancer, expression levels of CCR5 are higher in lymph node metastasis and correlate with a poor prognosis (Sugasawa et al., 2008). In pancreatic cancers, upregulated CCL5 and CCR5 have also been described in patients with advanced disease. Recently, Singh et al (2018) reported that pancreatic cancer cells display high expression of CCR5. The invasive potential of $CCR5^+$ cells is upregulated by CCL5 and downregulated by Maraviroc with F-actin polymerization. Taken together, these data suggest CCL5 and/or CCR5 are potential markers and/or mediators of cancer metastasis.

Despite their importance in other types of cancer, there are a paucity of reports regarding the role of the CCL5 and/or CCR5 in hepatobiliary cancers. CCR5 has been implicated in inflammatory-induced HCC where CCR5-deficient mice had reduced inflammation and less fibrosis, as well as deceased tumor incidence and size compared to control models (Barashi et al., 2013). The role of CCL5 in HCC was also studied by Bai et al (2014), who suggested CCL5 released from bone marrow stromal cells promote migration and invasion of the HCC cell line (HuH7) by PI3K/Akt signaling. In another study, Mohs et al (2017) reported overexpression of CCL5 and CCR5 in chronic liver disease patients. Subsequent animal models revealed that CCL5-deficient mice develop smaller and fewer HCC tumors as a result of reduced cell proliferation and diminished angiogenesis. The CCR5 inhibitor Maraviroc diminished tumor development in chronic liver disease models (Ochoa-Callejero et al., 2013). Regarding CCA, Zhong et al (2017) demonstrated CCL5 and CCR5 expression correlate with inflammation and metastasis of CCA cells. From both *in vitro* and *in vivo* assays, secreted factors from stimulated mesenchymal stem cells

(MSCs) promote CCA cell migration and metastasis. By incubating CCA cells with MSCs secreted supernatants, CCR5 expression in CCA is upregulated by interacting with CCL5. Moreover, alteration of the CCL5/CCR5 axis is associated with activation of Akt/NF-κB pathways by increased expression of MMP2 and MMP9. Maraviroc inhibits the effects MSCs on CCA cell migration (Zhong et al., 2017)

1.4 CURRENT GAP OF KNOWLEDGE

CCAs are often fatal, have limited treatment options and low therapeutic responses. Inter-tumoral and intra-tumoral heterogeneities in CCA have been a challenge in understanding this cancer. Specifically, different study cohorts have demonstrated various molecular profiling of surgical CCA samples in different genetic and epigenic subtypes, which may not correlate to clinical features or outcomes. The role of CSC in CCA remains to be elucidated, none of the current CSC research has identified the prevalence or phenotype of the CSC subpopulation in CCA development and prognosis. Additionally, there are still gaps in understanding the resistance to treatment in CCA. Current application of mono-therapy or combination-therapies appears to have limited efficacy and need to be approved upon.

1.5 RATIONAL

1.5.1 Part I: Differences in Tumor Biology and CSCs

The two anatomical subclasses, I-CCA and E-CCA differ in their growth patterns and responses to treatment. Clinical observations have revealed that I-CCA tends to be mass forming and frequently metastasize whereas E-CCA tends to grow parallel to tissue planes and rarely develop

distant metastases (Hirohashi et al., 2002; Nakeeb et al., 1996). Although numerous factors might explain these differences, the intrinsic biological features of I-CCA and E-CCA need to be documented and compared.

CSC is a subpopulation of tumor cells that are responsible for many tumor features including cell proliferation, migration, invasiveness and metastatic potential (Batlle & Clevers, 2017; Iacopino et al., 2014). Many of these features are associated with or influenced by SCSMs expressed by the CSCs. Whether the prevalence and SCSM expression profiles of CSCs differ in I-CCA versus E-CCA have yet to be determined.

1.5.2 Part II: I-CCA and E-CCA Chemoresistance

The majority of CCA tumors are unresectable. Therefore, for most patients, chemotherapy is often considered but response rates are low and prolongation of survival is limited (Mavros, Economopoulos, Alexiou, & Pawlik, 2014; Nakeeb & Pitt, 2005). The MRP genes in tumor cells play an important role in rescuing cells from chemotherapy by exporting chemotherapeutic agents out of tumor cells. To date, six distinct MRP (MRP1-6) genes have been identified with different expression profiles in different tissues and cancer types (Z. S. Chen & Tiwari, 2011). However, there have been no reports describing the expression profiles of MRPs and their functions in I-CCA and E-CCA cells or whether inhibiting key MRPs increase CCA chemosensitivity.

1.5.3 Part III: I-CCA and E-CCA Chemotaxis

In the setting of carcinoma, chemokine gradients within the tumor microenvironment influence tumor cell survival, growth and metastasis (Balkwill, 2004a). The CXCR4 and its ligand CXCL12 have been implicated in the development of tumor metastases in more than 23 distinct tumor types (Balkwill, 2004b). In addition, CR and chemokine interactions induce tumor promoting growth factors (Balkwill, 2004a; Chow & Luster, 2014). Despite the high mortality rates associated with CCA and importance of chemotaxis in regulating tumor cell biology, there are a paucity of reports describing chemotaxis in CCA (Leelawat et al., 2013; Ohira et al., 2006; Tan et al., 2014; Y. Xie et al., 2016; S. Zhao et al., 2014), and whether altering the expression profile and/or influence of the CCR subclass impacts I-CCA and E-CCA tumor cell biology (Sueoka et al., 2014; Zheng et al., 2010).

1.6 HYPOTHESIS

1.6.1 Part I: Differences in Tumor Biology and CSCs

Based on the different clinical features of I-CCA and E-CCA tumors and the importance of CSCs in regulating these features, we hypothesize that I-CCA and E-CCA cells will exhibit different intrinsic tumor biology and the prevalence and/or SCSM profiles of CSCs within the two cell types will also differ.

1.6.2 Part II: I-CCA and E-CCA Chemoresistance

Since chemotherapy is the most often utilized therapeutic option for CCA, and I-CCA may respond differently than E-CCA (Patel, 2011) and MRP play an important role in chemoresistance, we hypothesize there will be differences in the expression of MRPs between I-CCA and E-CCA. Moreover, inhibition of certain MRPs could enhance chemotherapeutic sensitivity.

1.6.3 Part III: I-CCA and E-CCA Chemotaxis

Chemokines and their receptors influence tumor biology including their propensity to invade and metastasize. Thus, we hypothesize that chemokines and their receptors are expressed but to a different extent in I-CCA and E-CCA, and inhibition of chemokine activity will alter these biologic properties.

2. MATERIALS AND METHODS

2.1 MATERIALS

2.1.1 Cell Lines

Table 2-1 List of cell lines

Name	Origin	Media	Description	Source
CCLP-1	I-CCA	Dulbecco's Modified Eagle Medium (DMEM), 10% fetal bovine serum (FBS), 2 mmol/L L-glutamine, 100	I-CCA cell line derived from a 48-year-old female	Dr. Gianfranco Alpini, Texas A&M University, USA

		U/mL penicillin and 100 μg/mL streptomycin	(Shimizu et al., 1992)	
HuCCT1	I-CCA	RPMI 1640 Medium, 10% FBS, 110 mg/L sodium pyruvate, 100 U/mL penicillin and 100 μg/mL streptomycin	I-CCA cell line derived from a 56-year-old male (Miyagiwa et al., 1989)	Sekisui XenoTech, USA
SG231	I-CCA	Minimum Essential Media (MEM), 25 mM HEPES pH 7.2, 10% FBS, 2 mmol/L L-glutamine, and 1 % penicillin/streptomycin	I-CCA cell line drived from a 42-year-old male (Storto et al., 1990)	Dr. Gianfranco Alpini, Texas A&M University, USA
HuH28	E-CCA	RPMI 1640 Medium, 10% FBS, 110 mg/L sodium pyruvate, 100 U/mL penicillin and 100 μg/mL streptomycin	E-CCA cell line derived from a 37-year-old female (Kusaka et al., 1988)	Dr. Gianfranco Alpini, Texas A&M University, USA
KMBC	E-CCA	RPMI 1640 Medium, 10% FBS, 110 mg/L sodium pyruvate, a100 U/mL penicillin and 100 μg/mL streptomycin	E-CCA cell line derived from a 74-year-old male (Yano et al., 1992)	ATCC, USA

TFK-1	E-CCA	RPMI 1640 Medium, 10% FBS, 110 mg/L sodium pyruvate, 100 U/mL penicillin and 100 µg/mL streptomycin	E-CCA cell line derived from a 63-year-old male (Saijyo et al., 1995)	Dr. Gianfranco Alpini, Texas A&M University, USA
H69	Non-malignant	DMEM (Low glucose, Gibco), 25 % Ham's F12, 10 % FBS, 4 mmol/L L-Glutamine, 180 µmol/L adenine, 5 mg/L insulin, 5 mg/L transferrin, 2 nmol/L triiodothyronine, 1,1 µmol/L hydrocortisone, 5,5 µmol/L epinephrine , 1.64 µmol/L epidermal growth factor (EGF), 100 U/mL penicillin and 100 µg/mL streptomycin	Intrahepatic cholangiocytes with retroviral transduction of SV large T (Grubman et al., 1994)	Dr. Gianfranco Alpini, Texas A&M University, USA

2.1.2 Reagents and Facilities

Table 2-2 List of reagents

Reagent	Source
Antibodies	

7-AAD	Beckman Coulter, USA
Allophycocyanin (APC)-anti human CD13	BD Biosciences, USA
APC-eFluor 780- anti human CD24	Life technologies, USA
eFlour 450- anti human CD44	Life technologies, USA
Phycoerythrin (PE)-Cy7- anti human CD90	BD Biosciences, USA
PE- anti human CD133	Miltenyi Biotec, USA
Fluorescein isothiocyanate (FITC)- anti human EpCAM	Miltenyi Biotec, USA
APC- anti human IgG1	BD Biosciences, USA
APC-eFluor 780- anti human IgG1	Life technologies, USA
PE-Cy7- anti human IgG1	BD Biosciences, USA
PE- anti human IgG1	Santa Cruz, USA
FITC- anti human IgG1	Miltenyi Biotec, USA
Rabbit anti-human MRP5	Life technologies, USA
Rabbit anti-human MRP6	Life technologies, USA
Mouse anti-human β-actin	ABCAM, USA
Goat anti-rabbit IgG, horseradish peroxidase (HRP)	Life technologies, USA
Goat anti-mouse IgG, HRP	Life technologies, USA
Cell cultures	
RPMI 1640 medium	Invitrogen, USA
Dulbecco's Modified Eagle Medium/Nutrient Mixture F-12 (DMEM/F12)	Invitrogen, USA

MEM	Invitrogen, USA
DMEM	Invitrogen, USA
DMEM (low glucose)	Invitrogen, USA
Ham's F12	Invitrogen, USA
L-Glutamine	Invitrogen, USA
Sodium pyruvate	Invitrogen, USA
HI- fetal bovine serum (FBS)	Invitrogen, USA
Penicillin-streptomycin	Invitrogen, USA
Heat inactivated HI-FBS	Invitrogen, USA
Adenine	Sigma-Aldrich, USA
Insulin	Invitrogen, USA
Transferrin	Sigma-Aldrich, USA
Triiodothyronine	Sigma-Aldrich, USA
Hydrocortisone	Sigma-Aldrich, USA
Epinephrine	Sigma-Aldrich, USA
EGF	Invitrogen, USA
bFGF	Invitrogen, USA
B-27 Serum-Free Supplement	Invitrogen, USA
Heparin	Stem cell Technologies, Canada
Trypsin-EDTA	Invitrogen, USA
EDTA	Sigma-Aldrich, USA

Nobel agar	Sigma-Aldrich, USA
Cell dissociation buffer	Invitrogen, USA
Luria-Bertani broth (LB) medium	Sigma-Aldrich, USA
Ampicillin	Invitrogen, USA
Puromycin	Sigma-Aldrich, USA
Hexadimethrine bromide	Sigma-Aldrich, USA
Kits	
TRIzol Plus RNA Purification	Thermo Scientific, USA
iScript™ cDNA synthesis kit Reverse Transcription Kit	Bio-Rad, USA
SYBR® Green PCR Master Mix	Invitrogen, USA
SuperSignal™ Wester Dura Extended Duration Substrate	Invitrogen, USA
QIAGEN Plasmid Midi Kit	Qiagen, USA
Pierce™ BCA Protein Assay Kit	Thermo Scientific, USA
Agnist, antagonist	
Gemcitabine	Sigma-Aldrich, USA
Maraviroc	Sigma-Aldrich, USA
CCL5 (RANTES)	Invitrogen, USA
Plasmids	
pLKO.1-puro vector stock	Lentiviral Core Platform, University of Manitoba, Canada

MRP5 shRNA plasmid bacteria stock	Lentiviral Core Platform, University of Manitoba, Canada
MRP6 shRNA sequences from MISSION® TRC shRNA	Sigma-Aldrich, USA
Others	
Protease inhibitor cocktail	Sigma-Aldrich, USA
4-20% Mini-PROTEAN TGX™ precast protein gels	Bio-Rad, USA
PVDF membranes	Millipore, USA
Pre-mixed WST-1 reagent	Takara Bro, USA
DH5α™ Competent Cells	Invitrogen, USA
p-Nitroblue tetrazolium choloride	Millipore, USA
Agarose agar	Sigma-Aldrich, USA
Ethidium bromide	Sigma-Aldrich, USA
Prestained dual color standards	Bio-Rad, USA
Ultra low range DNA ladder	Invitrogen, USA
1 Kb plus DNA ladder	Invitrogen, USA
4x Laemmli sample buffer	Bio-Rad, USA
BlueJuice™ gel loading buffer	Invitrogen, USA

Table 2-3 List of materials, facilities and applied software

Materials	Source

Cell cultures	
Housekeeping cell culture flasks, multiple-well plates, pipette, centrifuge tubes	FroggaBio, Canada
Ultra-low attachment 96-well plates	BD Falcon, USA
Transwell permeable supports with 8 μm pores	Corning, USA
75 mm polystyrene round-bottom test tubes	BD Falcon, USA
Cell scarper	Corning, USA
Facilities	
BD FACSCanto-II Digital Flow Cytometry Analyzer	BD Biosciences, USA
Synergy™ 4 Microplate Reader	Biotek, Wi, USA
Phase Contrast Microscope	Optika, Italy
Cellometer® Auto 2000 Cell Counter	Nexcelom Bioscience, USA
NanoDrop™ 2000 Spectrophotometer	Thermofisher, USA
Mastercycler	Eppendorf, Germany
ViiA™ 7 Real-time PCR System	Applied Bio-systems, USA
Wide Mini-Sub Cell GT electrophoresis	Bio-Rad, USA
Tetra Blotting Module	Bio-Rad, USA
FluorChcm™ 800 Imaging System	Applied Bio-systems, USA
Computer software	
FlowJo	FlowJo LLC, USA

ImageJ	LOCI, University of Wisconsin, USA
Oligo 7	Molecular Biology Insights, Inc., USA.
QuantStudio™ Real-Time PCR Software	Applied Bio-systems, USA
GraphPad Prism 6 statistical software	GraphPad Software, Inc, USA

2.1.3 Oligonucleotide Sequences

Table 2-4 List of primers for real-time polymerase chain reaction (qPCR)

Name		Sequence (5'-3')	Tm (°C)	Amplication Size
MRP1	sense	CTCTATCTCTCCCGACATGACC	55	94
	antisense	AGCAGACGATCCACAGCAAAA		
MRP2	sense	CCCTGCTGTTCGATATACCAATC	55	131
	antisense	TCGAGAGAATCCAGAATAGGGAC		
MRP3	sense	TGGGGTGAAGTTTCGTACTGG	56	77
	antisense	CACGTTTGACTGAGTTGGTGATA		
MRP4	sense	AGCTGAGAATGACGCACAGAA	55	125
	antisense	ATATGGGCTGGATTACTTTGGC		
MRP5	sense	AGTCCTGGGTATAGAAGTGTGAG	55	97
	antisense	ATTCCAACGGTCGAGTTCTCC		
MRP6	sense	AGATGGTGCTTGGATTCGCC	56	120
	antisense	GCCACACAGTAGGATGAATGAG		
MRP8	sense	GGTGACCGAATCCCACCATC	55	127

	antisense	CAGGGCAATTAGCAGCTTGG		
CCR1	sense	GACTATGACACGACCACAGAGT	60	117
	antisense	TACCAAGGAGTACAGAGGGGG		
CCR2	sense	AGTTCAGAAGGTATCTCTCGGTG	60	115
	antisense	GGCGTGTTTGTTGAAGTCACT		
CCR3	sense	GTCATCATGGCGGTGTTTTTC	60	155
	antisense	CAGTGGGAGTAGGCGATCAC		
CCR4	sense	AGAAGGCATCAAGGCATTTGG	60	137
	antisense	ACACATCAGTCATGGACCTGAG		
CCR5	sense	TTCTGGGCTCCCTACAACATT	60	93
	antisense	TTGGTCCAACCTGTTAGAGCTA		
CCR6	sense	TTCAGCGATGTTTTCGACTCC	60	134
	antisense	GCAATCGGTACAAATAGCCTGG		
CCR7	sense	TGAGGTCACGGACGATTACAT	60	134
	antisense	GTAGGCCCACGAAACAAATGAT		
CCR8	sense	GTGTGACAACAGTGACCGACT	60	173
	antisense	CTTCTTGCAGACCACAAGGAC		
CCR9	sense	ATGTCAGGCAGTTTGCGAG	60	105
	antisense	TGCAGTACCAGTAGACAAGGAT		
CCR10	sense	ATTACTCTGGGGATGAAGA	56	117
	antisense	CCACGGTCAGGGAGACACT		

CXCR1	sense	TGGGGACTGTCTATGAATCTGT	60	127
	antisense	GCAACACCATCCGCCATTTT		
CXCR2	sense	TGGATTTTTGGCACATTCC	55	249
	antisense	TGGGCTAACATTGGATGAGT		
CXCR3	sense	TTTGACCGCTACCTGAACATAGT	55	185
	antisense	GGGAAGTTGTATTGGCAGTGG		
CXCR4	sense	TACACCGAGGAAATGGGCTCA	55	63
	antisense	TTCTTCACGGAAACAGGGTTC		
CXCR5	sense	ACCTCCCGATTCCTCTACCAT	55	155
	antisense	AAGATGCTTGTCACCAGGATG		
CXCR6	sense	GACTATGGGTTCAGCAGTTTCA	55	169
	antisense	GGCTCTGCAACTTATGGTAGAAG		
CXCR7	sense	AGCACAGCCAGGAAGGCGAG	55	277
	antisense	TCATAGCCTGTGGTCTTGGC		
β-actin	sense	TCCTCTCCCAAGTCCACACAGG	60	131
	antisense	GGGCACGAAGGCTCATCATTC		

Table 2-5 List of shRNA sequences

MRP5 / ABCC5			
TRC number	Region	Clone ID	Sequence (5'-3')

TRCN0000060303 *(labeled as 303)*	CDS	NM_005688.1 -2691s1c1	CCGGCCCTTGGCATTCCTGGTTATTCTC GAGAATAACCAGGAATGCCAAGGGTT TTTG
TRCN0000060304 *(labeled as 304)*	CDS	NM_005688.1 -1461s1c1	CCGGGCTTTGAAAGTAACACCGTTTCT CGAGAAACGGTGTTACTTTCAAAGCTT TTTG
TRCN0000060305 *(labeled as 305)*	CDS	NM_005688.1 -4160s1c1	CCGGCCGCCACTGTAAGATTCTGATCT CGAGATCAGAATCTTACAGTGGCGGTT TTTG
TRCN0000060306 *(labeled as 306)*	CDS	NM_005688.1 -354s1c1	CCGGCCCAAGGGAAAGTACCATCATCT CGAGATGATGGTACTTTCCCTTGGGTT TTTG
TRCN0000060307 *(labeled as 307)*	CDS	NM_005688.1 -2288s1c1	CCGGCCACATCTTCAATAGTGCTATCT CGAGATAGCACTATTGAAGATGTGGTT TTTG
MRP6 / ABCC6			
TRC number	Region	Clone ID	Sequence
TRCN0000059713 *(labeled as 713)*	CDS	NM_001171.2 -3331s1c1	CCGGGCCTGTATGTGGTTAGCTCATCT CGAGATGAGCTAACCACATACAGGCTT TTTG

TRCN0000059714 *(labeled as 714)*	CDS	NM_001171.2 -3111s1c1	CCGGCGATCTCCCATCAGCTTCTTTCTC GAGAAAGAAGCTGATGGGAGATCGTT TTTG
TRCN0000059715 *(labeled as 715)*	CDS	NM_001171.2 -1692s1c1	CCGGGTGGCCGAGAATGCTATGAATCT CGAGATTCATAGCATTCTCGGCCACTT TTTG
TRCN0000059716 *(labeled as 716)*	CDS	NM_001171.2 -1961s1c1	CCGGCCACAGAATAAACCTCACGGTCT CGAGACCGTGAGGTTTATTCTGTGGTT TTTG
TRCN0000059717 *(labeled as 717)*	CDS	NM_001171.2 -3482s1c1	CCGGCGTAGATGAAAGCCAGAGGATC TCGAGATCCTCTGGCTTTCATCTACGTT TTTG

2.2 METHODS

2.2.1 Cell Culture

Cell lines were obtained and cultured in medium as described in Table 2-1 described. Cells were incubated in a humidified incubator at 37°C with 5% CO_2. Regarding cell expansion, cells were detached by Trypsin-EDTA at 80% confluency and then passaged at a ratio of 1:3 or 1:4.

2.2.2 Cell Proliferation and Doubling Times

Cells were seeded at a density of 2000 cells per well in 96-well plates with corresponding medium (Table 2-1) and incubated at 37ºC with 5% CO_2. The numbers of cells from these wells was

measured at days 0, 1, 3 and 6 days after plating, by adding a cell proliferation indicator: premixed WST-1 reagent and incubating at 37ºC for 3 hours. Absorbance of each well against a blank control was measured using a Synergy™ 4 microplate reader at 540 nm. The value of the blank (containing no cells) was subtracted from the value from samples. Growth curve for cell grown in culture were plotted in log graph. The cell doubling time was calculated in the exponential phase by using the equation:

$$\text{Doubling time} = duration \times \frac{log(2)}{log(final\ absorbency) - log\ (initial\ absorbency)}$$

where Duration= day 6 – day 3 (hours); Final absorbency: absorbency of day 6; Initial absorbency: absorbency of day 3.

2.2.3 Spheroid Formation

Cells were trypsinized and resuspended in DMEM/F12 medium, supplemented with 1 × B-27 serum-free supplement, 4 μg/mL heparin, 10 ng/mL EGF, and 10 ng/mL bFGF, 100 U/mL penicillin and 100 μg/mL streptomycin (J. Yang et al., 2018). Cells were subsequently seeded at a density of 200 cells per well in ultra-low attachment 96-well plates. After 0, 3 and 6 days of culture, spheroids were photographed under a microscope.

Regarding experiments performed in Part III, cells were seeded and treated with either 1000 nM Maraviroc, 20 ng/mL RANTES (CCR5 agonist), or a combination of Maraviroc/RANTES (1000 nM/ 20 ng/mL). Cells with medium alone served as the control. Spheroid/aggregation diameters were measured and analyzed by using ImageJ software.

2.2.4 Soft-Agar Colony Formation

Cells were seeded on dual layer soft agar. The bottom layer was composed of a 0.75 mL mixture of 1% Nobel agar and 2× corresponding completed medium (1:1), and the top layer a 0.75 mL mixture of 0.6% Nobel agar and 2× corresponding completed medium. The top layer contained approximately 5,000 cells (1:1). Plates were incubated for 21 days in a 37°C incubator. Each well was stained by 300 µL 10 mg/mL p-Nitroblue tetrazolium chloride and incubated at 37°C overnight. Photographs of wells containing stained colonies were analyzed using ImageJ software with the ColonyArea plugin. The colony intensity was calculated by using the formula (Guzman, Bagga, Kaur, Westermarck, & Abankwa, 2014):

$$\text{Colony intensity } \% = \frac{\sum pixel\ intensities\ in\ a\ region}{\sum maximum\ intensitites\ possible\ in\ the\ same\ region} \times 100$$

2.2.5 Wound Healing Assay

Cells (0.5×10^6/mL, 2 mL per well) were seeded in six-well plates and cultured with corresponding completed medium until confluence. Cells were washed with 1 x PBS. Then, monolayers were scratched with a 200 µL pipette tip to generate a wound according to the method described previously (J. Yang et al., 2018). Cell debris was removed by washing with 1x PBS. Control medium (medium supplement with 10% FBS or 5% heat inhibited FBS) or treatment solution were added to the wells. Cells were allowed to migrate to close the scratch. Phase contrast images were taken at initiation of the wound for each population and captured in certain time intervals until the wound was closed.

- *For experiments in Part I*, cells were cultured in medium and images were taken after 6, 12, 18, 24, 30, 36, 42, 48, 60, 72 and 84 hours until the wound closed.

- *For experiments in Part III*, cells were cultured in RPMI 1640 medium supplemented with 5% heat inactivated FBS (instead of 10% FBS) and exposed to either 1000 nM Maraviroc, 20 ng/mL RANTES (CCR5 agonist), or a combination of Maraviroc/RANTES (1000 nM/ 20 ng/mL). Images were captured at 0, 12 and 24 hours.

Images was acquired for each cell group in at least 10 different fields. Wound closure was analyzed quantitatively by using ImageJ software with MRI Wound Healing Tool (Cormier, Yeo, Fiorentino, & Paxson, 2015). By comparing images from each captured time point, the migration capacity of cells was measured as the extent of wound closure (gap) by calculating wound area. The half-closure time was calculated using the formula (Jonkman et al., 2014):

$$T_{1/2}\ \text{gap} = \frac{initial\ \text{gap area}}{2 \times slope}$$

Gap area was measured and plotted as a function of time (Rajakyla, Krishnan, & Tojkander, 2017).

2.2.6 Transwell Chamber Assay

Twenty-four well Transwell permeable supports with 8 μm pores were used to measure cell invasion. After trypsinization, cells were washed twice with 1 × PBS to remove remaining serum in the cell solution.

- *For experiments in Chapter 3:* The lower chambers were filled with 650 μL corresponding medium with or without 10% FBS. The upper chambers were added with 1×10^5 cells in 100 μL serum-free medium.

- *For experiments in Chapter 5:* The lower chambers were filled with 650 μL RPMI 1640 medium with no serum, 10% FBS, 5% heat inactivated FBS, 1000 nM Maraviroc, 20ng/mL Rantes, or Maraviroc-Rantes complex respectively. The upper chambers were added with 1×10^5 cells in 100 μL serum-free medium.

After 24 hours incubation, non-migrating cells in the upper chamber were removed with cotton swabs. The upper chambers were washed twice with 1x PBS and swabbed again until no apparent cell was observed. Migrated cells either on the opposite side of the insert or on the bottom of the well plate were dissociated and collected by a cell dissociation buffer with 650 μL volume. Collected cells were centrifuged and resuspended in 50 μL 1xPBS, and then counted by the Cellometer® Auto 2000 cell counter.

2.2.7 Flow Cytometry for SCSM staining

APC-conjugated anti-human CD13 monoclonal antibodies (mAbs), APC-eFluor 780--conjugated anti-human CD24 mAb, eFlour 450-conjuagted anti-human CD44 mAb, PE-Cy7 conjugated anti-CD90 mAb, PE-conjugated CD133 mAb, FITC-conjugated anti-human EpCAM mAb, and cell viability marker 7-AAD were used in the flow cytometry analysis. Briefly, cultured cells were trypsinized and resuspended with ice cold fluorescence-activated cell sorter (FACS) buffer

(phosphate-buffered saline (PBS) with 1.5% FBS, 25 mM HEPES pH7.0, and 2 mM EDTA) in a 50 mL tube. Cells went through a 40 μm cell mesh to allow cells individually suspended in the solution. A total of $0.5x10^6$ single suspended cells in 100 μL FACS buffer were added into a 75 mm polystyrene round-bottom test tube. Each sample of cells was stained with corresponding fluorescence-conjugated mAbs and incubated for 30 minutes in the dark. Optimized doses of CD13, CD24, CD44, CD90, CD133, EpCAM, and 7-AAD mAbs were 2.5 μL, 2.5 μL, 2.5 μL, 5 μL, 2.5 μL, 2μL, and 5μL respectively. Cells were rinsed twice with 2 mL FACS buffer and resuspended in a final volume of ice cold 300 μL FACS buffer for analysis. Corresponding fluorescence-conjugated isotype-matched mAbs or unstained samples served as controls to calibrate the analyzer for each experiment. The flow cytometry analysis was performed on BD FACSCanto-II Digital Flow Cytometry Analyzer at the University of Manitoba Flow Cytometry Core Facility and analyzed using FlowJo software. Cells thawed from the tank were cultured in corresponding medium supplemented with 10% FBS for up to 31 days.

2.2.8 RNA Extraction

Total RNA was extracted by a TRIzol Plus RNA Purification combination kit according to the protocol provided by the manufacturer. Briefly, cells were washed with ice cold 1× PBS, 300 μL TRIzol reagent was added to each well of a six-well plate where the cells were previously seeded and/or treated. The cell lysate was directly pipetted up and down, and then transferred into an Eppendorf tube. The homogenized sample was incubated for 5 minutes at room temperature and 60 μL chloroform was added. The mixture was shaken vigorously by hand for 15 seconds and incubated for 2 minutes at room temperature, and then centrifuged at 12,000 *g* for 15 minutes at

4ºC. The upper aqueous phase was transferred into a new tube and added same volume of 70% ethanol by pipetting up and down. The resulting mixture was applied to a spin tube and centrifuged for 30 seconds. The flow-through was discarded and the total RNA bound to the membrane was washed with Wash Buffer I and Wash Buffer II to eliminate contaminants. An additional centrifuge step for 2 minutes was performed to dry the membrane with bound RNA. The RNA was eluted with 50 µL of RNase-free water in a new collection tube. The yield and quality of isolated mRNA were determined by a NanoDrop™ 2000 spectrophotometer and assessed using a ratio of absorbance at 260 nm and 280 nm. Samples presenting A260/A280 ratio values around 2.0 were used for subsequent procedures. The sample mRNA was diluted to RNase-free water as 100 ng/µL and served as a stock solution. The diluted mRNA was stored at -80ºC.

2.2.9 Reverse Transcription (RT) of RNA to Obtain cDNA

In order to synthesize cDNA from the total RNA extracted, the first strand cDNA was synthesized by an iScript™ cDNA synthesis kit according to the manufacturer's instruction. Half microgram of stock total RNA solution (100 ng/µL) was used for each RT reaction. A mastermix of 4 μL 5× iScript™ reaction mix, 1 μL iScript™ reverse transcriptase and 10 μL RNase-free water were pre-mixed (in total of 15 µL). A resulting solution of 15 µL mastermix and 5 µL total RNA solution were incubated for RT reaction with 5 minutes at 25°C, 20 minutes at 46°C, and 1 minute at 95°C. Finally, the cDNA obtained was diluted with 200 µL of RNase-free water to a concentration of 100 ng/µL.

2.2.10 Quantitative qPCR

The reaction was performed using a Power SYBR® Green PCR Master Mix. Total reaction volume was 20 μL with 10 μL of 2× of Power SYBR® Green PCR Master Mix, 1μL of 10 μM forward and reverse primers (in total of 2 μL), 3 µL RNase-free water and 5 μL of cDNA solution. Specific primers are listed in Table 2-4 and were designed with the respective sequences from GenBank by Oligo 7 software. PCR amplification was initially held at 95ºC for 10 minutes, then carried out by applying 35 cycles comprised of denaturation at 95ºC for 15 seconds, annealing temperature at corresponding temperature for 1 minute (Table 2-4), followed by a final melting curve stage using a ViiA™ 7 Real-time PCR System. Data were analyzed by QuantStudio™ Real-Time PCR Software. The gene cycle threshold (CT) value of the target was normalized to β-actin. Gene expressions were calculated by using relative quantification method ($2^{-\Delta CT}$). Fold changes of interested gene expression were evaluated by the ($2^{-\Delta\Delta CT}$) method. The product was further tested by electrophoresis with 2.0% agarose gels (Livak & Schmittgen, 2001).

2.2.11 Agarose Gel Electrophoresis

The electrophoresis was used for the confirmation of PCR and plasmid extraction. The gel for electrophoresis consisted of 1.0% or 2.0 % agarose and Tris-acetate EDTA buffer. 0.05% of ethidium bromide was added to the gel solution and when solidified, the gel was placed in the electrophoresis apparatus which was immersed in 1x Tris-acetate EDTA buffer. The samples were mixed with 10× gel loading buffer, and then loaded on the gel with a Wide Mini-Sub Cell GT electrophoresis system. Ultra low range DNA ladder or 1Kb plus DNA ladder was employed as the ladder. The electric current used to perform the electrophoresis was 100 V for 40 minutes.

After the running time the separated bands on the gel were visualized under ultraviolet light by FluorChcm™ 800 imaging system.

2.2.12 Protein Extraction

Protein was extracted by employing a protein extraction buffer (1× buffer= 50 mM Tris, pH 8.0, 0.5 mM EDTA, 150 mM NaCl, 0.5% NP-40) containing 1× protease inhibitor cocktail (1:100, protease inhibitor: lysis buffer). Cells in six-well plates were washed with ice cold 1x PBS. Two hundred microliter of protein extraction buffer were added and cells were scrapped to an Eppendorf tube on ice. Each sample of cells was maintained at constant agitation for 30 minutes at 4°C. Samples were then centrifuged at 12,000 *g* for 15 minutes at 4°C. Supernatants of each sample were carefully collected, and protein concentrations determined by the BCA protein assay. In brief, triplicates for each sample were prepared by mixing 10 µL of cell lysate with 200 µL of BCA kit reagent mixture (50:1, Reagent A: B) and incubating for 30 minutes at 37°C. The lysis buffer served as the blank and bovine serum albumin (BSA) was used to generate a standard curve. The absorbance was measured at 562 nm using a spectrophotometer. The protein concentration was calculated based on the standard curved plotted.

2.2.13 Western Blot Analysis

Protein samples (20 µg each) were mixed with 4× Laemmli sample buffer. Samples were then incubated at 95°C for 10 minutes. Meanwhile, a 4-20% Mini-PROTEAN TGX™ precast protein gel was immersed in 1× sodium dodecyl sulfate (SDS) running buffer in the Bio-Rad Tetra Cell Module system. A dual color standard protein ladder and the pre-heated samples were loaded

into the wells of the gel and was run by electrophoresis at 160V constant voltage for 30 minutes. The gel containing separated proteins were electrically transferred to a PVDF membrane (8 cm × 7 cm) with 1× transferring buffer at 100V for 60 minutes. Next, the membrane was blocked by incubation with 5% BSA in 1× (tris-buffered saline) TBS-Tween (TBST) for one hour at room temperature, and incubated with primary antibodies against MRP5 at 1:2500, MRP6 at 1:2500 or β-actin at 1:10,000 overnight at 4°C respectively in 5% BSA in 1×TBST. Subsequently, the membrane was washed three times with TBST, 5 minutes each, with 1× TBST, and incubated with HRP-conjugated secondary antibodies, goat anti-rabbit IgG (1:5000) or goat anti-mouse IgG (1:50,000) for one hour at room temperature in 5% BSA in 1× TBST. The membrane was then washed 5 times with TBST, 5 minutes each with 1× TBST. All bands were visualized by an enhanced chemiluminescent kit: SuperSignal™ Wester Dura Extended Duration Substrate. In brief, a 500 µL mixture of chemiluminescent reagents (1:1) were added to the membrane and incubated for 5 minutes at room temperature. The signal was captured by FluorChcm™ 800 imaging system with an exposure duration of 20 minutes. The quantification of signal was analyzed with ImageJ software.

2.2.14 Drug Effects on Proliferation and Cytotoxicity

- *For experiments in Chapter 4:* Cells were seeded at a density of 2000 cells per well in 96-well plates. Different concentrations of gemcitabine (0, 0.1 nM, 1 nM, 10 nM, 100 nM, 1 µM, 10 µM and100 µM) were added to cells after 24 hours of cell seeding and incubated for 3 days after plating. At the end of treatment, cells were incubated with fresh medium. A premixed WST-l reagent was added and incubated at 37°C for 3 hours. Cells treated with gemcitabine

and shRNAs were exposed to either the same dilution of lentivirus plus different concentrations of gemcitabine or the same concentration of gemcitabine plus different dilutions of lentivirus for 3 days. At the end of treatment, WST-1 reagent was added and incubated at 37ºC for 3 hours.

- *For experiments in Chapter 5:* HuCCT-1 and KMBC cells were seeded onto 96-well plates at a density of 2000 cells per well in 100 μL of RPMI completed medium and incubated for 24 hours. The following day, cell culture media was replaced with 5% heat inactivated FBS. During concentration-dependent experiments, cells were exposed to a range of Maravirocs (0.1 to 1000 nM) and RANTES (1 to 50 ng/mL) concentrations for 3 days. Based on the initial results, time-dependent proliferative activity was tested from days 1 to 6 at a constant Maraviroc concentration of 1000 nM, RANTES 20 ng/mL or a combination of Maraviroc/RANTES (1000 nM/20 ng/mL). The blank cell medium served as negative control while untreated cells were used as positive controls. At the end of treatments, the cell proliferation of tested samples was measured by adding a premixed WST-1 reagent and incubating at 37ºC for 3 hours.

Absorbance of each well against a blank control was measured using a microplate reader (Synergy™ 4, Biotek Wi, USA) at 540 nm. The value of the blank (containing no cells) was subtracted from the value of the samples. Data were expressed as the fold of the values of treated cells compared to the value of non-treated cells (control). The formula is:

$$\%\ \text{proliferation (survial)} = 100 \times \frac{(Experimental\ absorbency - Blank\ absorbency)}{(Control\ absorbency - Blank\ absorbency)}$$

2.2.15 Preparation of Lentivirus Packaged of shRNA Library

Five predesigned shRNA sequences for MRP5 were selected from the shRNA bacteria library of the Lentiviral Core Platform at the University of Manitoba. Five predesigned MRP6 shRNA sequences from MISSION® TRC shRNA purified plasmid DNA were purchased from the Sigma-Aldrich. A nonsilencing pLKO.1-puro control was employed as a negative control. These predesigned MRP shRNAs are shown in Table 2-5, where the target sequence is indicated by underlined lower case letters.

2.2.15.1 Transformation and Amplification of Plasmid DNA (MRP6)

Purchased human MRP6 shRNA plasmid were transformed prior to replication. Two microliters of different MRP6 plasmid DNA was mixed gently into 50 µL competent cells in a 15 mL centrifuge tube and incubated on ice for 30 minutes. After using the heat-shock method for each transformation, 250 µL LB medium was added to the bacteria and grown in a 37ºC shaking incubator for 40 minutes. Expanded bacteria were plated onto a 10 cm LB agar plate containing 100 µg/mL ampicillin and incubate at 37 ºC overnight. Only cells containing the plasmid formed colonies on plates. At least 3 colonies were selected and expanded for the further purification. Regarding MRP5 shRNA library, the glycerol bacteria stock was recovered by streaking the bacteria stock onto previously prepared LB agar plates, and incubated at 37ºC overnight without shaking. Formed colonies were selected and expanded for further purification.

2.2.15.2 MRP shRNA Plasmids Isolation

Following proper growth of bacteria, a single colony of each sample from selective LB agar plates was picked and cultured in LB medium supplemented with 100 μg/mL ampicillin on a 37ºC shaker via a two-step cell expansion, reaching a final volume of 100 mL bacterial cells. Plasmid DNA was purified using a QIAGEN plasmid midi kit according to the manufacture is protocol. The harvested plasmid DNA were resuspended in 300 μL Tris-EDTA (TE) buffer (pH 8.0) and tested by electrophoresis with 1.0% agarose gel. Each sample of plasmid DNA was stored at -80ºC.

The yield and quality of purified DNA were determined by a NanoDrop™ 2000 spectrophotometer. Plasmid samples with DNA concentration greater than 500 ng/μL were sent to Lentiviral Core Platform at the University of Manitoba to perform lentivirus packaging.

2.2.16 Lentivirus Transduction

Transductions of HuCCT1 or KMBC cells with lentiviral vectors were carried out in 24-well plates with serial dilutions of lentiviral vector preparations following the puromycin selection method (M. J. Li & Rossi, 2007). Prior to transduction, optimization of the puromycin test was performed on HuCCT1 and KMBC cells. Fifty thousand cells of each cell line were plated in a 24-well plate. A range of 0.5 μg/mL to 10 μg/mL puromycin was added to cells for 7 days. It was determined that 2 μg/mL was the optimized concentration for both cell lines.

2.2.16.1 Lentivirus Titer Determination

By processing the lentivirus titer transduction, 50,000 cells were seeded on 24-well plates and cultured overnight. The next day, culture medium was removed and a total of 200 μL of serial dilution of viral stock in RPMI 1640 medium containing 8 μg/mL hexadimethrine bromide was added to each well to reach ratios of 1:10, 1:50, 1:100, 1:500, and 1:1000. The plates were gently rocked back and forth to ensure even distribution. After 20 hours incubation, wells were refreshed with 500 μL medium and cultured for 24 hours. Fresh 500 μL medium containing 2 μg/mL puromycin was then added, and medium replaced with fresh puromycin containing medium every 3 days until all control cells were killed and resistant colonies in transduced wells were identified. After removal of culture medium from each well, each well was gently washed by 1×PBS. The number of colonies generated in each well was counted under a microscope. Viral titer was determined by colony number per well, multiplying by 5 and the dilution fold to determine the number of infectious units per milliliter (TU/mL). The average lentiviral titer of MRP5 and/or MRP6 on cells was approximately 2×10^5 transducing units/mL (TU/mL).

2.2.16.2. Transduction with lentivirus

Concurrent with lentivirus titer determinations, HuCCT1 and KMBC cells were transduced with packaged MRP5 or MRP6 shRNA pools. Briefly, 1.5×10^5 of HuCCT1 and KMBC cells were plated per well of 24-well plates and cultured overnight. The next day, cells reached approximately 70% confluence. RPMI 1640 medium containing 8 μg/mL hexadimethrine bromide and lentiviral supernatant was added to each well to achieve a multiplicity of infection (MOI) of 0.08 (1:10) for MRP5 and MRP6 shRNA library screening. After 20 hours incubation,

wells were refreshed with 500 μL medium and cultured for 24 hours. Fresh 500 μL medium containing 2 μg/mL puromycin was then added, and medium replaced with fresh puromycin containing medium every 3 days until all control cells were killed and resistant colonies in transduced wells were identified. At least 6 puromycin-resistant colonies were selected and expanded.

2.2.17 Verification of Transduced shRNA Cells

After puromycin-resistant colonies expanded, shRNA-transduced cells were preceded by qRT-PCR and western blot analyses to assay for knockdown of target genes and proteins respectively as descried above. Only samples with the most reduced mRNA were followed by protein analysis. After screening for potential shRNA (Table 2-5), the MRP5 shRNA target sequence of 5'-CCGGCCACATCTTCAATAGTGCTATCTCGAGATAGCACTATTGAAGATGTGGTTTTTG -3' was selected to inhibit MRP5 and the MRP6 shRNA target sequence of 5'-CCGGCGATCTCCCATCAGCTTCTTTCTCGAGAAAGAAGCTGATGGGAGATCGTTTTTG - 3' was used to inhibit MRP6.

2.2.18 Statistical Analysis

All assays were performed in triplicate and experiments were repeated on a minimum of three occasions. Significant differences were determined by repeated measures of ANOVA and/or Tukey's multiple comparison post-hoc test. A Student's t-test was used for comparisons between groups. Significant correlations were demonstrated by Pearson correlation coefficients test. Data

were analyzed by GraphPad Prism 6 statistical software. Differences with p values less than 0.05 were considered statistically significant.

3. RESULTS

3.1 PART I: DIFFERENCE IN TUMOR BIOLOGY AND CSCS

3.1.1 Cell Morphologies

The six CCA cell lines (CCLP-1, HuCCT1, SG231, HuH28, KMBC and TFK-1) and one non-malignant cholangiocyte H69 cell line displayed different cell morphologies while growing in adherence cultures (Table 3-1, Figure 3.1). When cells were growing under 80% confluence, HuCCT1, HuH28, TFK-1and H69 grew in monolayers consisting of stretched cells, displaying an irregular pattern. CCLP-1, SG231 and KMBC also grew in monolayers, but were less adherent, forming a layer of individual cells. When cells reached 100% confluence in culture, cell lines started to grow as either a monolayer or stacked (Figure 3.5 and 3.6). As shown in the wound healing experiments, HuCCT1, HuH28, TFK-1, and H69 cells grew as non-overlapping monolayers, which spread out and pressed neighboring cells. The other cell lines CCLP-1, SG231, and KMBC grew in a stacked pattern and formed clumps of overlapped cells. Overall, there were no clear distinctions between the cell morphologies of I-CCA and E-CCA cell lines during growth.

Table 3-1 Cell morphologies of I-CCA, E-CCA and non-malignant cholangiocytes cell lines

Cell types	Cell lines	Morphologies
I-CCA	CCLP-1	Stacked
	HuCCT1	Monolayer
	SG231	Stacked

E-CCA	HuH28	Monolayer
	KMBC	Stacked
	TFK-1	Monolayer
Non-malignant	H69	Monolayer

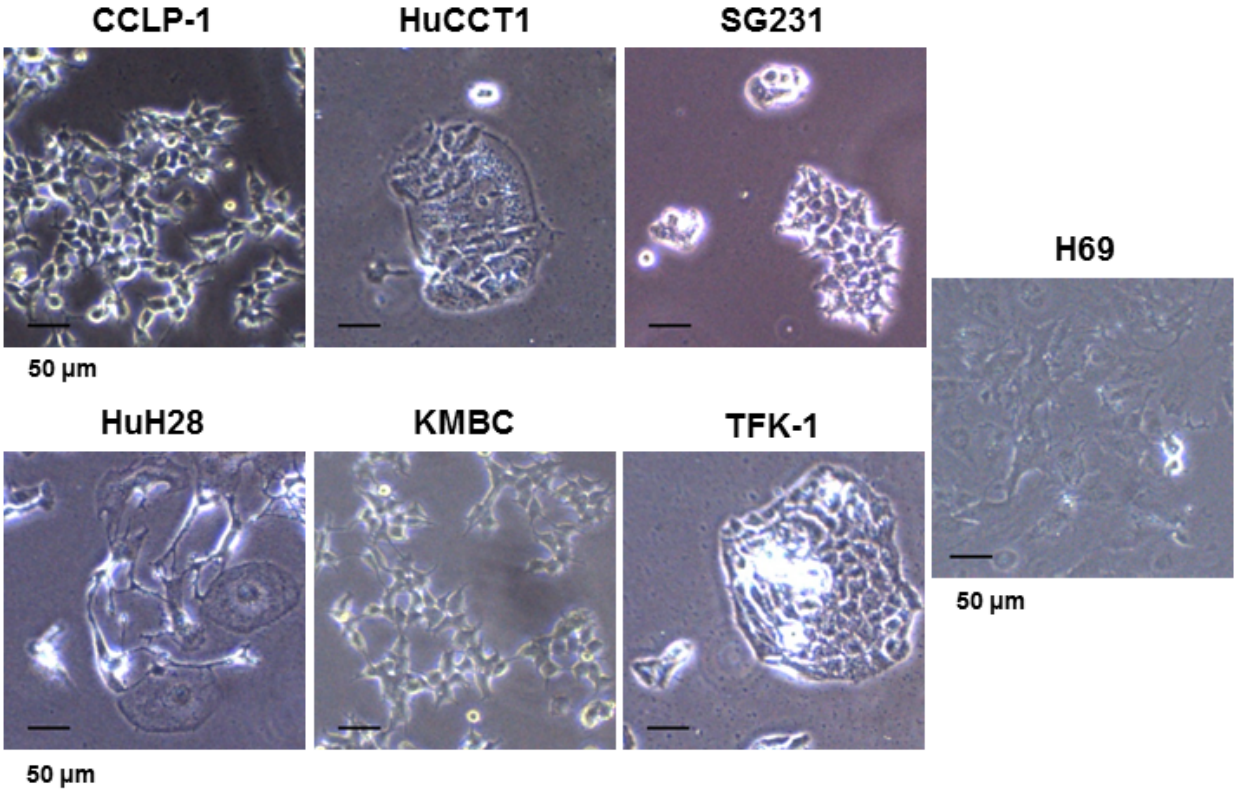

Figure 3.1 Phase contrast images of I-CCA, E-CCA and non-malignant cholangiocytes.

The morphologied I-CCA (CCLP-1, HuCCT1, SG231), E-CCA (HuH28, KMBC, TFK-1), and non-malignant cholangiocytes (H69) in adherent culture were captured by phase contrast microscopy. Cells were plated and grown as a monolayer in a 37°C incubator with a humidified

atmosphere of 5% CO2 in air. Images were obtained using 10× objectives 3 days after plating. Scale bar: 50 μm.

3.1.2 Proliferation and Doubling Times

Cell proliferation of the three I-CCA cell lines, three E-CCA cell lines and one non-malignant cholangiocyte cell line were examined by the WST-1 assay as shown in Figure 3.2. The three I-CCA cell lines showed similar proliferation rates, wherein a sharp increase in proliferation was detected at day 3. E-CCA cells exhibited more varied proliferative activities. On day 6, the proliferative activity of the three I-CCA cell lines was significantly increased compared to E-CCA cells ($p=0.0004$). The I-CCA cell lines also had shorter doubling times compared to E-CCA cell lines (39.9 ± 2.6 versus 54.6 ± 9.1 hours $p=0.009$). The doubling time in non-malignant H69 cholangiocytes (47.3 ± 8.9 hours) was between I-CCA and E-CCA cells.

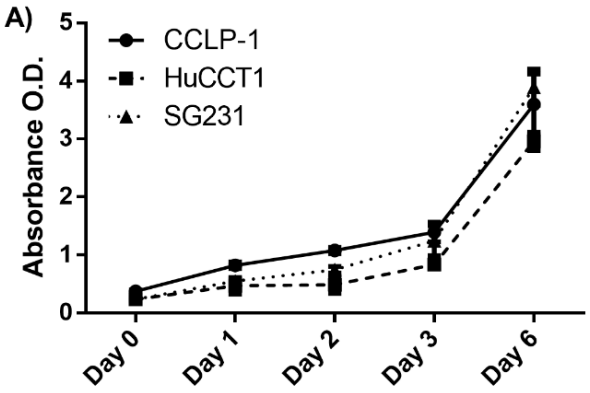

I-CCA cell lines	Doubling time (hrs)
CCLP-1	44.4±2.7
HuCCT1	39.7±3.6
SG231	35.4±1.9

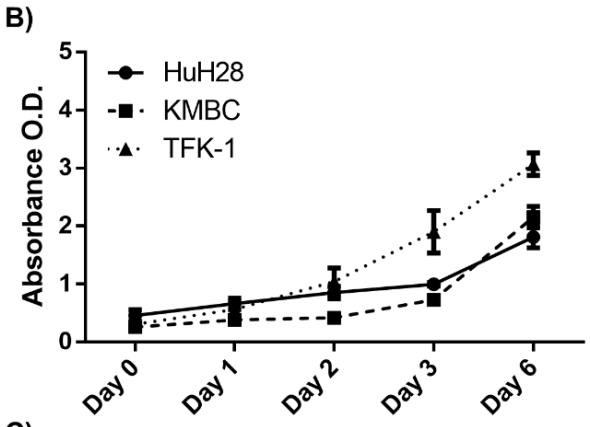

E-CCA cell lines	Doubling time (hrs)
HuH28	72.6±6.4
KMBC	48.2±3.5
TFK-1	43.1±1.3

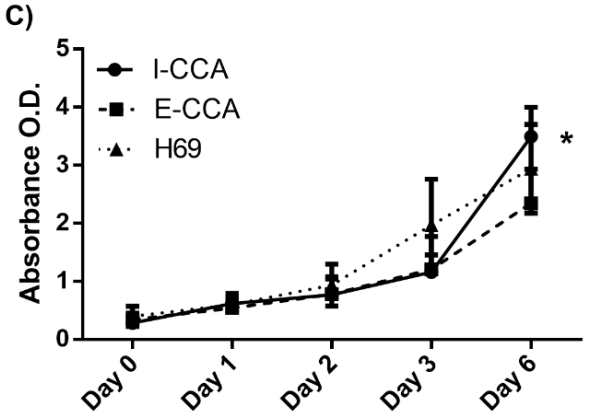

Cell lines	Doubling time (hrs)
I-CCA	39.9±2.6 *
E-CCA	54.6±9.1
Non-malignant	47.3±8.9

Figure 3.2 Proliferative activity of I-CCA, E-CCA and non-malignant cholangiocytes

Five thousand cells of each cell line were cultured for 1, 2, 3, and 6 days. Cell proliferation of I-CCA (upper panel), E-CCA (middle panel) and comparisons of cell populations including non-malignant H69 cells (lower panel) were measured by the WST-1 assay. Significant differences in cell proliferation were observed on day 6 between I-CCA and E-CCA cells (multiple t tests, Day

*6: p=0.004). Cell doubling times of each cell line were analyzed using data derived from the WST-1 assay. I-CCA cells exhibited more rapid doubling times compared to E-CCA cells (p=0.009). Data presented as the mean ± SD. *: p<0.01.*

3.1.3 Spheroid Formation

Spheroid formation for I-CCA, E-CCA and non-malignant H69 cholangiocytes were determined on days 0, 1, 2, 3 and 6. On day 6, all cell lines had generated spheroids or aggregate masses with different morphologies between cell lines (Figure 3.3).

One I-CCA (CCLP-1), two E-CCA (KMBC and TFK-1), and the non-malignant H69 cell lines formed the largest aggregates. Spheroid formation of these cells began with aggregating neighbouring cells and the formation of cell masses, whereas the I-CCA cell lines (HuCCT1 and SG321) and one E-CCA cell line (HuH28) developed small spheroids by self-replication or self-renewal rather than cell aggregation.

When spheroid sizes were quantified for each cell line, there were no differences on day 6 between I-CCA and E-CCA cells (137±32.1 μm and 144±31.0 μm respectively, p=0.40). However, significantly larger spheroids were observed with non-malignant H69 cholangiocytes (177±15.8 μm) compared to either I-CCA or E-CCA cells (p<0. 001 and 0. 01, respectively).

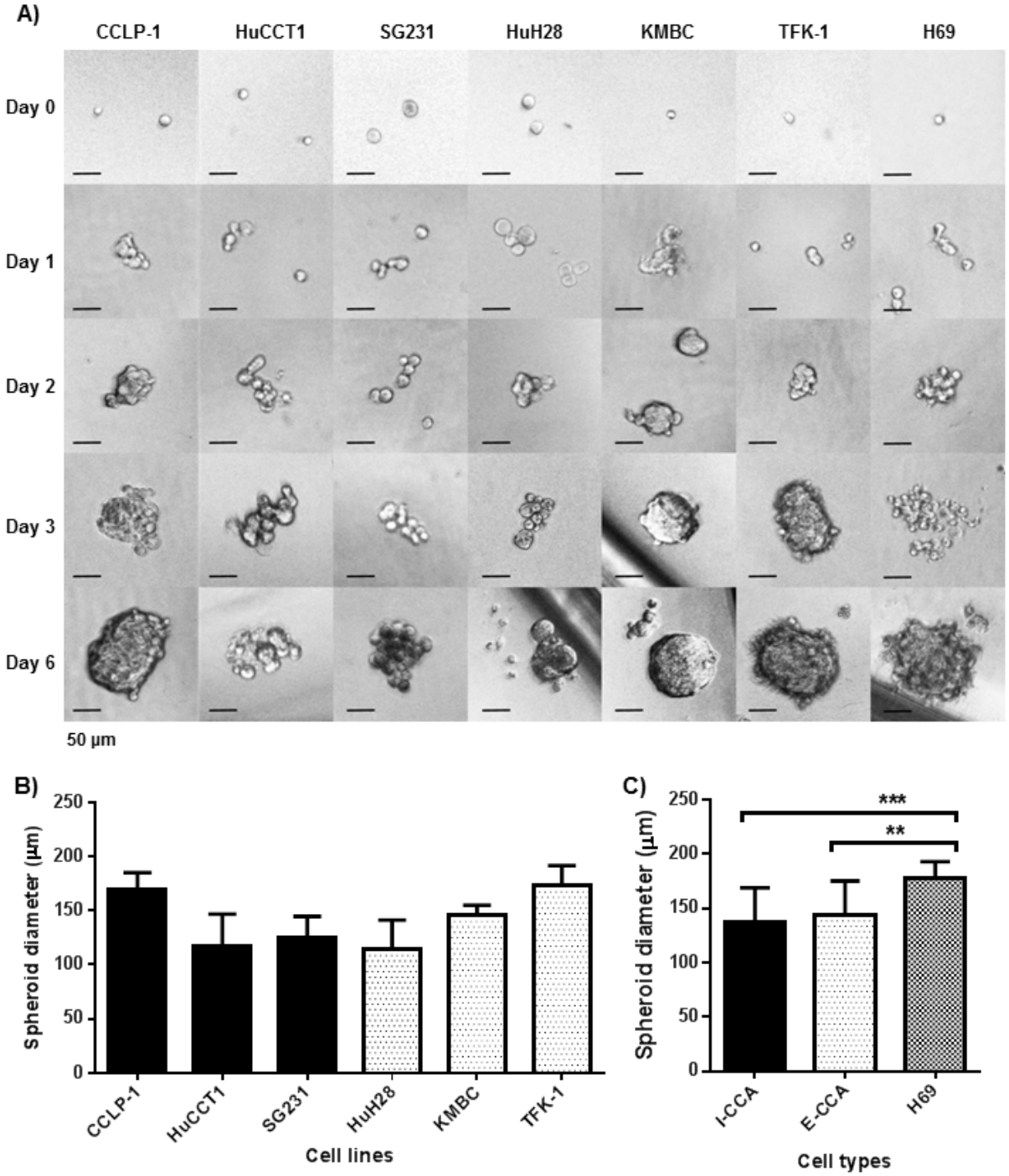

Figure 3.3 Spheroids formed by I-CCA, E-CCA and non-malignant cholangiocytes.

*Cells were seeded at densities of 200 cells/well at ultra-low 96-well plates to generate spheroids. Scale bar: 50 μm. Spheroid/aggregation diameters analyzed for I-CCA, E-CCA, and non-malignant H69 cells are provided in panels B and C respectively. Although there were differences in the mechanisms of spheroid formation (see text), no differences in spheroid size detected between I-CCA and E-CCA cells, but significant differences in H69 compared to both CCA cell subpopulations. Data presented as the mean ± SD. **: p<0.01; ***: p<0.001.*

3.1.4 Colony Formation on Soft-Agar

Colony-forming capacities of I-CCA, E-CCA and non-malignant H69 cholangiocytes in anchor-free medium were documented by the soft-agar colony formation assay. As shown in representative photographs in Figure 3.4A, both I-CCA and E-CCA cells were able to form colonies in soft agar to similar extents (colony intensity: 51.3±7.4% versus 45.9±20.1%, respectively, p=0.46). The colony intensity of H69, non-malignant cholangiocytes (63.0±5.0%), was not significantly different from I-CCA or E-CCA cells (p=0.05 and 0.19 respectively) (Figures 3.4B and C).

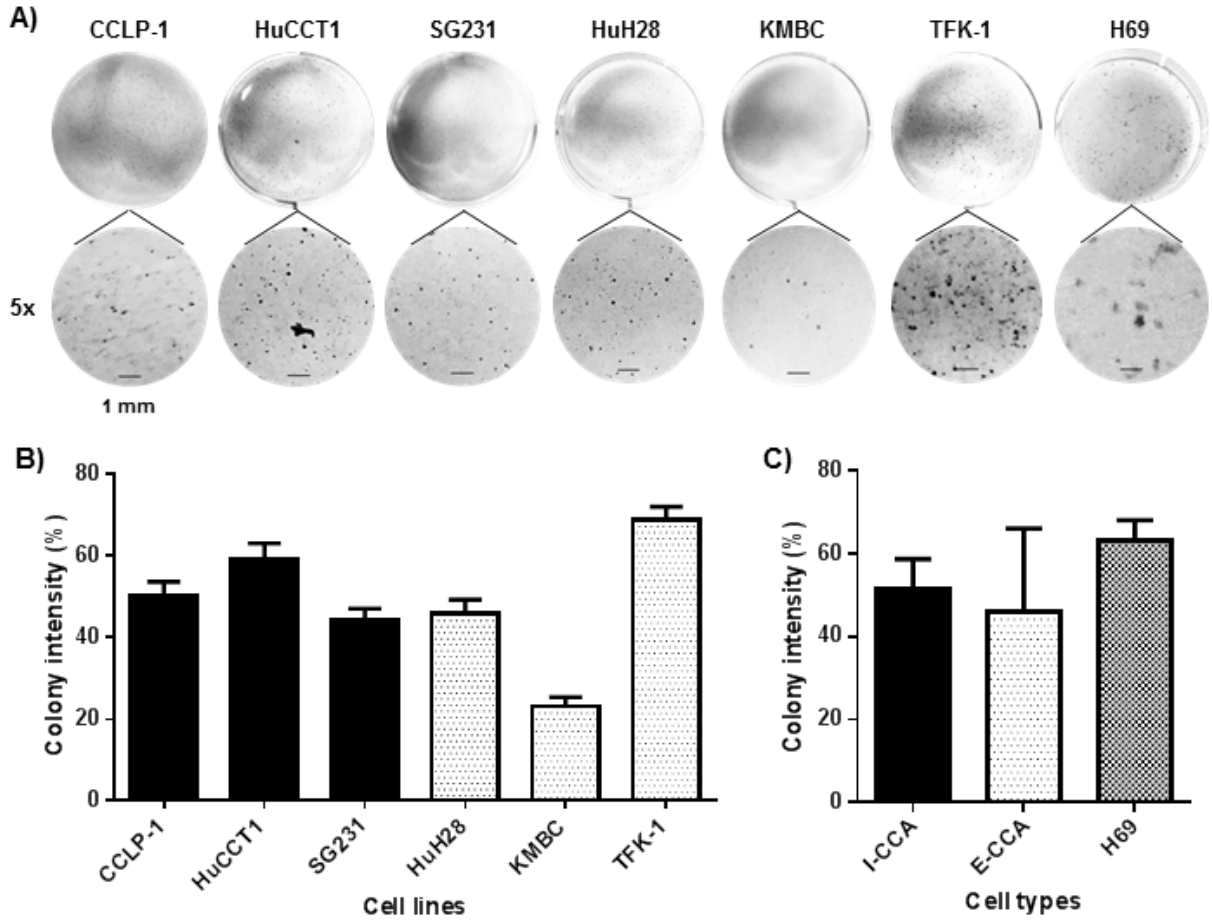

Figure 3.4 Soft-agar colony formation of I-CCA, E-CCA and non-malignant cholangiocytes. Panel A: representative photographs of colonies formed on soft agar plates from 5000 cells after 21 days of incubation. A five-times optical zoom of corresponding soft agar plates are shown in scale bar of 1 mm. Panels B and C demonstrate the quantification of colony intensity in percentage by ImageJ analysis. There were no significant differences in colony formation between I-CCA and E-CCA cells (p=0.46). Data presented as the mean ± SD.

3.1.5 Cell migration by Wound Healing

The two-dimensional migration abilities of I-CCA, E-CCA and non-malignant H69 cholangiocytes were demonstrated by the wound healing assay. Figures 3.5 and 3.6 provide the complete migration activity of each cell line. Representative photographs of scratch closure were captured at several time points until wound closure. Quantification of wound healing revealed the extent of migration varied among cell lines, and completion of wound healing ranged from 18 to 84 hours. Amongst I-CCA cell lines, SG231 cells exhibited more delayed wound closure compared to CCLP-1 and HuCCT1 cells, whereas for E-CCA cells, TFK-1 wound closure was delayed relative to HuH28 and KMBC cells. Figures 3.7 suggest that overall, I-CCA tend to migrate more rapidly than E-CCA cells. However, mean times to one half wound closure (17.0±10.3 hours for I-CCA versus 24.4±11.8 hours for E-CCA cell lines) were similar ($p=0.179$), as were times to complete closure (38±29.6 versus 50 ±30.8 hours respectively, $p=0.652$). Wound closure for non-malignant H69 cholangiocytes was similar to I-CCA and E-CCA cell lines (42.0±0 hours).

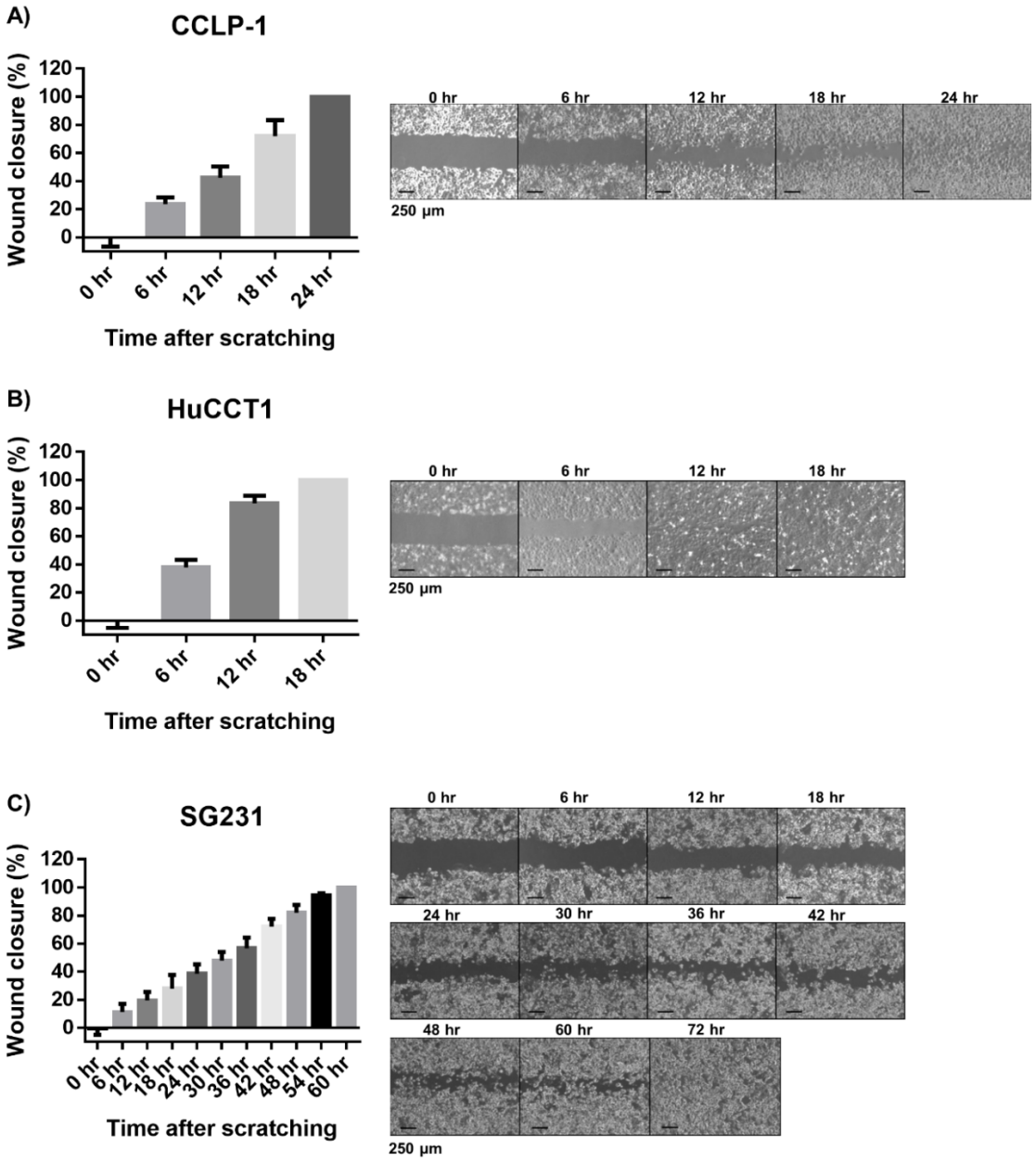

Figure 3.5 Wound healing activity of I-CCA cell lines.

Left panels: ImageJ analysis of cell migration and area closures from phase-contrast images. $T_{1/2gap}$ *of A) CCLP-1, B) HuCCT1, and C) SG231: 13.2±1.95, 7.68±1.35, and 30.1±3.48 hours, respectively. Lower panels: phase contrasts of cell migration were photographed after scratching until closure. Scale bar: 250 µm. Data presented as the mean ± SD.*

October 18th, 2019

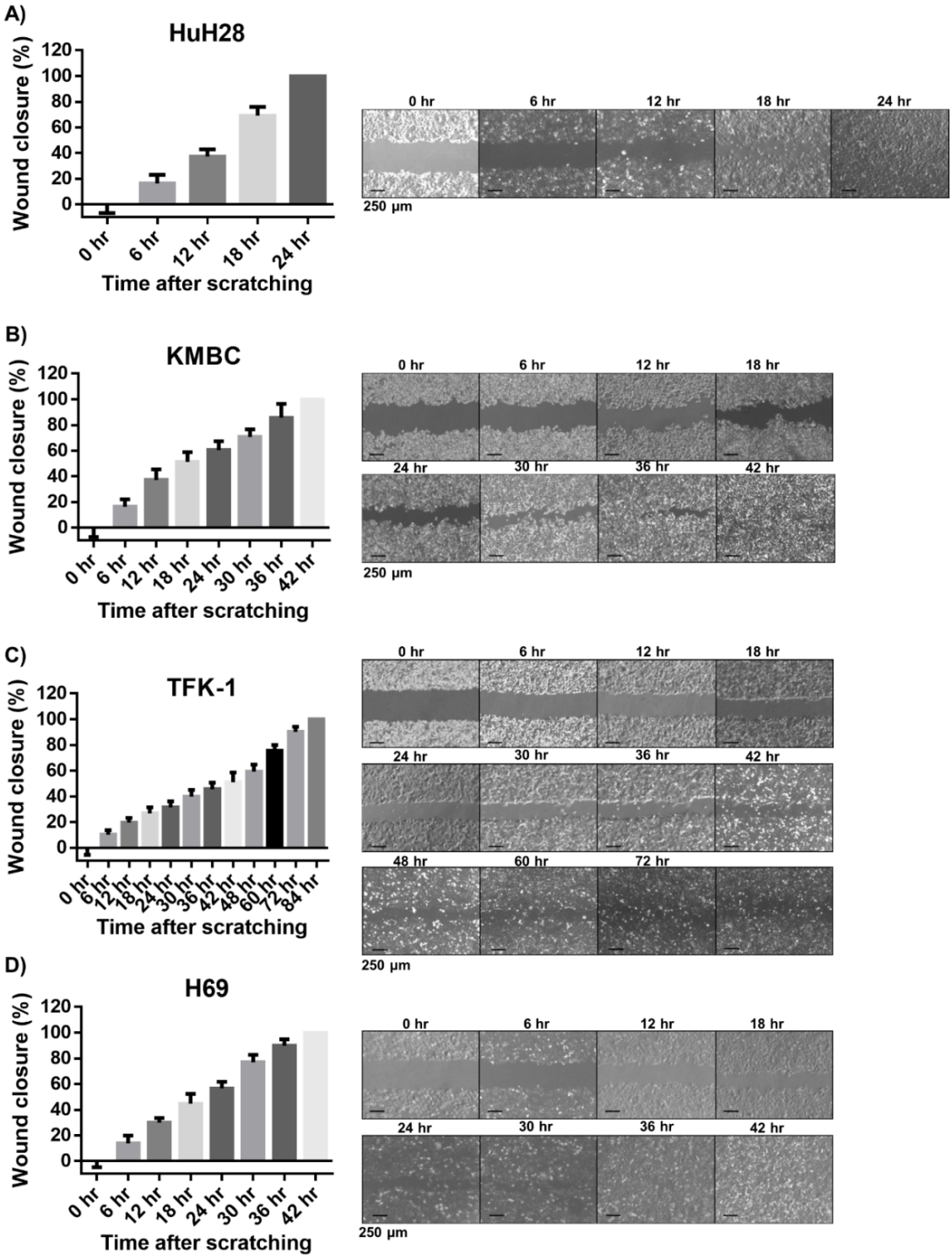

Figure 3.6 Wound healing activity of E-CCA and non-malignant cells.

Left panels: ImageJ analysis of cell migration and area closures from phase-contrast images. $T_{1/2gap}$ of A) HuH28, B) KMBC, C) TKF-1, and D) H69: 14.9±1.83, 18.5±2.56, 39.7±3.25 and 20.8±2.47 hours, respectively. Lower panels: phase contrasts of cell migration were photographed after scratching until closure. Scale bar: 250 µm. Data presented as the mean ± SD.

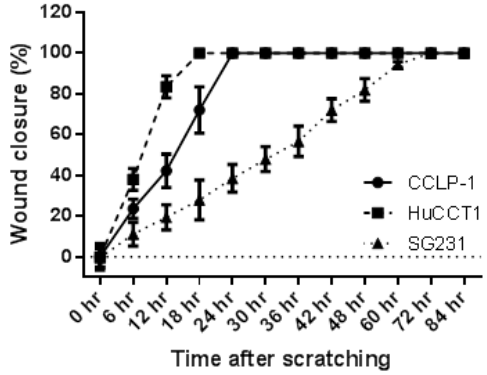

I-CCA cell lines	T ½ gap (hours)
CCLP-1	13.2 ± 1.95
HuCCT1	7.68 ± 1.35
SG231	30.1 ± 3.48

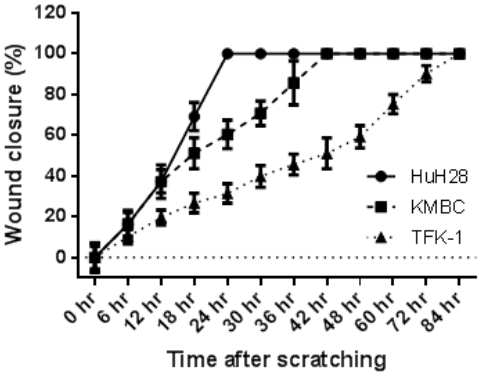

E-CCA cell lines	T ½ gap (hours)
HuH28	14.9 ± 1.83
KMBC	18.5 ± 2.56
TFK-1	39.7 ± 3.25

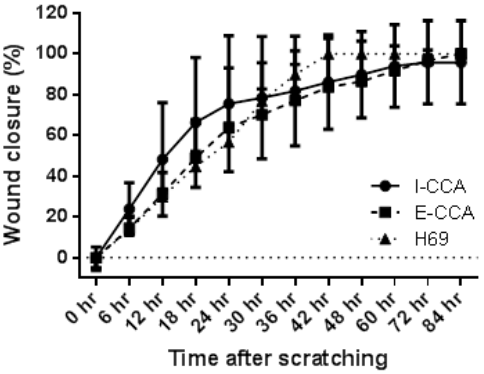

Cell lines	T ½ gap (hours)
I-CCA	17.0 ± 10.3
E-CCA	24.4 ± 11.8
H69	20.8 ± 2.47

Cell lines	Wound complete (hours)
I-CCA	38 ± 29.6
E-CCA	50 ± 30.8
H69	42 ± 0

Figure 3.7 Summary of wound healing capacities of I-CCA, E-CCA, and non-malignant cholangiocytes.

A significant difference in the extent of migration was observed at 6 hours in I-CCA cells versus E-CCA cells (p=0.0018) but not at subsequent time points. Data presented as mean ± SD.

October 18th, 2019

3.1.6 Cell invasion with Transwell Chambers

To demonstrate cell invasion properties, the Transwell invasion assay for I-CCA, E-CCA and non-malignant H69 cholangiocytes was performed. Figure 3.8A illustrates that two I-CCA cell lines (HuCCT1 and SG231) have the highest capacity to invade followed by one E-CCA cell line (KMBC), Figure 3.8 B suggests that overall, I-CCA cells had a significant increased ability to invade compared to E-CCA cells (cell number: 4466±1531 versus 2692±1030, $p<0.05$). Significant differences were also observed in I-CCA versus H69 (cell number: 562±78.9) and E-CCA versus H69 ($p<0.001$ and 0.05, respectively). All CCA cell lines demonstrated greater invasion properties than H69 cells.

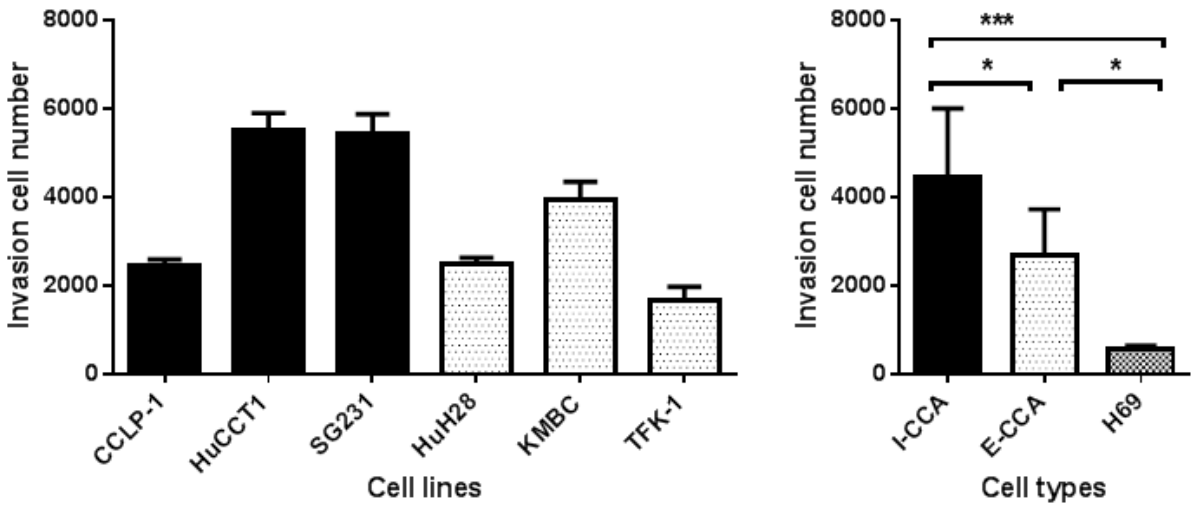

Figure 3.8 Transwell invasion ability of I-CCA, E-CCA and non-malignant cholangiocytes

*Cells that had invaded to lower chambers after 24 hours of incubation were counted for each cell line. The results are shown in panel A and collectively, panel B. Data presented as mean ± SD. *: p<0.05; ***: p<0.001.*

3.1.7 CSC Prevalence and SCSM Expression

CSC prevalences and CD13, CD24, CD44, CD90, CD133 and EpCAM SCSM profiles were documented by flow cytometry in all six CCA cell lines and non-malignant H69 cholangiocyte (Figures 3.9 and 3.10).

Among the six CCA cell lines, the I-CCA HuCCT1 cell line appeared to have the highest expression of all six SCSMs, while the E-CCA KMBC cell line expressed only CD90. Although high expression of certain CSC markers was observed in all CCA lines, there was no consistent distribution of SCSM in either I-CCA or E-CCA. CD90 was the one SCSM expressed in all cell lines (11.2% to 81.5%), while CD133 was detected in more than 90% of HuCCT1 cells but less than 5% in others. Overall, there were no significant differences in the prevalence of these SCSMs between I-CCA and E-CCA cell lines. In non-malignant H69 cholangiocytes, CD13 and CD90 SCSMs were expressed.

To determine whether SCSMs were consistently expressed (i.e. a feature of stemness), cells were cultured for 30 days and marker expression documented at the end of the culture period. SCSM expression was documented by flow cytometry every five days. The results are provided in Figures 3.11 and 3.12. There were no significant changes in SCSM prevalences over time.

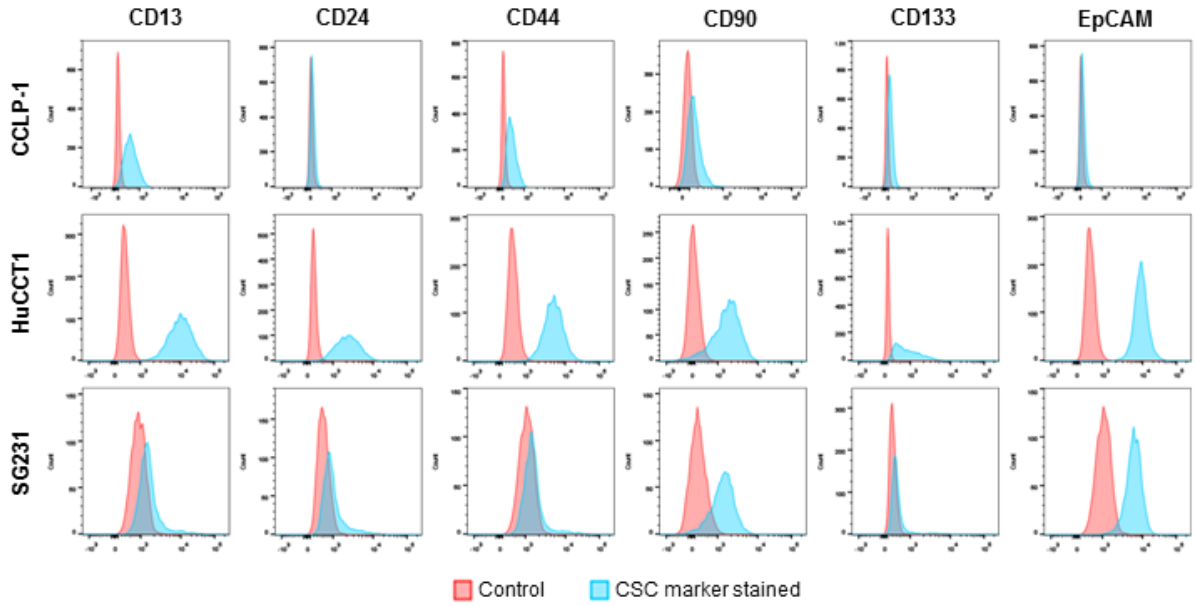

CSC marker expression (%)						
Cell lines	CD13	CD24	CD44	CD90	CD133	EpCAM
CCLP-1	61.7 ± 4.54	3.41 ± 1.16	35.1 ± 5.78	11.2 ± 1.75	9.17 ± 2.90	2.21 ± 1.06
HuCCT1	100 ± 0.06	97.2 ± 1.05	97.8 ± 2.82	80.4 ± 3.57	90.7 ± 1.9	99.9 ± 0.01
SG231	11.8 ± 1.28	16.1 ± 2.85	8.27 ± 2.44	48.0 ± 3.87	9.74 ± 0.84	99.0 ± 0.50

Figure 3.9 The expression of SCSMs in I-CCA cell lines.

CCLP-1, HuCCT1 and SG231 cell lines were stained with isotype-matched mABs (IgG1) or fluorescence-conjugated mAbs against CD13, CD24, CD44, CD90, CD133, and EpCAM respectively and analyzed by flow cytometry. Top panels are representative of marker expression. Cells stained with IgG1 (control/red colour) and mAs against SCSM (blue colour). Lower panel presents SCSM positive population in each cell line. Data presented as the mean ± SD.

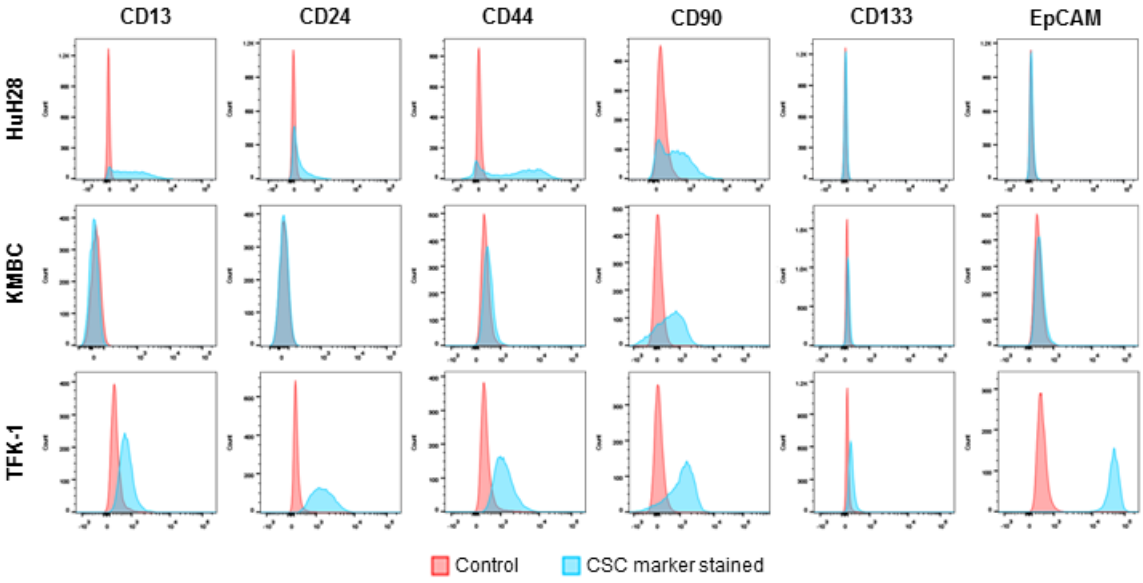

CSC marker expression (%)						
Cell lines	CD13	CD24	CD44	CD90	CD133	EpCAM
HuH28	88.3 ± 2.18	46.2 ± 3.26	90.8 ± 1.37	68.6 ± 6.61	2.49 ± 1.40	0.35 ± 0.47
KMBC	0.67 ± 0.54	0.99 ± 0.07	3.96 ± 1.64	52.8 ± 2.82	0.45 ± 0.13	0.92 ± 0.29
TFK-1	18.2 ± 4.65	97.2 ± 3.73	58.0 ± 3.36	81.5 ± 4.50	2.45 ± 1.40	99.3 ± 1.01

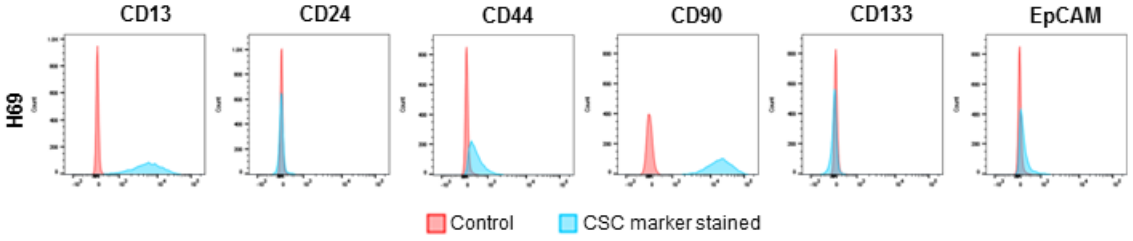

CSC marker expression (%)						
Cell lines	CD13	CD24	CD44	CD90	CD133	EpCAM
H69	99.1 ± 0.72	1.16 ± 0.53	31.4 ± 2.05	100 ± 0.06	0.61 ± 0.26	8.23 ± 1.17

Figure 3.10 SCSMs in E-CCA and non-malignant cell lines.

HuH28, KMBC, TFK-1, and H69 cell lines. were stained with isotype-matched mABs (IgG1) or fluorescence-conjugated mAbs against CD13, CD24, CD44, CD90, CD133, and EpCAM respectively and analyzed by flow cytometry. Data presented as the mean ± SD.

October 18th, 2019

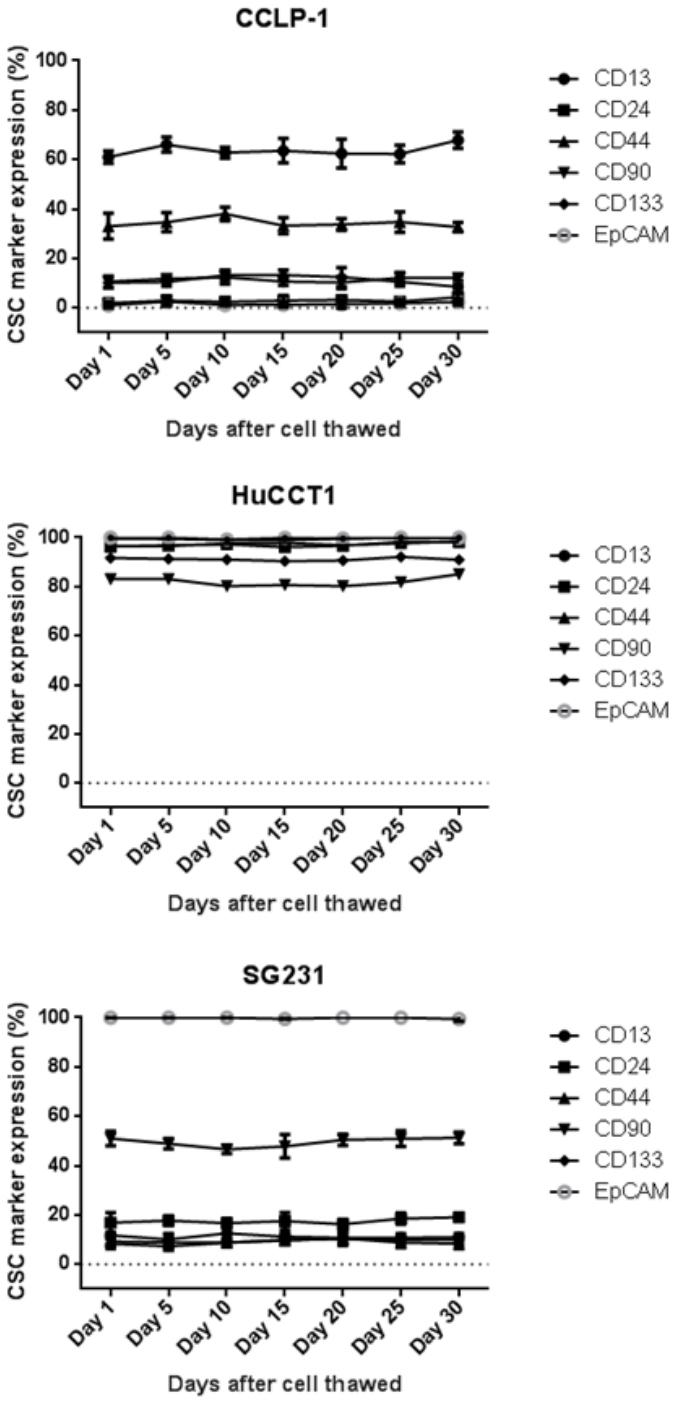

Figure 3.11 SCSM expression in I-CCA after 30 days in culture.

Data presented as the mean ± SD.

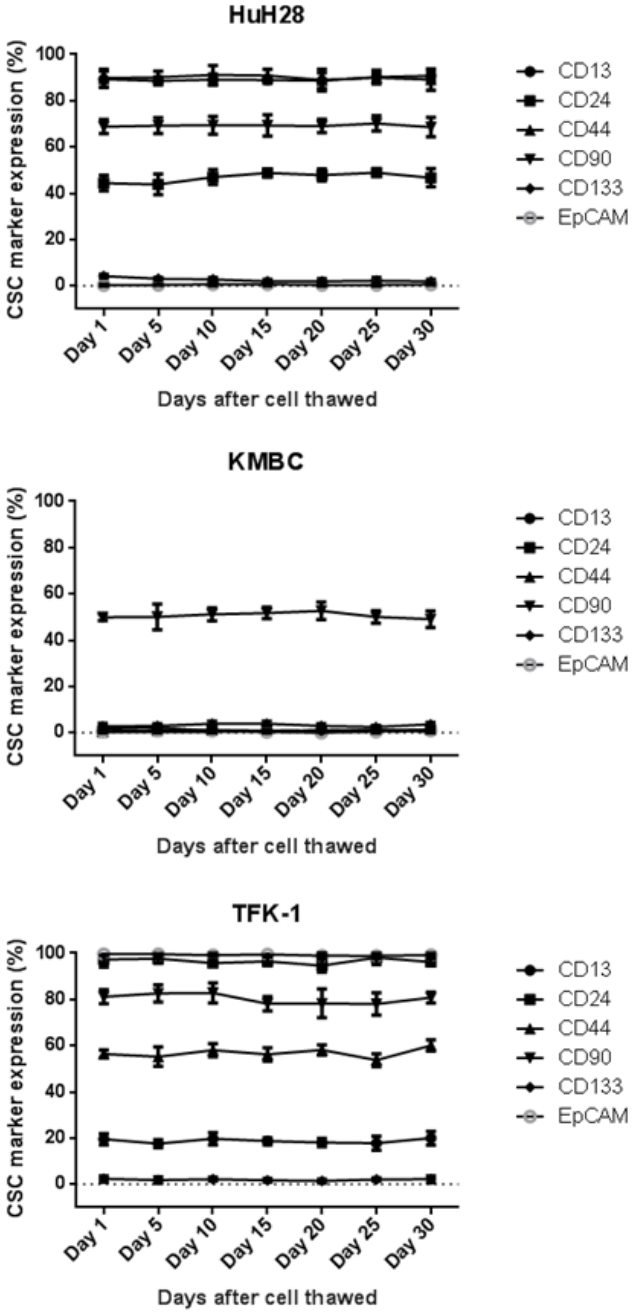

Figure 3.12 SCSM expression in E-CCA after 30 days in culture.

Data presented as the mean ± SD.

3.1.8 Association of SCSMs with Growth Features

To determine whether specific SCSMs associate with certain growth feature, correlation coefficients were calculated for each SCSM and cell proliferation, colony/spheroid formation, migration and invasion. P values of correlations are provided in Table 3-1. The results revealed there were no significant correlations between specific SCSMs and cell growth properties. The correlation between CD24 to colony-formation activity was highest but not significant (p=0.054). Other SCSMs with the highest correlations with growth features were CD44 to proliferation (p=0.40), CD13 to spheroid size (p=0.36), CD13 to migration (p=0.094) and CD133 to invasion (p=0.15).

Table 3-2 Correlations between tumor features, CSC prevalence, and SCSMs in CCA cells.

p-value of correlation	Cell proliferation	Spheroid size	Colony formation	Cell migration	Cell invasion
CD13	0.4389634	0.3626529	0.4700548	0.09415884	0.8848501
CD24	0.9160627	0.8638522	0.05399868	0.7914219	0.954834
CD44	0.3972887	0.4706831	0.206752	0.4406875	0.8530665
CD90	0.7874514	0.4746822	0.4577624	0.6899347	0.8429261
EpCAM	0.5195574	0.3843364	0.4931796	0.2538196	0.1502015

3.2 PART II: I-CCA AND E-CCA CHEMORESISTANCE

3.2.1 MRP1-6 Expression

To demonstrate whether transcripts of MRPs are expressed in CCA, mRNA levels of MRP1-6 were determined in the six CCA cell lines. In general, CCA cell lines expressed these MRPs to different extents (Figures 3.13). SG231 (I-CCA) and HuH28 cells (E-CCA) expressed mRNA of all MRPs. In CCLP-1 (I-CCA) and HuCCT1 (I-CCA) cells, mRNA expression of all MRPs except MRP3 were detected, while in KMBC (E-CCA cells MRP1, MRP3, MRP4 and MRP5 mRNA were detected, TFK-1 (E-CCA) expressed all MRPs mRNA except MRP6.

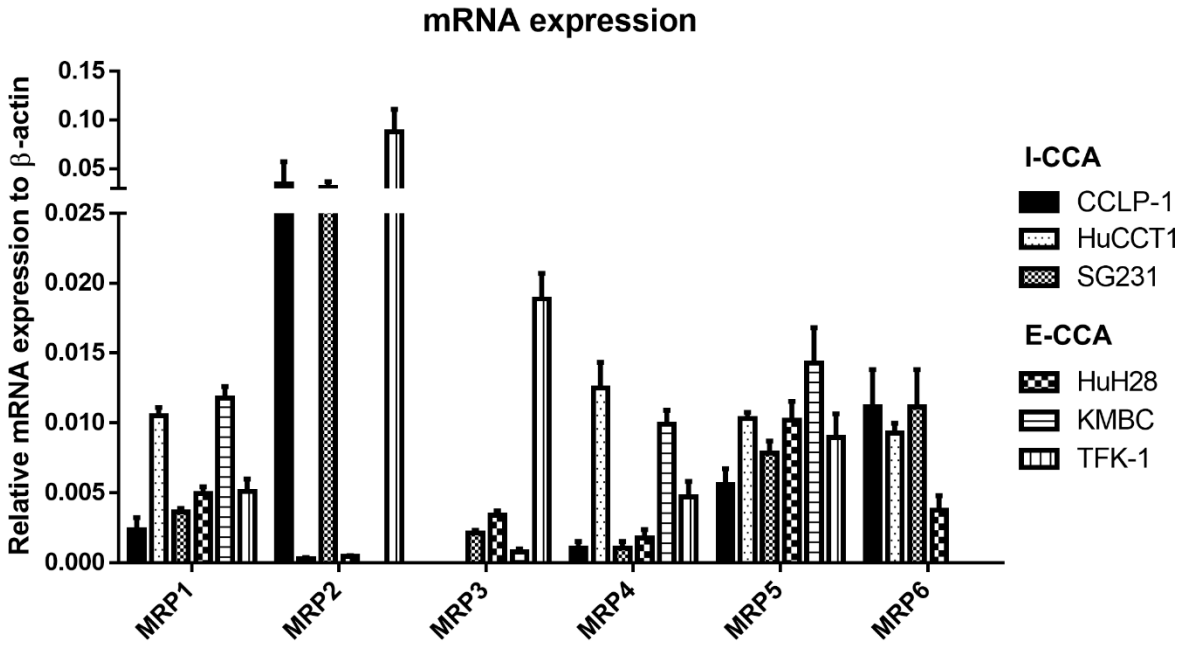

Figure 3.13 mRNA expression of MRPs in CCA cells.

MRP1-6 mRNA expression in CCA cells prior to gemcitabine exposure and after normalization to β-actin transcript abundance. Data presented as mean ± SD.

3.2.2 Response to Gemcitabine

Given that gemcitabine and related adjuvant treatments are the first line of chemotherapy against CCA (Morizane et al., 2018), we documented the chemosensitivity of CCA cell lines exposed to gemcitabine. Figures 4.2 provides the results of cytotoxicity experiments with different concentrations of gemcitabine in I-CCA and E-CCA cells. Gemcitabine induced cytotoxicity in all CCAs in a concentration-dependent manner. Gemcitabine achieved similar cytotoxicity among I-CCAs, which was approximately 80% at 100 μM (Figure 3.14 upper panel). In E-CCA cells, cytotoxicity achieved by gemcitabine followed a similar pattern until the concentration reached 100 nM (Figure 3.14 middle panel). TFK-1 was the most resistant cell line to gemcitabine at 100 μM with a cytotoxicity of 60%, while KMBC death was 95% at the same concentration. By comparing gemcitabine induced cytotoxicity between I-CCA and E-CCA (Figure 3.14 lower panel), cytotoxicity effects were significantly lower in I-CCA than E-CCA cells ($p=0.0016$). Regarding the relative half-maximal inhibitory concentration (IC_{50}) values, the effects of gemcitabine in CCA cell lines varied over a wide range of concentrations, from nanomolars to micromolars.

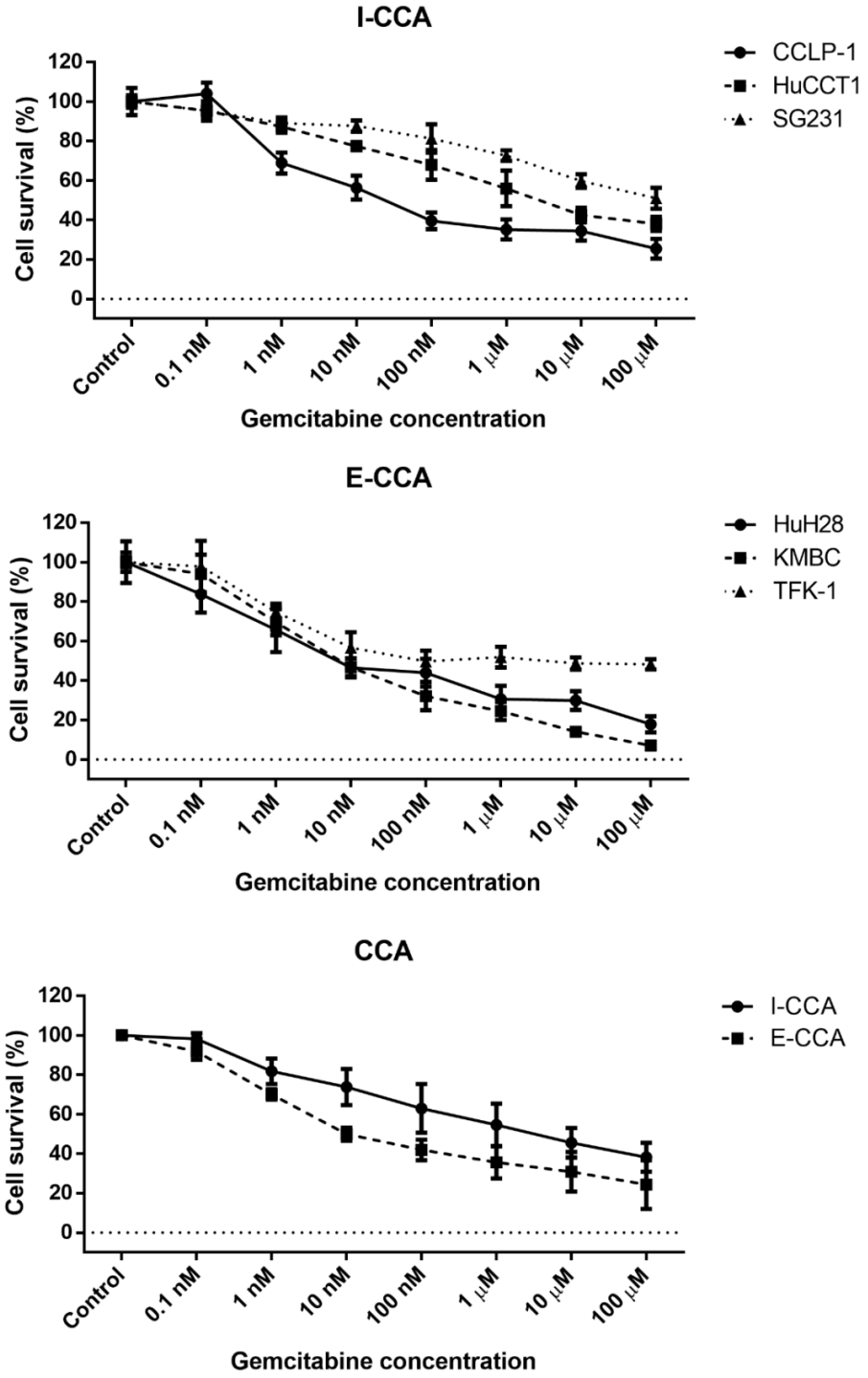

Figure 3.14 Cytotoxicity of concentration-dependent gemcitabine on CCA cells.

All I-CCA (upper panel) and E-CCA (middle panel) cell populations were treated for 72 hours with increasing concentrations of gemcitabine (0.1 nM to 100 μM). The IC_{50} value for I-CCA cells: CCLP-1, HuCCT1, and SG231 cells were 13.9±4.47 nM, 381.6±88.7 nM and 24.8±6.22 μM respectively. IC_{50} values for E-CCA cells: HuH28, KMBC and TFK-1 cells were 13.5±5.66 nM, 54.4±29.5 nM and 92.5±33.4 nM respectively. Panel C reveals that lower gemcitabine induced cytotoxicity was observed in I-CCA than E-CCA cells (p=0.0016). Significant difference was supported by considering IC_{50} values (p=0.0432). Data presented as mean ± SD.

3.2.3 MRP Upregulation After Exposure to Gemcitabine

To determine whether the activity of MRP efflux pumps was associated with sensitivity to gemcitabine in CCAs, we exposed these six CCA cell lines to gemcitabine at a concentration of 1 nM, which represents the concentration that achieved 20% cytotoxicity for most cell lines. As shown in Figures 3.15 and 3.16, changes in mRNA expression of MRP1-6 pumps are presented following 24 to 48 hours of exposure to gemcitabine. Gemcitabine induced significant increases in MRP1-6 mRNA expression in most cell lines. The most significant upregulation occurred with MRP5 and MRP6 in both I-CCA and E-CCA cell lines, where greater than five fold changes of MRP5 mRNA were observed in HuCCT1, SG231, HuH28 and KMBC cells, while MRP6 mRNA expression was increased 20 fold in HuCCT1 cells at 48 hours. On the other hand, MRP2, MRP3, or MRP4 expression were not affected or only slightly altered in these CCA cell lines. As a result, incubating CCA cell lines with gemcitabine at a cytotoxic concentration of 1 nM induced a rescue response in cells by upregulating MRPs and in particular, MRP5 and MRP6.

To evaluate whether alterations of MRP5 and/or MRP6 occurred at a protein level, we selected one CCA cell line from each I-CCA and E-CCA groups to perform Western blot analysis. HuCCT1 was the I-CCA which presented the most SCSMs (as described in Part I) and exhibited the largest increases in MRP5 and MRP6 mRNA expressions after exposure to gemcitabine, while KMBC was the selected E-CCA because it expressed the least CSC markers and upregulated predominantly MRP5 mRNA after exposure to gemcitabine. Figure 3.17 illustrates the results of protein expression of MRP5 and MRP6 by Western blot. The results confirm that CCA cells responded to the cytotoxic concentration of gemcitabine by increasing MRP5 and/or MRP6 protein expression.

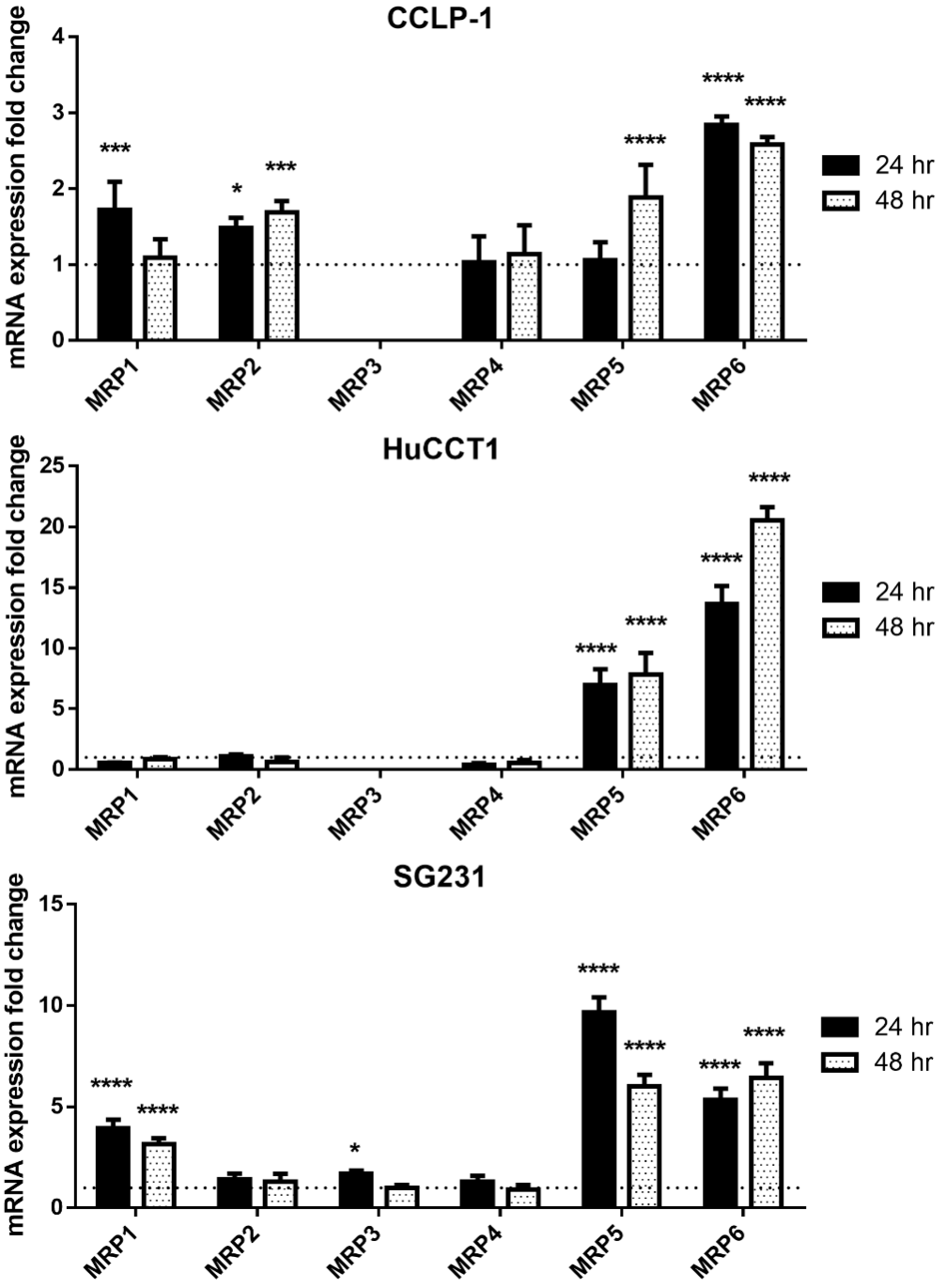

Figure 3.15 Fold changes in MRPs mRNA in I-CCA cells following gemcitabine exposure. Cells were incubated with gemcitabine (1 nM) for 24 and 48 hours prior to mRNA isolation. MRP mRNA expression in CCLP-1, HuCCT1, and SG231 cells was quantified by qRT-PCR.

October 18th, 2019

*Individual expression levels of the indicated MRPs were normalized to mRNA expression of β-actin. The results are shown as x-fold relative to the normalized expression in control cells (set as 1). Data presented as mean ± SD. *: p<0.05, ***: p<0.001, ****: p<0.0001.*

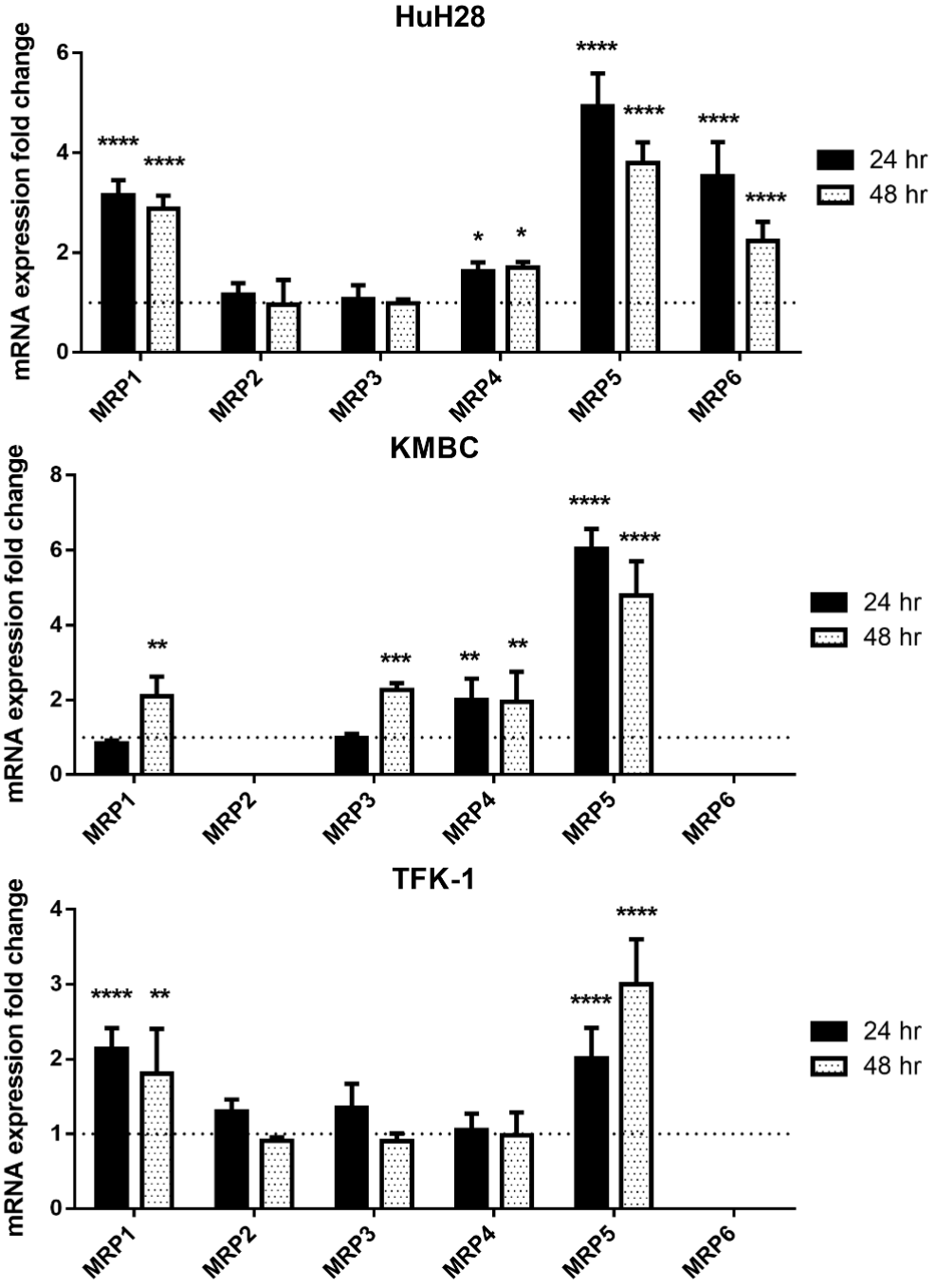

Figure 3.16 Fold changes in MPRs mRNA in E-CCA cells following gemcitabine exposure. Cells were incubated with gemcitabine (1 nM) for 24 and 48 hours prior to mRNA isolation. MRP mRNA expression in HuH28, KMBC, and TFK-1 cells was quantified by qRT-PCR.

*Individual expression levels of the indicated MRPs were normalized to mRNA expression of β-actin. The results are shown as x-fold relative to the normalized expression in control cells (set as 1). Data presented as mean ± SD. *: p<0.05, **: p<0.01, ***: p<0.001, ****: p<0.0001.*

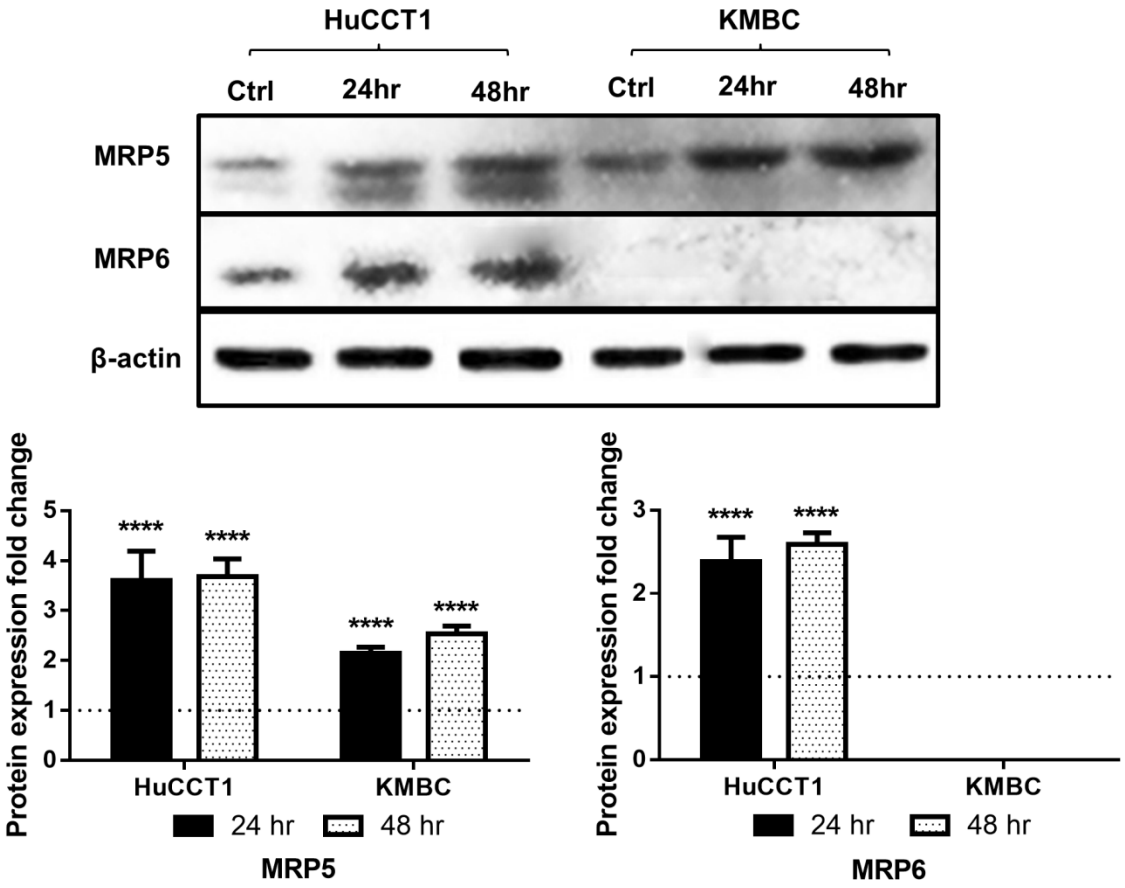

Figure 3.17 MRP5 and MRP6 protein expression in CCA with following gemcitabine exposure. Cells were incubated with gemcitabine (1 nM) for 24 and 48 hours prior to protein isolation. Upper panel is representative Western blot analysis of MRPs protein expressions in HuCCT1 and KMBC cells following gemcitabine exposure. Lower panel is quantification of protein alteration in MRP5 and MRP6. Individual expression levels of the indicated MRPs were normalized to protein expression of β-actin. The results are shown as x-fold relative to the normalized expression in control cells (set as 1). Data presented as mean ± SD.

*****: $p<0.0001$.*

3.2.4 Preparation and Transduction of MRP5 and MRP6 ShRNA into CCA

To further explore the roles of MRP5 and/or MRP6 in gemcitabine resistance, we silenced the MRP5 and MRP6 transporters in HuCCT1 and MRP6 in KMBC cells by specific RNAi. Five different shRNA oligonucleotides of MRP5 and MRP6 were generated. In total, ten shRNA oligonucleotides were employed. Each shRNA targeted a specific region of the MRP5 or MRP6 mRNA sequences (Table 2-5).

When packaged lentiviral particles (five MRP5 shRNA and five MRP6) were achieved, both MRP5 and/or MRP6 shRNA were titered to HuCCT1 and KMBC cells with ratios from 1:1000 to 1:10. After transduction and puromycin selection, MRP5-shRNA vectors including 303-307 were transduced into HuCCT1 cells, while 303, 304, 305, and 307 were transduced into KMBC cells. MRP6-shRNA packaged lentiviral particles including 714, 715, 716 and 717 were transduced into HuCCT1 cells. The calculated titer of these lentivirus vectors was approximately 2×10^5 TU/mL. By using an MOI of 0.08 for the lentiviral-based MRP5- or MRP6-shRNA as well as a nonsilencing pLKO.1-puro control, each viral particle was transduced into HuCCT1 and/or KMBC cells to perform further target knockdown verification.

3.2.5 Verification of ShRNA Knockdown

To verify that MRP5 or MRP6 expression was inhibited in transduced HuCCT1 and/or KMBC cells, qRT-PCR experiments were performed. In Figure 3.18, MRP5 mRNA expressions are presented after transduction of all the shRNA library pools. These MRP5-shRNAs showed large differences of mRNA knockdown in the two cell lines. Vectors 303 and 307 inhibited 80%

expression of MRP5 in HuCCT1, while 303, 305 and 307 achieved similar knockdown in KMBC cells. Since the lentivirus 307 achieved maximum mRNA knockdown in both HuCCT1 and KMBC, 307-MRP5-shRNA (5'-CCGGCCACATCTTCAATAGTGCTATCTCGAGATAGCACTATTGAAGATGTGGTTTTTG-3') transduced HuCCT1 and KMBC cells were employed for further verification analysis.

The mRNA knockdown verification in MRP6 is provided in Figure 3.19. Most vectors including 714, 715 and 716 approached 80% inhibition in HuCCT1, while 714 demonstrated the greatest MRP6 mRNA knockdown, Thus, 714-MRP6-shRNA (5'-CCGGCGATCTCCCATCAGCTTCTTTCTCGAGAAAGAAGCTGATGGGAGATCGTTTTTG - 3') transduced HuCCT1 cells were employed for further verification analysis.

To demonstrate whether lentivirus transduced shRNA exhibited dilution-dependent effects in MRP knockdown, we evaluated both mRNA and protein analysis in cells with different lentivirus dilutions (as previously performed for titers). Figures 3.20 to 3.22 indicate that shRNA inhibited MRP5 in a dilution-dependent manner. In HuCCT1 cells, MRP5 mRNA and protein expression were significantly inhibited at lentivirus shRNA dilutions of 1:500 and lower (Figures 3.20 upper panel and 3.21), while in KMBC cells MRP5 mRNA and protein inhibition were significant at lentivirus shRNA dilutions of 1:100 and lower (Figure 3.20 lower panel and 3.22). Similar results are also found in Figures 3.23 and 3.24 where MRP6-shRNA revealed dilution-dependent effects in both mRNA and protein levels. In HuCCT1 cells, significant MRP6 knockdown occurred at lentivirus shRNA dilutions of 1:100 and lower.

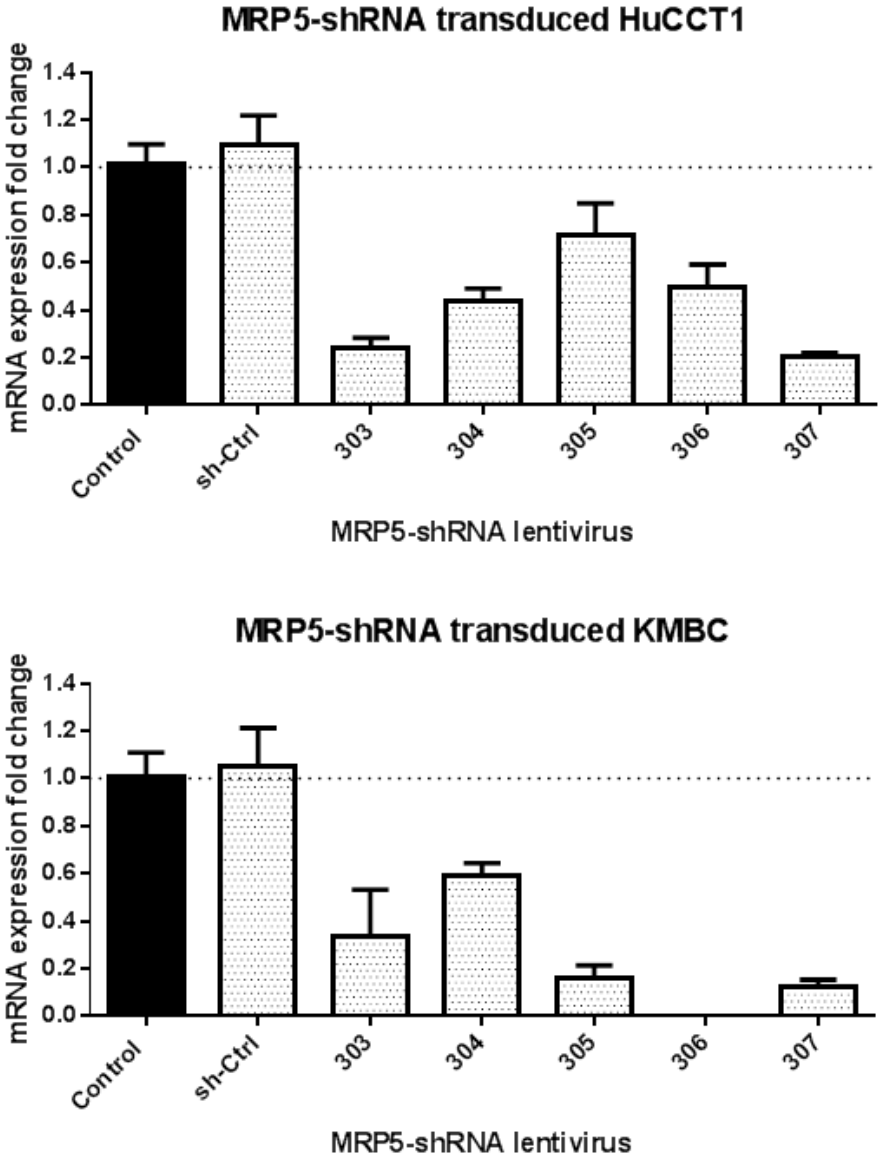

Figure 3.18 MRP5 mRNA knockdown verification.

Total mRNA was isolated from HuCCT1 and KMBC cells with either non-silencing shRNA (PLKO control) or MRP5-shRNA. Gene knockdown was verified at the mRNA level by qRT-PCR analysis. A reduction in the mRNA level of over 80% was obtained with 307-shRNA-MRP5 in

both cell lines. Individual expression levels of MRP5 were normalized to mRNA expression of β-actin. The results are shown as x-fold relative to the normalized expression in control cells (set as 1). Data presented as mean ± SD.

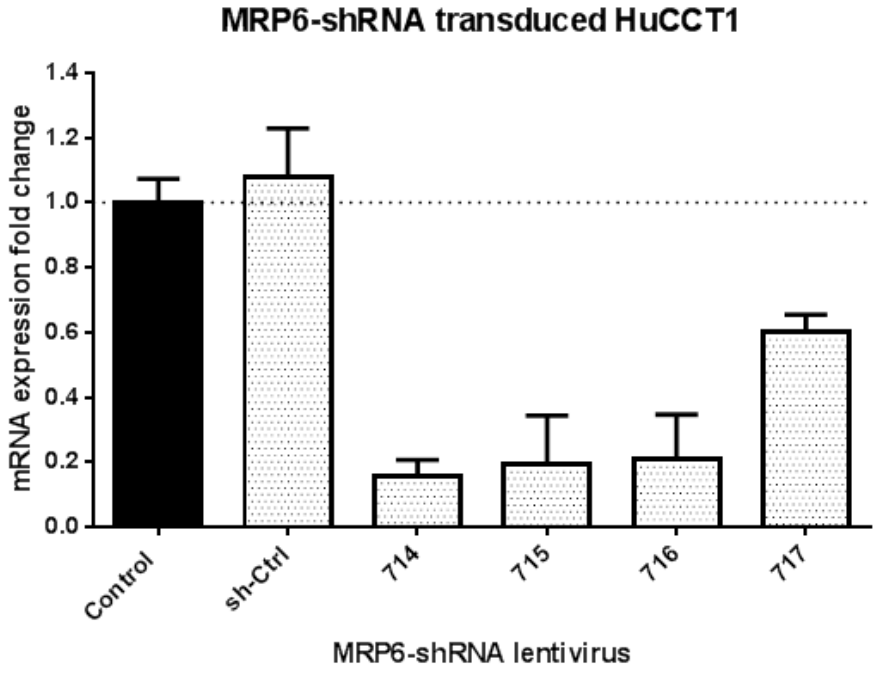

Figure 3.19 MRP6 mRNA knockdown verification.

Total mRNA was isolated from HuCCT1 cells with either non-silencing shRNA (PLKO control) or MRP6-shRNA. Gene knockdown was verified at the mRNA level by qRT-PCR analysis. A reduction in the mRNA level of 80% was obtained with 714,715, and 716 MRP6-shRNA in HuCCT1 cells. Individual expression levels of the MRP6 were normalized to mRNA expression of β-actin. The results are shown as x-fold relative to the normalized expression in control cells (set as 1). Data presented as mean ± SD.

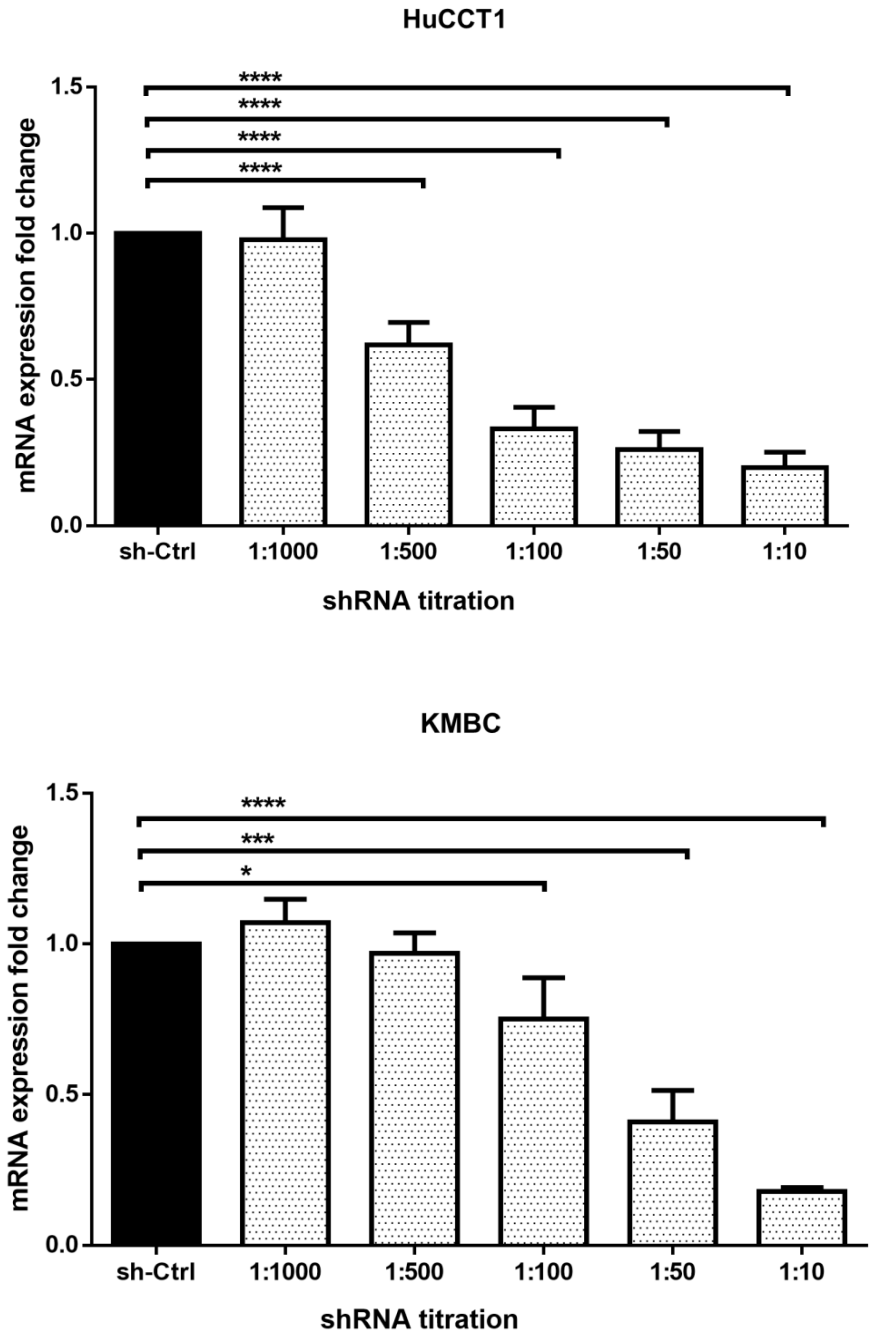

Figure 3.20 Optimization of the lentivirus dilution for shMRP5 in HuCCT1 and KMBC cells.

*Total mRNA was isolated from cells following exposure to either PLKO control (sh-Ctrl) or serial dilutions (1:1000 to 1:10) of MRP5-shRNA. Significant MRP5 mRNA was inhibited at MRP5-shRNA dilutions of 1:500 and lower in HuCCT1 cells and 1:100 and lower in KMBC cells. Individual expression levels of MRP5 were normalized to mRNA expression of β-actin. The results are shown as x-fold relative to the normalized expression in control cells (set as 1). Data presented as mean ± SD. *: p<0.05; ***: p<0.001; ****: p<0.0001.*

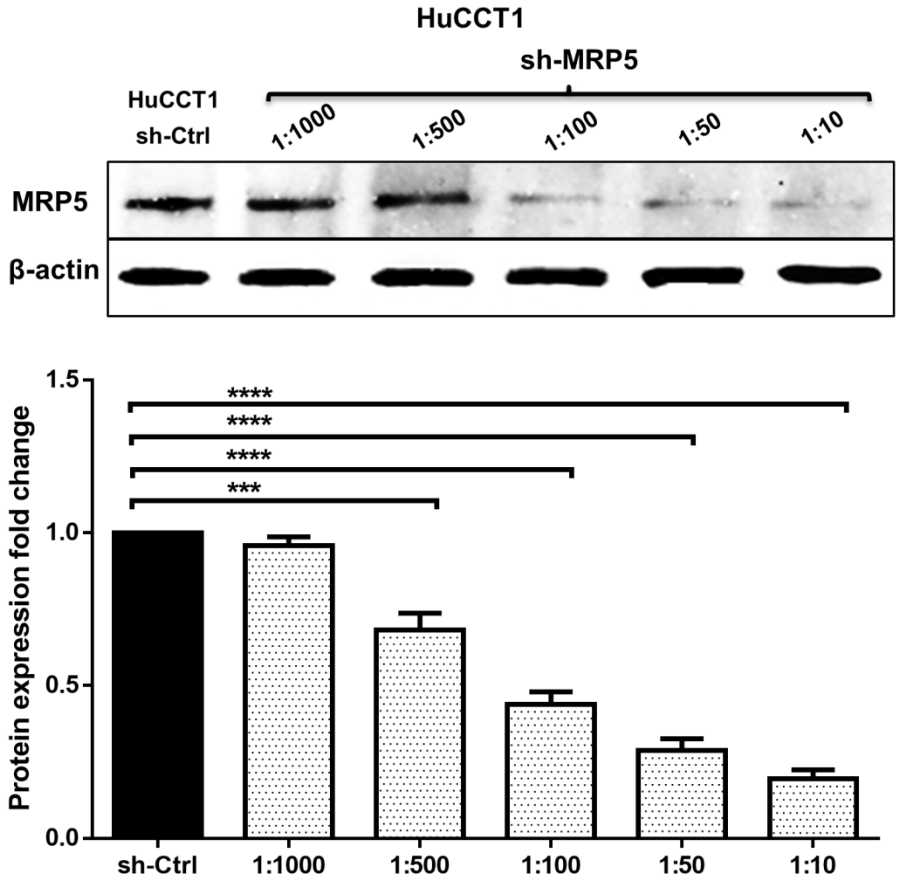

Figure 3.21 Optimization of the lentivirus dilution for shMRP5 in HuCCT1 cells.

*Total protein was isolated from cells following exposure to either PLKO control (sh-Ctrl) or serial dilutions (1:1000 to 1:10) of MRP5-shRNA. Upper panel: representative Western blot expression of MRP5 knockdown. Lower panel: quantification of Western blot determinations in HuCCT1 cells. Individual expression levels of the MRP5 were normalized to the protein expression of β-actin. The results are shown as x-fold relative to the normalized expression in control cells (set as 1). Data presented as mean ± SD. ***: p<0.001; ****: p<0.0001.*

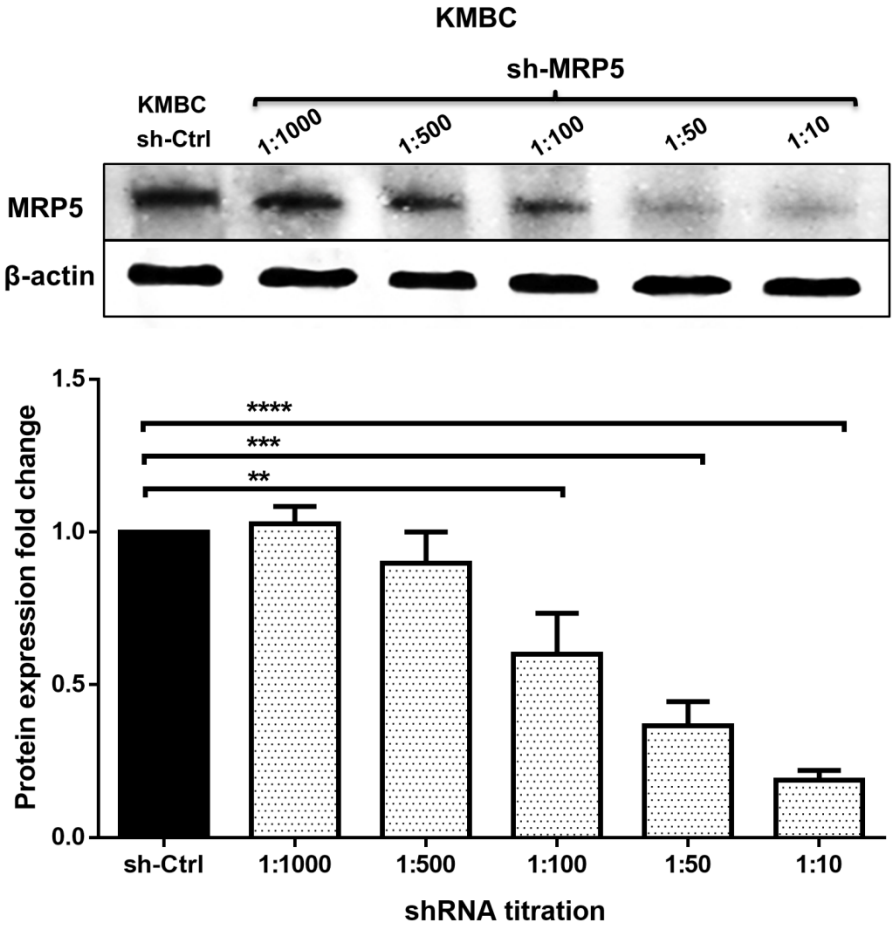

October 18th, 2019

Figure 3.22 Optimization of the lentivirus dilution for shMRP5 in KMBC cells.
*Total protein was isolated from cells following exposure to either PLKO control (sh-Ctrl) or serial dilutions (1:1000 to 1:10) of MRP5-shRNA. Upper panel: representative Western blot expression of MRP5 knockdown. Lower panel: quantification of Western blot determinations in KMBC cells. Individual expression levels of the MRP5 were normalized to the protein expression of β-actin. The results are shown as x-fold relative to the normalized expression in control cells (set as 1). Data presented as mean ± SD. **: p<0.01; ***: p<0.001; ****: p<0.0001.*

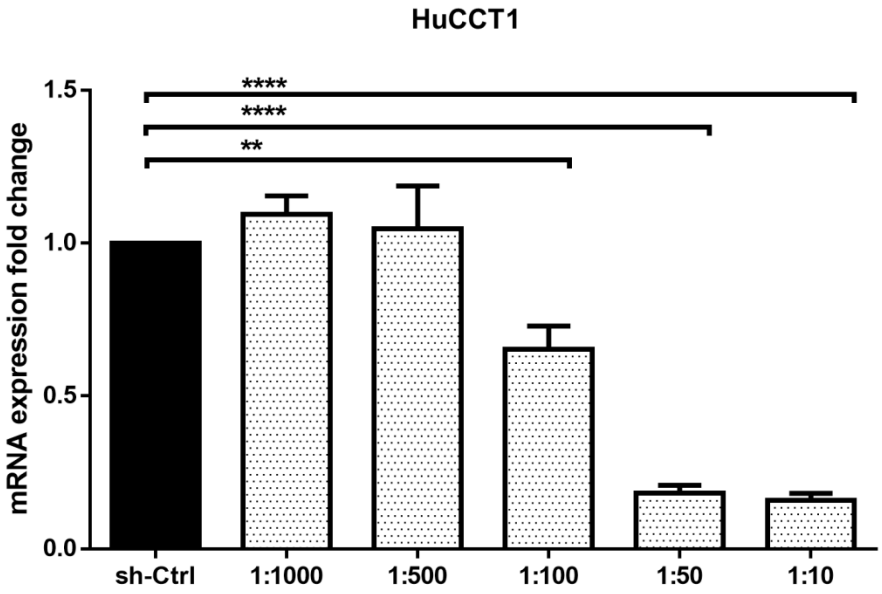

Figure 3.23 Optimization of the lentivirus dilution for shMRP6 in HuCCT1 cells.
Total mRNA was isolated from HuCCT1 cells and determined by qRT-PCR. Significant inhibition of MRP6 mRNA was obtained at an MRP6-shRNA dilution of 1:100 and lower. Individual expression levels of the MRP6 were normalized to mRNA expression of β-actin. The

*results are shown as x-fold relative to the normalized expression in control cells (set as 1). Data presented as mean ± SD. **: p<0.01; ****: p<0.0001.*

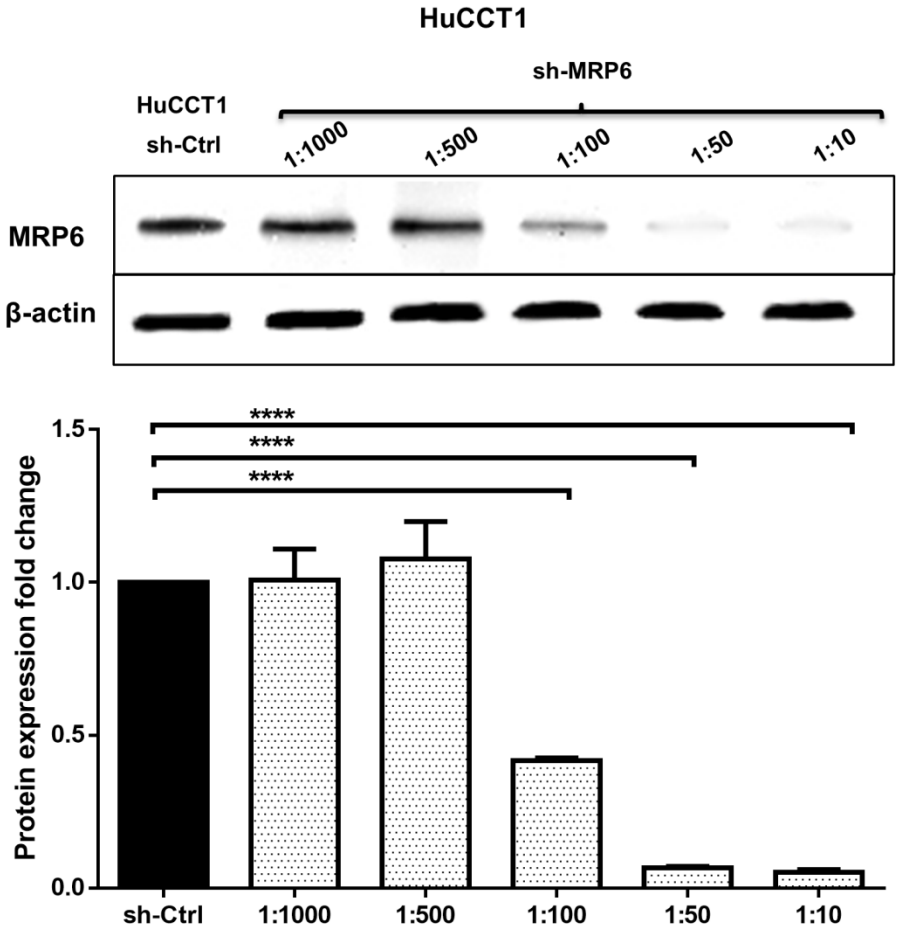

Figure 3.24 Optimization of the lentivirus dilution for shMRP6 in HuCCT1 cells.
Total protein was isolated from HuCCT1 cells following exposure to either PLKO control (sh-Ctrl) or serial dilutions (1:1000 to 1:10) of MRP6-shRNA and quantified by Western blot analyses. Significant inhibition of MRP6 protein expression was obtained at an MRP6-shRNA dilution of 1:100 and lower. Individual expression levels of the MRP6 were normalized to

*protein expression of β-actin. The results are shown as x-fold relative to the normalized expression in control cells (set as 1). Data presented as mean ± SD. ****: p<0.0001.*

3.2.6 Gemcitabine Enhanced Cytotoxicity in MRPs

The results of experiments designed to determine whether the extent of MRP5 and MRP6 knockdown with different dilutions of lentivirus shRNA enhance the cytotoxicity of gemcitabine are provided in Figures 3.25 and 3.26. At a constant gemcitabine concentration of 10 nM, lentivirus containing MRP5 shRNA at different dilutions increased both HuCCT1 and KMBC cytotoxicity at dilutions of 1:100 or lower (Figure 3.25). MRP6 inhibition at a constant lentivirus shRNA dilution of 1:100 and lower significantly increased gemcitabine-induced HuCCT1 cytotoxicity (Figure 3.26).

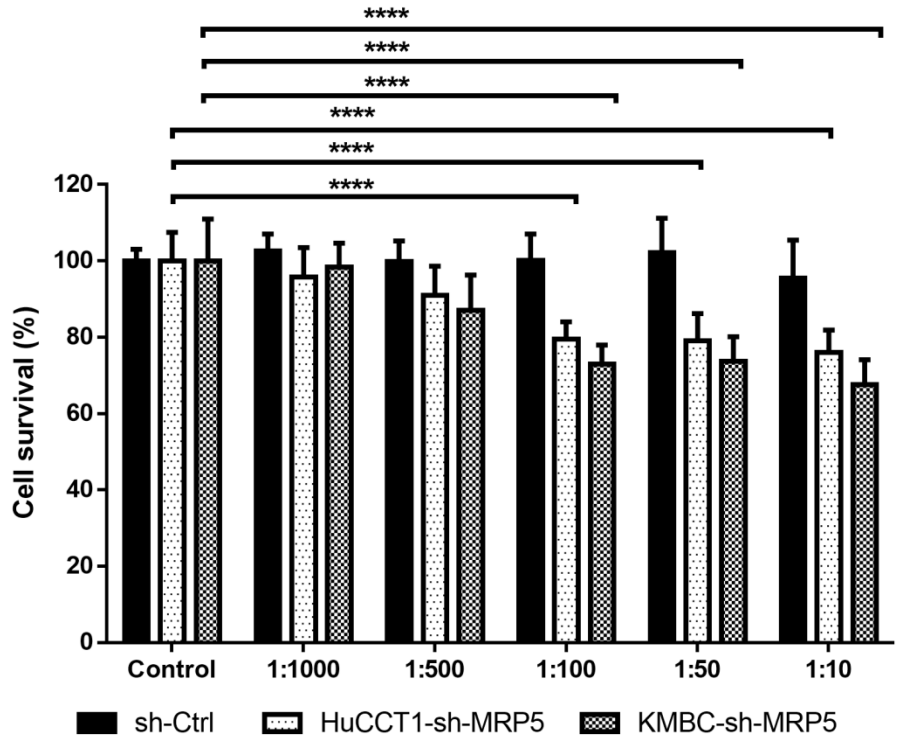

Figure 3.25 Lentivirus shRNA of MRP5 and MRP6 dilution-dependent cytotoxicity of gemcitabine (10 nM) in HuCCT1 and KMBC cells.

*ShRNA dilutions of 1:1000 to 1:10 were employed. HuCCT1 and KMBC survival were determined after three days of gemcitabine exposure. The cell cytotoxicity of control cells induced by 10 nM gemcitabine was normalized as "100%" (i.e. Control). The cell survival of each experimental group was documented by which compared to the Control. Data presented as mean ±SD. ****: p<0.0001. sh-Ctrl: HuCCT1-sh-MRP5: MRP5 shRNA knockdown in HuCCT1 cells; KMBC-sh-MRP5: MRP5 shRNA knockdown in KMBC cells.*

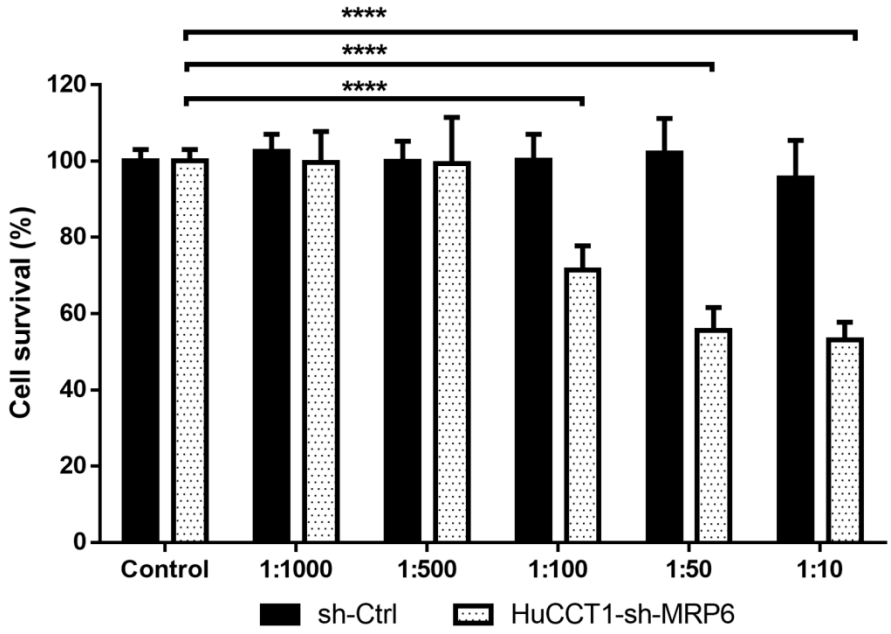

Figure 3.26 Lentivirus shRNA of MRP6 dilution-dependent cytotoxicity of gemcitabine (10 nM) in HuCCT1 cells.

*ShRNA dilutions of 1:1000 to 1:10 were employed. HuCCT1 was were determined after three days of gemcitabine exposure. The cell cytotoxicity of control cells induced by 10 nM gemcitabine was normalized as "100%" (i.e. Control). The cell survival of each experimental group was documented by which compared to the Control. Data presented as mean ±SD. ****: p<0.0001. HuCCT1-sh-MRP6: MRP6 shRNA knockdown in HuCCT1 cells.*

3.2.7 Gemcitabine Cytotoxicity at Different Concentrations Following ShRNA Knockdown

Figures 3.27- 3.29 provide the results of concentration-dependent gemcitabine cytotoxicity in HuCCT1 and KMBC cells, gemcitabine-induced cytotoxicity was similar at all concentrations in cells with or without MRP5 knockdown (IC_{50}. 430.5±39.8 nM versus 124.1±43.6 nM; $p<0.01$) (Figure 3.27). However, MRP6 knockdown significantly enhanced gemcitabine toxicity of HuCCT1 cells at all gemcitabine concentrations with almost complete killing of cells at a concentration of 1 mM (IC_{50}. 430.5±39.8 nM versus 25.6±8.36 nM; $p<0.01$) (Figure 3.28). In KMBC cells, MRP5 knockdown significantly enhanced gemcitabine cytotoxicity at concentrations of 1 nM and higher (IC_{50}. 39.5±8.94 nM versus 4.57±2.92 nM; $p < 0.05$) (Figure 3.29).

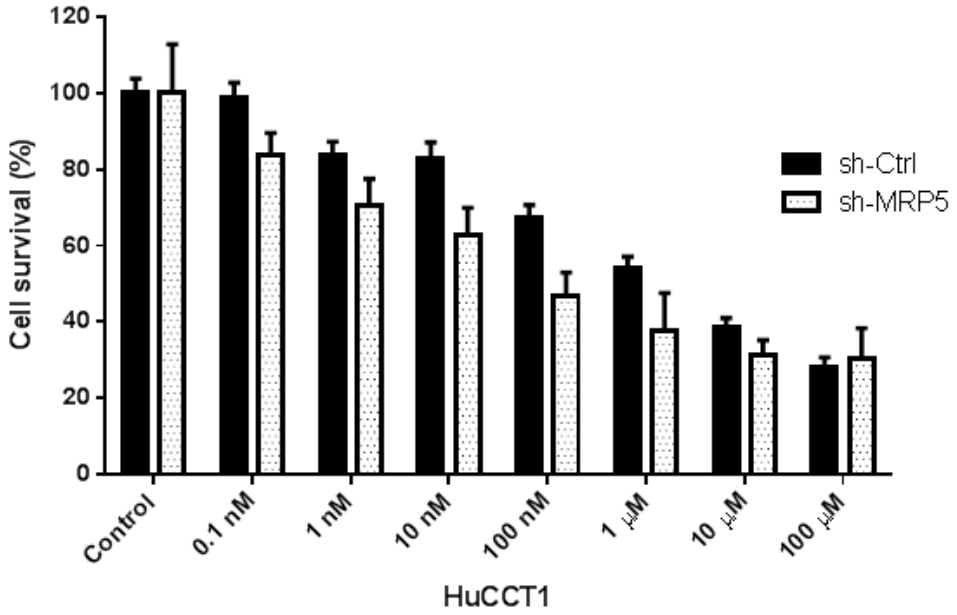

Figure 3.27 Gemcitabine induced cytotoxicity of HuCCT1 cells following inhibition of MRP5 expression.

ShRNA dilutions of 1:10 were employed. HuCCT1 cell survival was determined after three days of gemcitabine exposure. Data presented as mean ±SD.

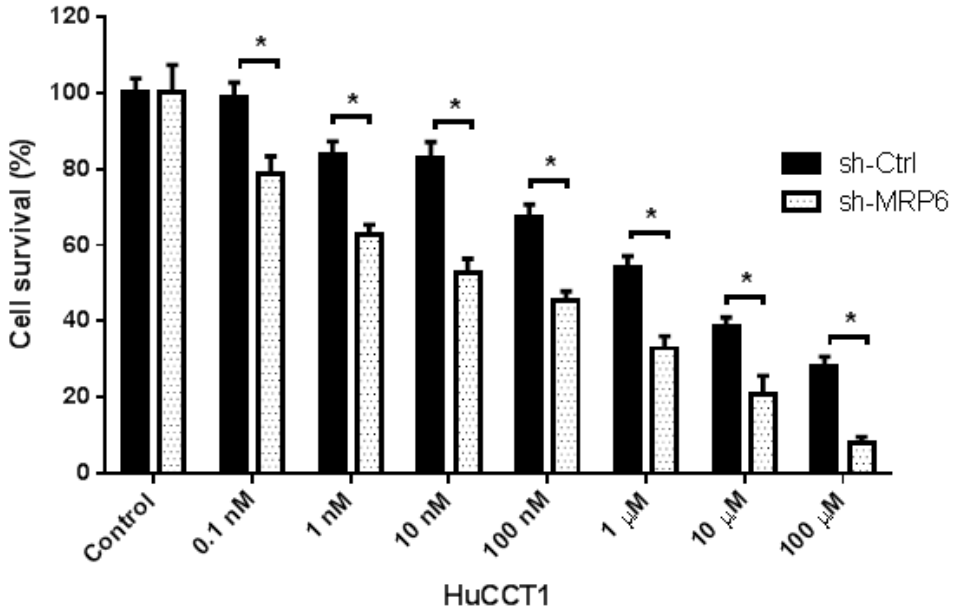

Figure 3.28 Gemcitabine induced cytotoxicity of HuCCT1 cells following inhibition of MRP6 expression.

*ShRNA dilutions of 1:50 were employed. HuCCT1 cell survival was determined after three days of gemcitabine exposure. Data presented as mean ±SD. *: $p<0.05$.*

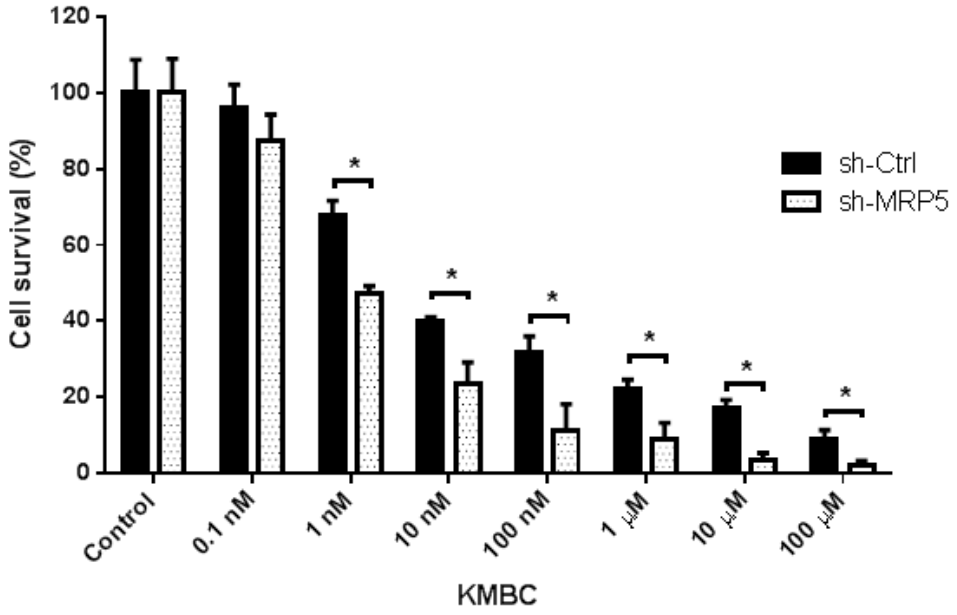

Figure 3.29 Gemcitabine induced cytotoxicity of KMBC cells following inhibition of MRP5 expression.

*ShRNA dilutions of 1:10 were employed. KMBC cell survival was determined after three days of gemcitabine exposure. Data presented as mean ±SD. *: $p<0.05$.*

3.3 PART III: I-CCA AND E-CCA CHEMOTAXIS

3.3.1 CCR Expression Profile in CCA Cells

The CCR expression profiles of HuCCT1 and KMBC cells are provided in Figure 3.30. All CCRs (CCR1-10) were expressed in HuCCT1 cells, while six (CCR4, CCR5, CCR6, CCR8, CCR9 and CCR10) were detected in KMBC cells. The most abundant CCR subtype expressed in HuCCT1 cells was CCR5 followed by CCR7. In KMBC cells, CCR6 expression was most abundant followed by CCR5.

Regarding CXCR subtypes, both HuCCT1 and KMBC cells expressed CXCR1, CXCR3, CXCR4, CXCR6 and CXCR7 mRNA. CXCR4 expression was the most abundant in both cell lines, and more than 15-fold higher than other CXCRs. The second most abundant CXCR expressed in HuCCT1 was CXCR3 followed by CXCR7. In KMBC cells, second most abundant was CXCR7 followed by CXCR6, CXCR3 and CXCR1.

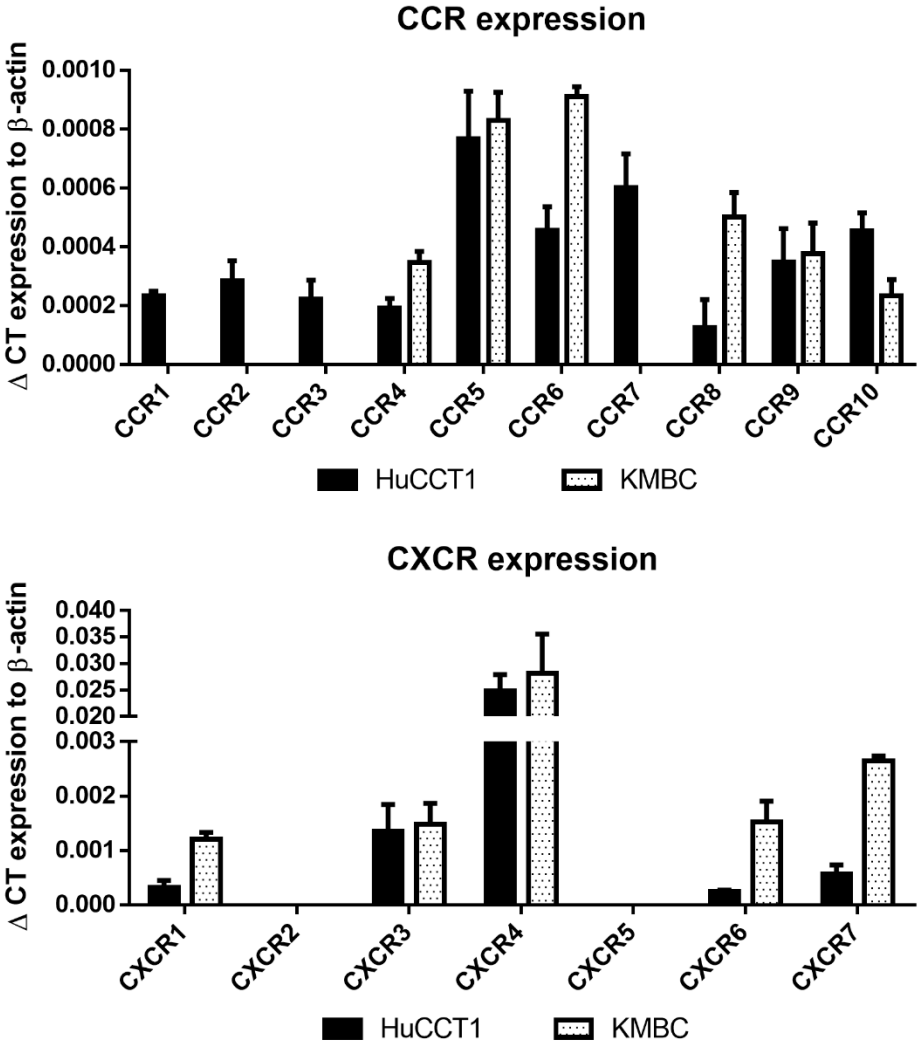

Figure 3.30 CCR and CXCR subtype mRNA expressions in HuCCT1 and KMBC cells as determined by qRT-PCR.

Human activated peripheral blood mononuclear cells (PBMCs) served as positive controls. Data presented as mean ± SD of these determinations.

3.3.2 Altered CCR5 Activity and CCA Cell Proliferation

As one of the most abundantly expressed CCR subtypes, the effects of the CCR5 antagonist Maraviroc, agonist RANTES and Maraviroc/RANTES combination on I-CCA and E-CCA cell proliferation were explored.

As shown in Figures 3.31 and 3.32, in HuCCT1 cells, there were no concentration-dependent alterations in cell proliferation with Maraviroc, RANTES or Maraviroc/RANTES. However, in KMBC cells (Figures 3.33 and 3.34), proliferation was inhibited at the highest concentration of Maraviroc (1000 nM) and increased at all RANTES concentrations higher than 1 ng/mL with maximum increases occurring at 20 ng/mL. Based on these findings, all further experimentation was performed at a Maraviroc concentration of 1000 nM, RANTES 20 ng/mL and Maraviroc/RANTES (1000 nM/20 ng/mL).

The time-dependent effects of Maraviroc, RANTES or Maraviroc/RANTES on proliferation are provided in Figures 3.35-3.38. There was no time-dependent effect of Maraviroc on HuCCT1 cell proliferation over six days (Figure 3.35). In RANTES exposed HuCCT1 cells, proliferation was also not affected over the six-day period compared to the non-RANTES exposed control (Figure 3.36).

In KMBC cells, an inhibitory effect of Maraviroc on cell proliferation was evident on days 3 and 6 ($p<0.05$ and 0.0001 respectively) (Figure 3.37), whereas RANTES increased cell proliferation over the six days of exposure with significant increases relative to day 1 (Figure 3.38). In the

presence of both Maraviroc and RANTES, the inhibitory effects of Maraviroc and increased proliferation with RANTES were no longer evidence in KMBC cells (Figure 3.39).

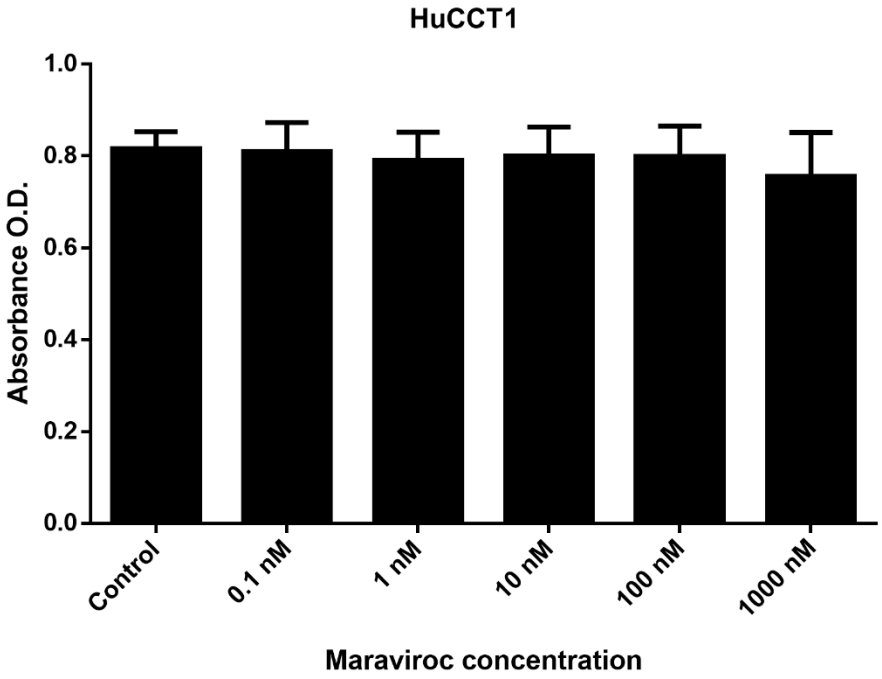

Figure 3.31 Dose-dependent effects of a CCR5 antagonist on HuCCT1 cell proliferation. HuCCT1 cells were exposed to the CCR5 antagonist Maraviroc in a range of 0.1 to 1000 nM for 3 days. Data are expressed as the absolute absorbance reading of cells in each group. Data presented as mean ± SD.

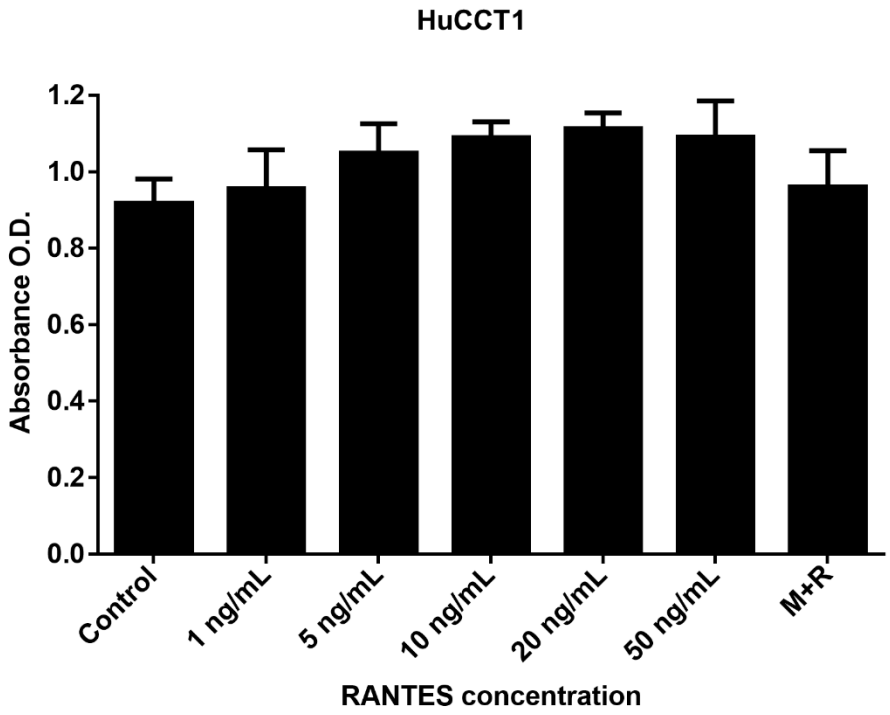

Figure 3.32 Dose-dependent effects of a CCR5 agonist on HuCCT1 cell proliferation. HuCCT1 cells were exposed to the CCR5 agonist RANTES in a range of 1 -50 ng/mL for 3 days. Data are expressed as the absolute absorbance reading of cells in each group. Data presented as mean ± SD.

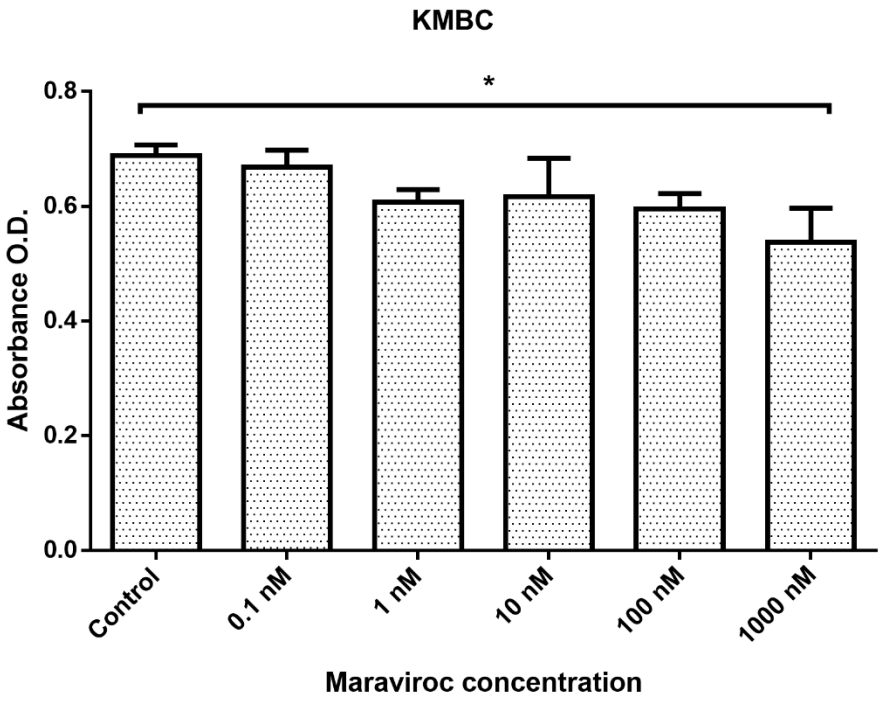

*Figure 3.33 Dose-dependent effects of a CCR5 antagonist on KMBC cell proliferation. KMBC cells were exposed to the CCR5 antagonist Maraviroc in a range of 0.1 to 1000 nM for 3 days. Data are expressed as the absolute absorbance reading of cells in each group. Data presented as mean ± SD. *: $p<0.05$.*

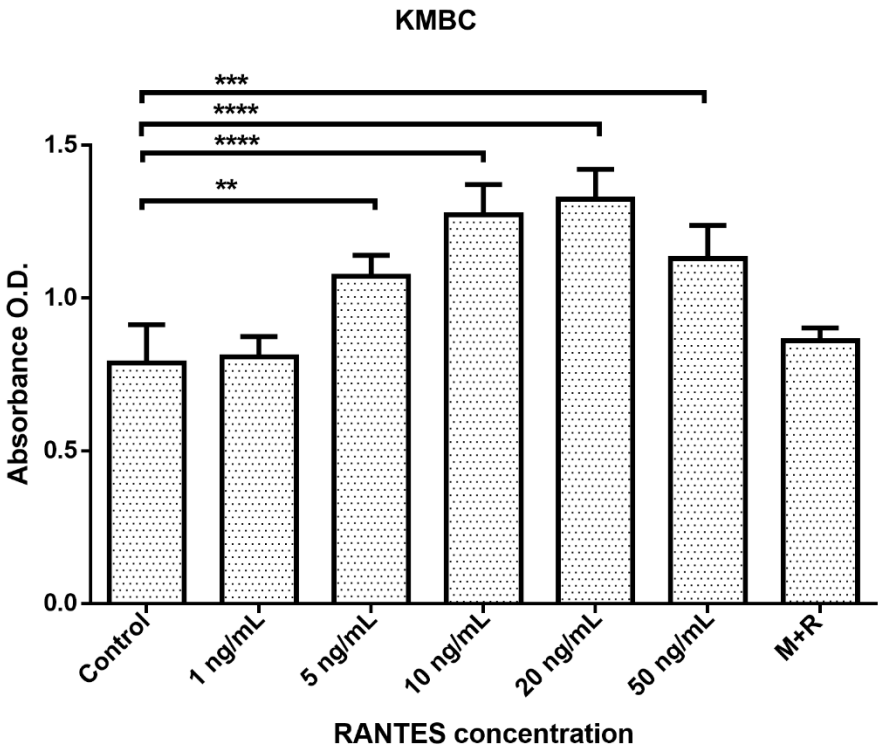

Figure 3.34 Dose-dependent effects of a CCR5 agonist on KMBC cell proliferation.

*KMBC cells were exposed to the CCR5 agonist RANTES in a range of 1 -50 ng/mL for 3 days. Data are expressed as the absolute absorbance reading of cells in each group. Data presented as mean ± SD. **: p<0.01, ***: p<0.001, ****: p<0.0001.*

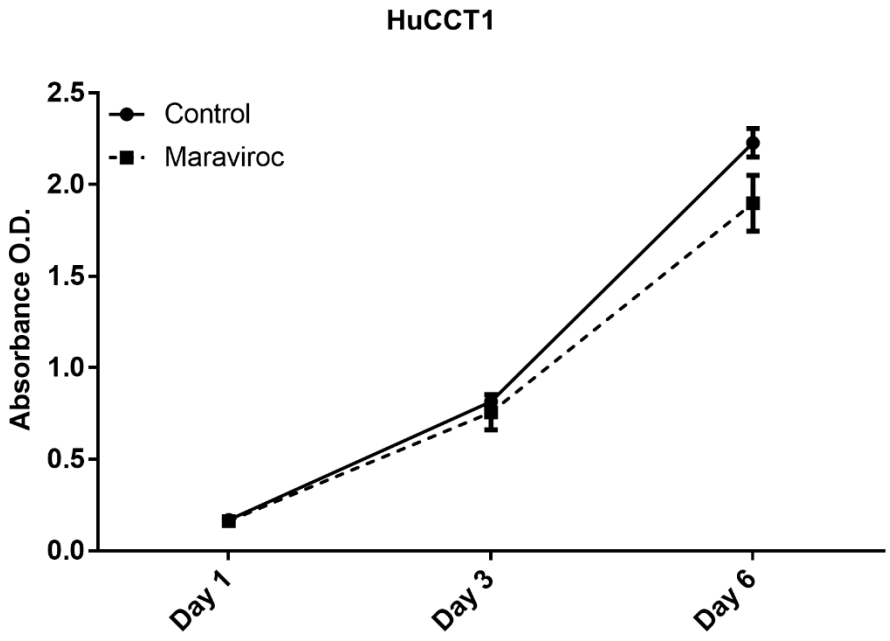

Figure 3.35 Time-dependent effects of a CCR5 antagonist on HuCCT1 cell proliferation. HuCCT1 cells were exposed to Maraviroc at a constant concentration of 1000 nM for 1, 3, and 6 days. Data are expressed as the absolute absorbance reading of cells in each group. Data presented as mean ± SD.

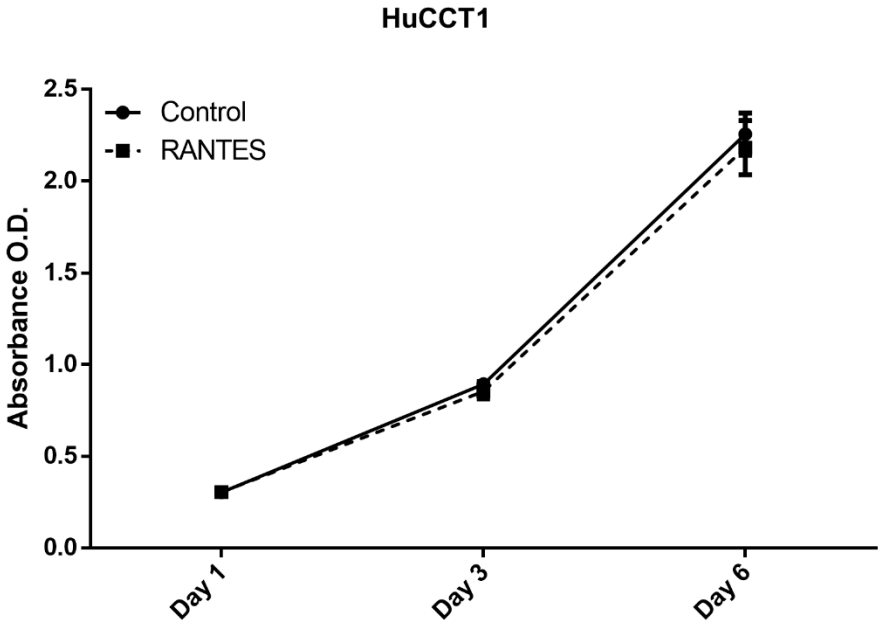

Figure 3.36 Time-dependent effects of a CCR5 agonist on HuCCT1 cell proliferation. HuCCT1 cells were exposed to RANTES at a constant concentration of 20 ng/mL for 1, 3, and 6 days. Data are expressed as the absolute absorbance reading of cells in each group. Data presented as mean ± SD.

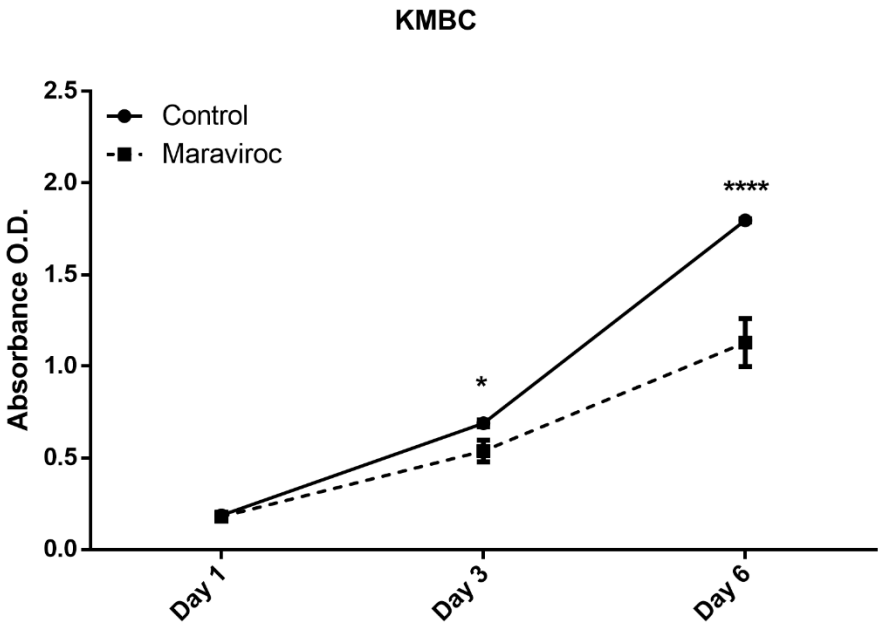

*Figure 3.37 Time-dependent effects of a CCR5 antagonist on KMBC cell proliferation. KMBC cells were exposed to Maraviroc at a constant concentration of 1000 nM for 1, 3, and 6 days. Data are expressed as the absolute absorbance reading of cells in each group. Data presented as mean ± SD. *: p<0.05, ****: p<0.0001.*

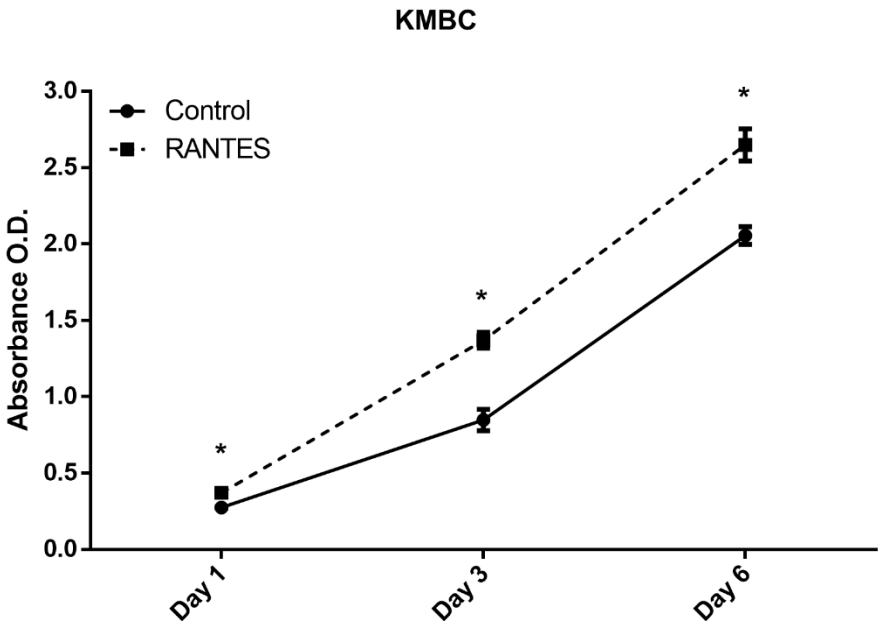

*Figure 3.38 Time-dependent effects of a CCR5 agonist on KMBC cell proliferation. KMBC cells were exposed to RANTES at a constant concentration of 20 ng/mL for 1, 3, and 6 days. Data are expressed as the absolute absorbance reading of cells in each group. Data presented as mean ± SD. *: $p<0.05$.*

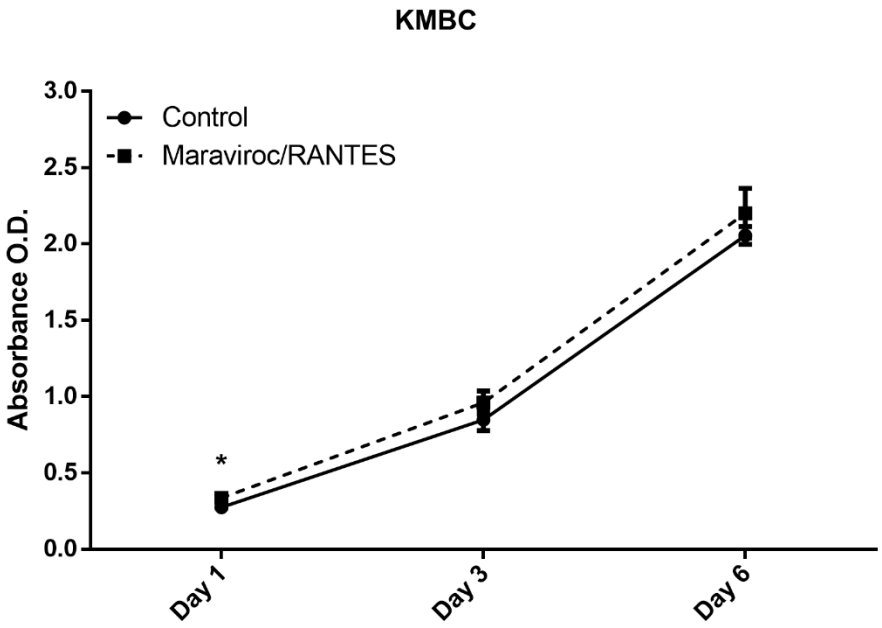

Figure 3.39 Time-dependent effects of CCR5 antagonist and agonist combination on KMBC cell proliferation.

*KMBC cells were exposed to constant concentration of 1000 nM Maraviroc and 20 ng/mL RANTES for 1, 3, and 6 days. Data are expressed as the absolute absorbance reading of cells in each group. Data presented as mean ± SD. *: $p<0.05$.*

3.3.3 Altered CCR5 Activity and CCA Spheroid Formation

Figures 3.40 and 3.41 demonstrate the results of spheroid formation in HuCCT1 and KMBC cells following exposure to Maraviroc, RANTES, or Maraviroc/RANTES. Neither Maraviroc, RANTES nor Maraviroc/RANTES altered spheroid information in HuCCT1 cells (Figure 3.40).

In KMBC cells, spheroid formation was significantly inhibited following exposure to Maraviroc (Day 3 dimensions for Maraviroc: 145±6 μm versus control: 245±11 μm, $p<0.0001$; Day 6: Maraviroc: 171±18 μm versus control: 323±24 μm, $p<0.0001$), while RANTES alone had no effect. In the presence of both Maraviroc and RANTES (Maraviroc/RANTES), the inhibitory effect of Maraviroc alone was no longer evident (Figure 3.41).

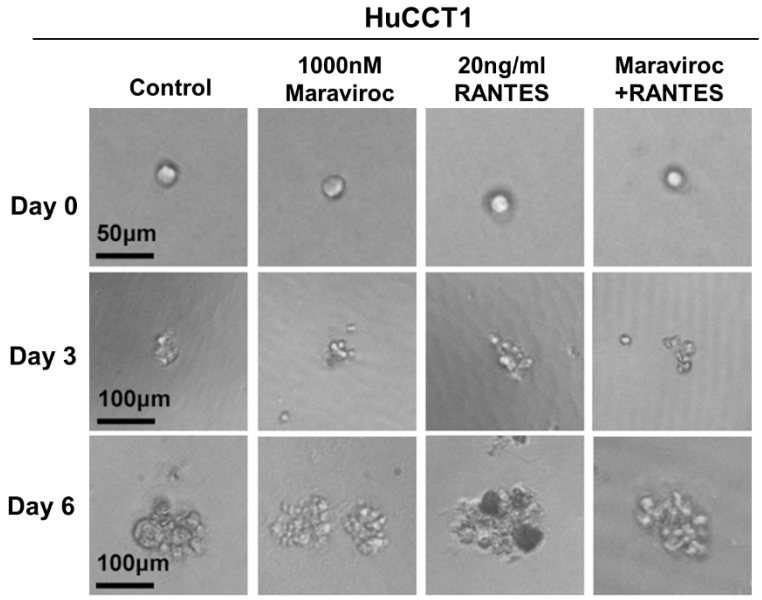

Figure 3.40 Spheroid formation by HuCCT1 cells with altered CCR5 activity.

HuCCT1 cells formed spheroids in the presence of a CCR5 antagonist Maraviroc (1000 nM), agonist RANTES (20 ng/mL), and Maraviroc/RANTES combination (1000 nM/20 ng/mL). Cells were seeded at densities of 200 cells /well in ultra-low 96-well plates to generate spheroids. The dimensions of spheroid formation in HuCCT1 were not influenced visually by Maraviroc, RANTES, or Maraviroc/RANTES. Scale bar: 50 µm and 100 µm.

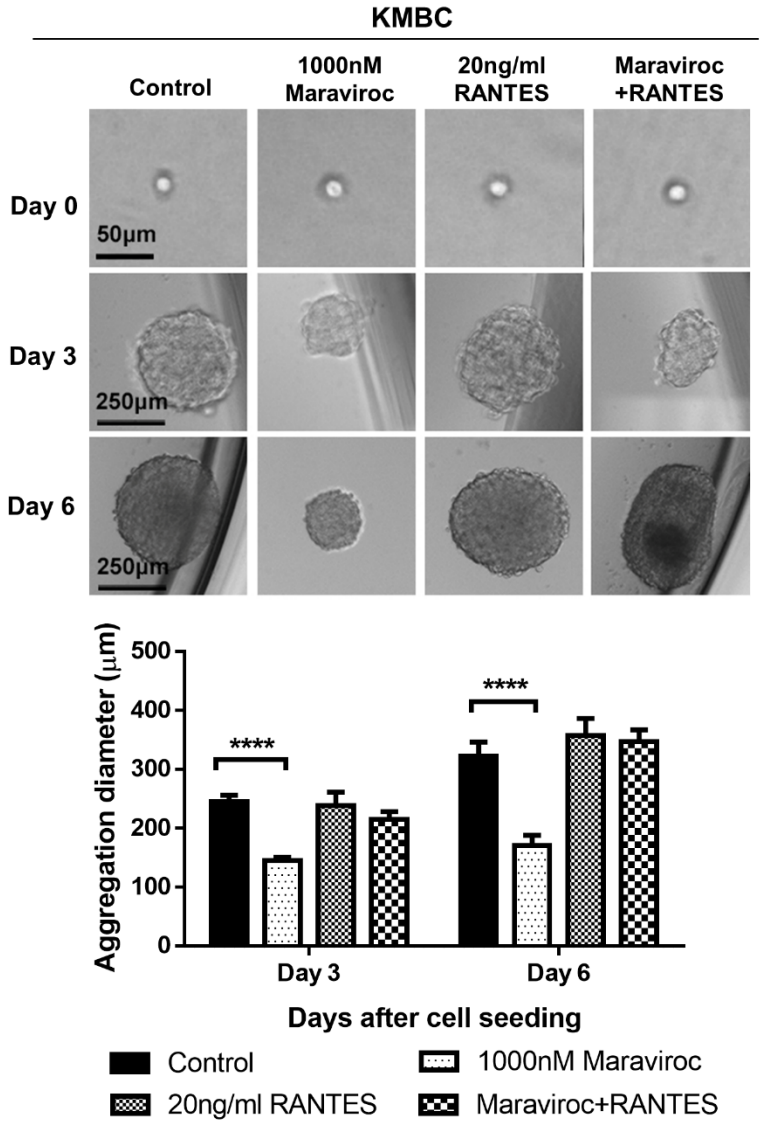

Figure 3.41 Spheroid formation by KMBC cells with altered CCR5 activity.

KMBC cells formed spheroids in the presence of a CCR5 antagonist Maraviroc (1000 nM), agonist RANTES (20 ng/mL), and Maraviroc/RANTES combination (1000 nM/20 ng/mL). Cells were seeded at densities of 200 cells /well in ultra-low 96-well plates to generate spheroid. Upper panel: Large aggregates of KMBC cells developed following seeding. The presence of Maraviroc, inhibited cell aggregation. Scale bar: 50 µm and 250 µm. Lower panel: The

*diameters of cell aggregation were measured by software ImageJ. Data presented as mean ± SD. ****: p<0.0001.*

3.3.4 Altered CCR5 Activity and CCA Cell Migration

The effects of Maraviroc, RANTES and Maraviroc/RANTES on cell migration were documented by the wound healing assay (Figures 3.42 and 3.43). In HuCCT1 cells Maraviroc inhibited cell migration at 12 hours, while RANTES had no significant effect. The inhibitory effect of Maraviroc was no longer evident in the presence of Maraviroc/RANTES (Figures 3.42). In KMBC cells, inhibition of Maraviroc at 12 and 24 hours was observed but the differences did not reach statistical significance. Increases in migration occurred with RANTES exposure at both time intervals. In the presence of Maraviroc, the increases associated with RANTES were no longer evident (Figure 3.43).

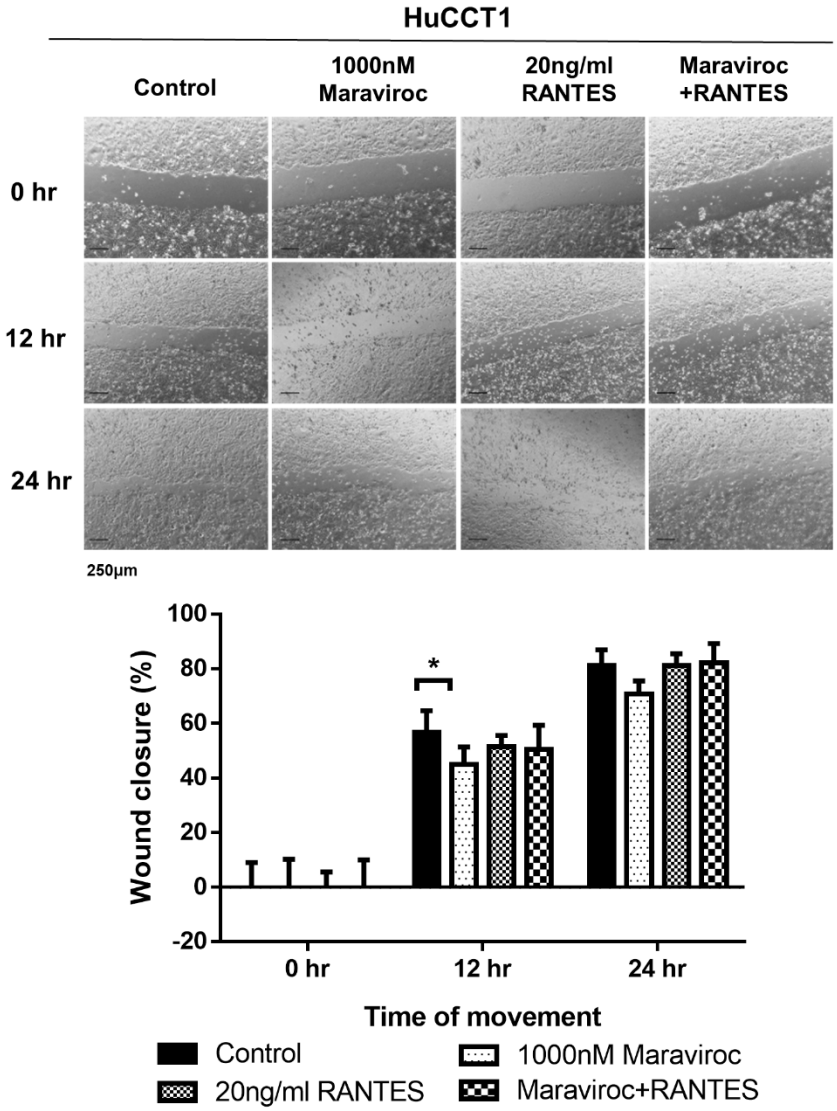

Figure 3.42 Migration of HuCCT1 cells with altered CCR5 activity.

Cell migration of HuCCT1 after exposure to a CCR5 antagonist Maraviroc (1000 nM), agonist RANTES (20 ng/mL) and Maraviroc/RANTES combination (1000 nM/20 ng/mL).

*Upper panel: phase contrast of cell migration was photographed at 0, 12, and 24 hours after scratching. Scale bar: 250 µm. ImageJ analysis of cell migration was determined by measuring area closure from phase-contrast images. Data presented as mean ± SD. *: $p<0.05$.*

October 18th, 2019

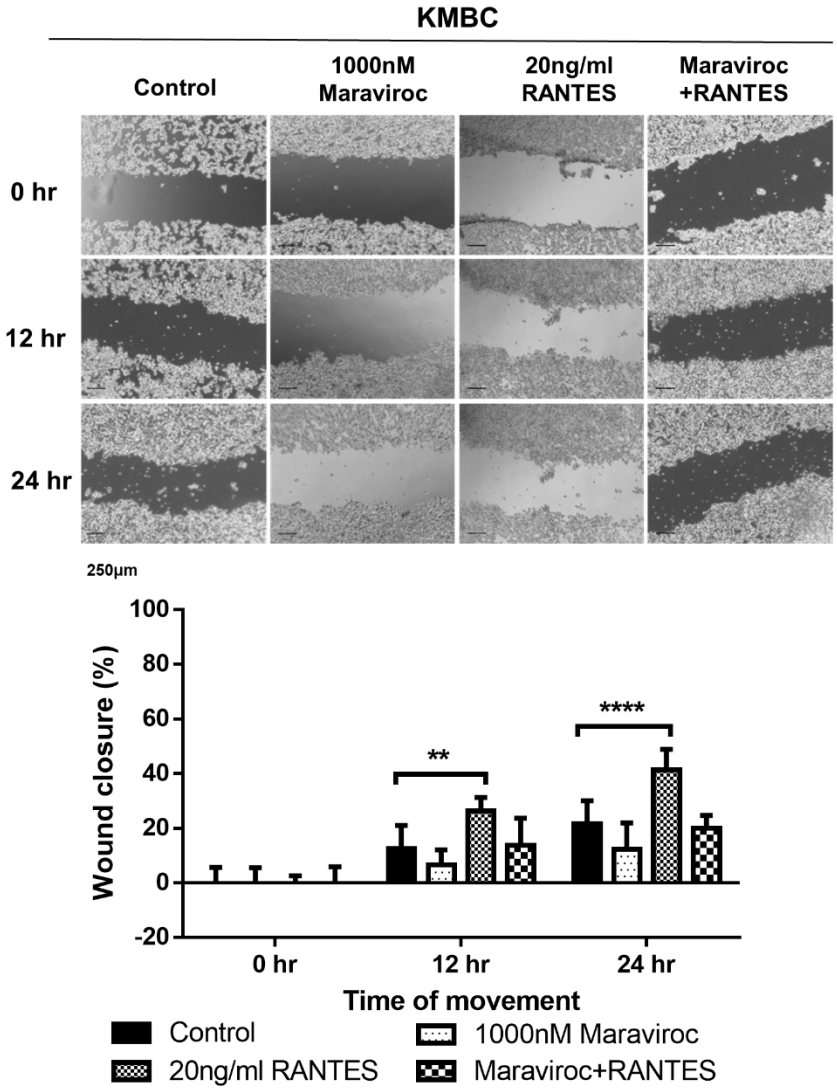

Figure 3.43 Migration of KMBC cells with altered CCR5 activity.

Cell migration of KMBC after exposure to a CCR5 antagonist Maraviroc (1000 nM), agonist RANTES (20 ng/mL) and Maraviroc/RANTES combination (1000 nM/20 ng/mL).

Upper panel: phase contrast of cell migration was photographed at 0, 12, and 24 hours after scratching. Scale bar: 250 µm. ImageJ analysis of cell migration was determined by measuring

*area closure from phase-contrast images. Data presented as mean ± SD. **: p<0.01; ****: p<0.0001.*

3.3.5 Altered CCR5 Activity and CCA Invasion

Regarding cell invasion, HuCCT1 and KMBC cells were seeded in the upper chamber of an 8.0 μm pore membrane Transwell as previously described (see Methods). Medium with either Maraviroc, RANTES, and Maraviroc/RANTES was loaded in the lower chamber. Cells were allowed to migrate for 24 hours. The results described in Figure 3.44 indicate that Maraviroc inhibited the migration of HuCCT1 cells ($p<0.05$), whereas RANTES had no effect. The inhibitory effect of Maraviroc was no longer evident in the presence of RANTES (Maraviroc/RANTES).

In KMBC cells, Maraviroc inhibited while RANTES increased cell invasion (Figure 3.45). Of note, the increase observed with RANTES persisted in the presence of Maraviroc.

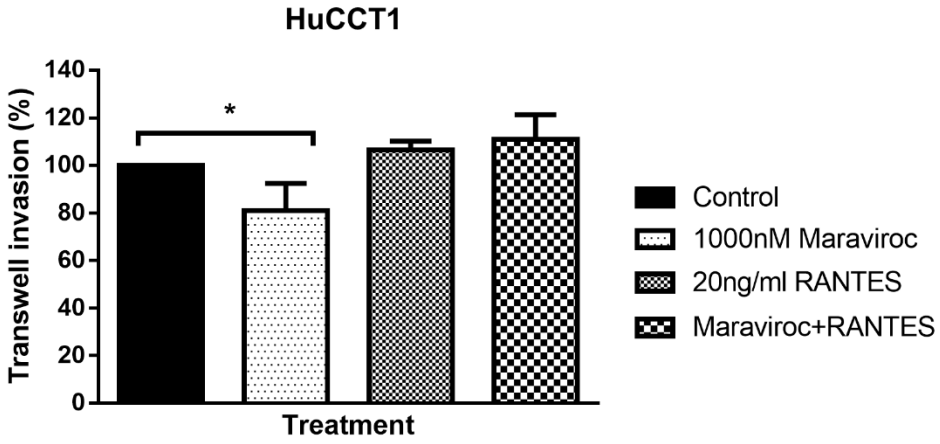

Figure 3.44 Cell invasion of HuCCT1 cells.

*Results were obtained from Transwell invasion chambers, in the presence of Maraviroc (1000 nM), RANTES (20 ng/mL) and Maraviroc/RANTES combination (1000 nM/20 ng/mL). Data presented as mean ± SD. *: $p<0.05$.*

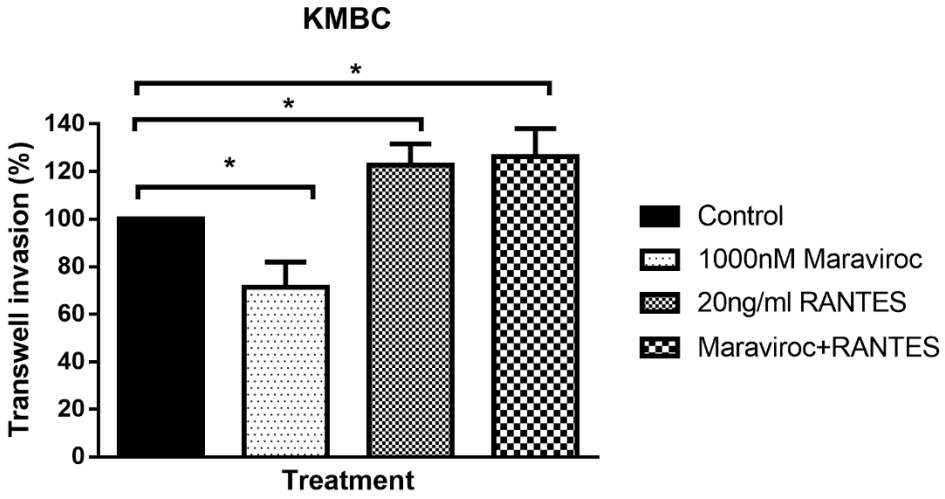

Figure 3.45 Cell invasion of KMBC cells

*Results were obtained from Transwell invasion chambers, in the presence of Maraviroc (1000 nM), RANTES (20 ng/mL) and Maraviroc/RANTES combination (1000 nM/20 ng/mL). Data presented as mean ± SD. *: $p<0.05$.*

4. DISCUSSION

4.1 Differences in Tumor Biology and CSCs

Numerous previous clinical studies have documented significant differences in I-CCA and E-CCA growth patterns. Specifically, I-CCAs form masses with well demarcated nodules that grow in a radial pattern. Less often, they are sclerosing or polypoid in nature. Microscopically, ductular morphology with mucin production or features of hepatocellular differentiation may be present. On the other hand, E-CCAs tend to be sclerosing or polypoid and non-mucin producing (Komuta et al., 2012; Nakanuma & Sato, 2012). They tend to grow within bile duct lumens, along the bile duct wall or parallel to adjacent tissue planes. In addition, the derivation of I-CCA and E-CCA differs with I-CCA thought to be derived from malignant transformation of hepatic stem cells (Bragazzi et al., 2018; Cardinale et al., 2013), whereas E-CCAs are thought to develop from epithelial to mesenchymal transformation of ductular cholangiocytes or cells within peribiliary glands (Nakanuma & Sato, 2012).

The results of this research suggest some of the differences observed could result from intrinsic differences in I-CCA and E-CCA tumor cell biology. Specifically, I-CCA cell proliferation and invasion were increased in I-CCA compared to E-CCA and non-malignant cholangiocytes. These findings could help to explain the more aggressive clinical course observed in I-CCA versus E-CCA patients. On the other hand, no differences in spheroid/colony formation and migration were observed.

The reasons for the lack of consistent differences in biological features may be multifactorial. For example, certain cell lines may have been misclassified. The current anatomic location-based classification is based on different guidelines, which may provide different definitions of CCA subtypes in clinics and derived samples. In general, classification and staging of CCA are defined by guidelines published from the American Joint Committee on Cancer (AJCC), Union for International Cancer Control (UICC), World Health Organization (WHO) and/or the Liver Cancer Study Group of Japan (LCSGJ). Although these institutions have reached a general consensus on the primary site of I-CCA (from the segmental bile ducts to the ductules) and d-CCA (from common bile duct and near the head of the pancreas), the definition of p-CCA is controversial. Based on the UICC guideline, p-CCA is defined as a cancer arising from the cystic duct into the extrahepatic biliary tree. However, the WHO offers that perihilar CCA, also called Klatskin tumors, develop from the right and left hepatic ducts near their junction but do not include the cystic bile duct insertion. P-CCA in the WHO classification renders it unclear whether that P-CCA originates from intrahepatic large bile ducts (*International classification of diseases for oncology (ICD-O-3.1)*, 2011). Secondly, a diagnosis of CCA is usually established at an advanced stage, where the primary site, especially of p-CCA, is difficult to determine whether originally I-CCA or E-CCA. Approximately 30% to 40% of CCA cases are classified as "site not otherwise specific" ducts (*International classification of diseases for oncology (ICD-O-3.1)*, 2011). Thirdly, by the continuous update of ICD codes, the classification of CCA has changed with time and following different versions of codes provide different CCA classifications. These controversies are relevant to efforts undertaken to distinguish differences in clinical features and cell biology in I-CCA versus E-CCA. In the current study, the cell lines employed were derived from different patients with

various disease stages and different institutions in different timelines. Thus, the variability in results could reflect differences in tumor subtype classifications.

Another consideration is that cellular origin rather than anatomy may be more responsible for the distinct tumor features (Cardinale et al., 2012; Komuta et al., 2012). Relevant to this possibility are reports that CCAs may originate from hepatic stem cells; non-mucin-producing cuboidal cholangiocytes in the canals of Hering; peribiliary glands; or the surface epithelium of bile ducts (Bragazzi et al., 2018; Cardinale et al., 2013). These different origins may manifest different phenotypic behaviors and prognosis in the clinical setting. Moreover, CCA subtypes based on anatomic location may present different phenotype and vice versa. For example, some p-CCAs are developed from mucin-secreting cholangiocytes or peribiliary glands (Nakanuma & Sato, 2012), and I-CCAs can be further classified into small bile duct (non-mucin) or mixed I-CCAs and large bile duct (mucin) I-CCAs (Komuta et al., 2012). In these instances, both I-CCAs and E-CCAs may consist of non-mucin and mucin secreting phenotypes. With these considerations in mind, Komuta et al (2008) has proposed classifying CCAs according to the maturation grade of the original cells as primary liver parenchymal CCA and primary biliary CCA.

In the present study, either I-CCA or E-CCA cells exhibited diverse cell migration capacities and showed no significant differences amongst cell subpopulations. A major concern of this finding is that the cell migration demonstrated by wound healing assays might be influenced by overall cell proliferation effects (C. C. Liang et al., 2007). Specifically, CCLP-1 and HuCCT1 cells had similar capacities in cell proliferation and migration, while HuCCT1 invaded two-fold as many

cells as CCLP-1 by the Transwell invasion assay. Additionally, cells with different morphologies could also affect the time to complete wound closure. The results demonstrated that SG231 had higher abilities of cell proliferation and invasion, but it completed the wound closure in 72 hours as the second lowest migrating CCA cell line. This finding could be explained by its stacked morphology when growing on culture plates.

Yet another consideration is that the interaction between stromal cells and CCAs. This possibility is supported by previous studies wherein CCA cell lines exhibited different tumorigenicity in nude mice compared to their original tumors (Shimizu et al., 1992). For example, the I-CCA cell line; CCLP-1 formed more highly differentiated tumors in nude mice than the original tumor which grew in a more glandular structure. Moreover, the E-CCA, HuH28 cell line, is not at all tumorigenic in nude mice (Kusaka et al., 1988), and KMBC cells develop less differentiated tumors than the original tumor and grow in a smaller glandular formation with few fibrous structures (Yano et al., 1992). Not to be ignored, however, are other studies wherein SG231 cells generated histologically similar tumors in nude mice compared to the original tumor sources (Storto et al., 1990). Thus, the tumor microenvironment appears to play an important role in tumor behavior. Thus, the specific component(s) of the tumor microenvironment responsible for these properties need to be identified. Because tumor stroma, chemokines, bile salts, and micropeptides influence CCA tumor biology (Banales et al., 2019; Leyva-Illades, McMillin, Quinn, & Demorrow, 2012; Sombattheera et al., 2015), these variables should be studied in future experiments.

Finally, the prevalence of CSCs and the SCSM profiles they express could have impacted on the findings of I-CCA versus E-CCA tumor cell biology. Although the prevalence of CSCs as defined by the expression of SCSM markers was similar in I-CCA and E-CCA cell lines, there was pronounced heterogeneity with respect to the SCSMs being expressed including CD13 (Haraguchi et al., 2010), CD44 (Gu & Choi, 2014), and CD90 (Sukowati et al., 2013), CD133 (Nakanuma & Sato, 2012) and EpCAM (Sulpice et al., 2014). In the present study, most of these markers were expressed at high levels in one or the other cell line. For example, 99% of SG231 (I-CCA) cells were EpCAM positive and 48% CD90 positive, while other makers were present in less than 20% of these cells. In the E-CCA cell line HuH28, 91% expressed CD44, 88% CD13, 46% CD24, 69% CD90 and less than 2% CD133 and EpCAM positive. An interesting finding was obtained with respect to EpCAM expression in these cells. EpCAM is considered as a cholangiocyte marker (B. Li et al., 2017). In the current study, CCLP-1, HuH28, KMBC and H69 were EpCAM negative. Although the precise explanation for this remains to be determined, a possible reason is that some of the cell lines might be "transdifferentiated" from hepatocytes (Doffou et al., 2018; J. Wang et al., 2018). Notwithstanding these differences, there was no clear suggestion that I-CCA or E-CCA cell lines have a predominance of certain SCSMs. Moreover, there were no associations between SCSMs and tumor cell biology. Overall, the results indicate the prevalence of CSCs and SCSM profiles are similar in I-CCA and E-CCA cells and hence, are unlikely to explain the different growth features of these tumors.

It should be noted that spheroid/colony formation and migration in non-malignant H69 cholangiocytes were similar to CCA cell lines. This finding is in keeping with those previously

described for malignant versus non-malignant cells (Hanahan & Weinberg, 2011) and could be explained by the transformed phenotype of normal cholangiocytes. Indeed, the H69 cell line is an SV40 immortalized cholangiocyte cell line with inherent anti-apoptotic properties. Thus, they are not "normal" cells. As demonstrated in spheroid and soft-agar colony formation, where H69 cells formed spheroids and colonies in an anchorage-independent culture (Pipas, 2009).

There are a number of limitations to this research that warrant emphasis. First, although I-CCA and E-CCA cell lines were defined according to current standards, various differences in classifying I-CCA and E-CCA, particularly for cells derived from tumors within the hilar region of the liver render such definitions not absolute. Second, limited CCA cell sources and SCSMs were employed in investigating tumor growth properties and CSC prevalences and SCSM profile. Thus, type I or II errors may have occurred when analyzing correlations. Finally, *in vivo* studies are required to compare the relative contributions of tumor cells and the microenvironment to tumor growth. Such experimentation is also required to identify the specific features within the tumor microenvironment responsible for any differences observed.

In summary, although I-CCA cell populations exhibit more proliferative activity, shortened doubling times, and more invasive properties than E-CCA cells, other tumor cell properties are similar in the two cell populations. In addition, the prevalences of CSCs and SCSM profiles expressed within these cells are similar and do not associate with tumor subclass or biology. Overall, these findings suggest that both intrinsic tumor biology and the tumor microenvironment play important roles in determining the course of I-CCA and E-CCA in humans.

4.2 I-CCA and E-CCA Chemoresistance

A key feature of CCA is its relative resistance to chemotherapy. As discussed previously, several factors contribute to this chemoresisitance. Principal amongst these is the expression of drug efflux pumps such as MRPs within the tumor. Although overexpression of specific MRP subtypes have been described in a number of human tumors, to date, there have been no reports describing the complete MRP expression profile in CCA. Thus, the current study documented mRNA expression profiles of MRP1-6 for both I-CCA and E-CCA cell lines. The expression levels of MRPs varied amongst these cells. Specifically, SG231 and HuH28 cells expressed mRNA of all MRPs, while other cell lines expressed varied MRP subtypes prior to chemotherapeutic exposure.

Although there is limited benefit of anticancer drugs for CCAs, gemcitabine-based regimens are the standard first-line chemotherapy for advanced disease (Morizane et al., 2018). Gemcitabine, also known dFdC (2′, 2′-difluorodeoxycytidine), is a commonly used anticancer agent for various solid tumors (Wong, Soo, Yong, & Innocenti, 2009). It is a deoxycytidine nucleoside analog mainly inhibiting DNA synthesis and blocking G1/S-phase transition during cell cycle progression (Huang, Chubb, Hertel, Grindey, & Plunkett, 1991). In the clinical setting, gemcitabine is administered at doses ranging from 800 mg/m^2 to 1,000 mg/m^2, resulting in an average peak concentration (C_{max}) of 100 μM (Fujiwara et al., 2015). Thus, in most *in vitro* studies, a concentration range including 100 μM is typically employed.

The results obtained in the described experiments suggest that CCA cell lines were differentially sensitive to gemcitabine in a concentration-dependent manner and at concentrations similar to those achieved *in vivo* during the treatment of CCA in patients (Park et al., 2015). This apparent paradox of *in vitro* sensitivity and *in vivo* resistance highlights the importance of drug delivery systems and/or the *in vivo* tumor microenvironment. They also raise concerns about the extrapolation of *in vitro* findings to clinical outcomes.

Notwithstanding the adobe reservations, in our experiments I-CCA cells were more resistant to gemcitabine than E-CCA cells. This finding supports clinical outcomes wherein patients with I-CCA tend to be more resistant to chemotherapy than E-CCA patients, although different chemotherapeutic agents were used in the two patient populations (Gabriel et al., 2017). The explanation for this finding may relate to the CCA cell lines employed in the present study. Specifically, in excess of 90% of HuCCT1 cells express SCSMs as compared to less than 5% of KMBC cells (Part I) and it is well established that CSC cells are more chemoresistant than mature cancer cells (J. Zhao, 2016). Moreover, different gradients of MRP5 or MRP6 knockdown correlated within the extent of gemcitabine-sensitivity. These findings suggest MRP5 and/or MRP6 contribute to acquired gemcitabine resistance in I-CCA and E-CCA.

Following gemcitabine exposure, upregulation of specific MRPs including MRP1, MRP5 and MRP6 in CCAs were observed, suggesting these MRPs in particular, may be involved in gemcitabine elicited resistance. Most striking were significant increases in MRP5 and/or MRP6 abundance in all CCA cells studied. MRP1 is the most extensively studied MRP and is found in most normal tissues and cancers. The drug efflux capacity of MRP1 has been demonstrated in

different diseases, including clinical depression, epilepsy, and solid cancers. In cancer studies, it has been widely reported that MRP1 mediates resistance to a number of therapeutic agents, such as doxorubicin, methotrexate, vincristine and etoposide (J. F. Lu, Pokharel, & Bebawy, 2015). More recently, MRP5 and/or MRP6 have emerged as specific targets in drug resistant cancers. MRP5 is a nucleoside transporter, which can mediate the efflux of 3',5'-cyclic nucleotides, cAMP and cGMP (Jedlitschky, Burchell, & Keppler, 2000; Wielinga et al., 2003). Although there have been no previous reports documenting MRP5 expression and its potential role in CCA, MRP5 associated gemcitabine-induced resistance has been described in pancreatic cancers (Hagmann, Jesnowski, & Lohr, 2010). MRP6, a homologue of MRP1, is highly expressed in liver and kidney but minimally expressed in other tissues. The role of MRP6 in chemotherapeutic agent associated resistance has not been investigated.

The post-exposure MRP findings described differ somewhat from those reported by Rau et al (2008) and Cirqueira et al. (2018) who described significant induction of MRP2 and MRP3 expression in human CCA tissues and MRP1-3 mRNA expression in a human CCA cell line following exposure to chemotherapeutic agents (Tepsiri et al., 2005). Although the precise explanation for the discrepancy remains to be determined, perhaps differences in the chemotherapeutic agents (doxorubicin and/or pararubicin versus gemcitabine) and/or the CCA cell lines employed are relevant (Rogers et al., 2014).

Inhibition of gene expression can be achieved by several strategies including RNA interference (RNAi) with exogenous siRNA. However, naked siRNA is easily degraded by plasma nucleases

and therefore, several RNAi delivery systems have been developed. One of the most effective of these is the lentiviral shRNA delivery system (Singer & Verma, 2008). In the present study, in excess of 80% of gemcitabine-induced upregulation of MRP5 and MRP6 mRNA and protein expressions in HuCCT1 cells and MRP5 in KMBC cells were inhibited by lentiviral shRNA constructs. When considering this approach to CCA treatment (i.e. inhibition of MRP expression), it will be important to determine whether pharmacologic agents can achieve similar efficacy. Moreover, different gradients of MRP5 or MRP6 knockdown correlated within the extent of gemcitabine-sensitivity. These findings suggest MRP5 and/or MRP6 contribute to acquired gemcitabine resistance in I-CCA and E-CCA.

In terms of the potential clinical relevance of these findings, it is important to note that following MRP6 knockdown, significant eradication of HuCCT1 and KMBC cells was achieved with a gemcitabine concentration of 100 μM, which as mentioned earlier, is well within the range achieved in humans treated with this agent (Fujiwara et al., 2015). Overall, gemcitabine-based regimens may benefit from inhibiting the expression of certain MRPs.

CSCs are responsible for chemoresistance in tumors due in large part to overexpressed ABC transporters and/or their upregulation after exposure to chemotherapeutic agents (Dean, 2009). By correlating gemcitabine-induced cytotoxicity as well as MRP profiles prior to and following exposure to gemcitabine to CSC prevalence and SCSM expression, upregulation of MRP6 at both 24 and 48 hours was significantly associated with CD133 expression (Table 4-1). This

suggests that CD133 expression may serve as an indicator to predict, or be involved in MRP6 regulated chemoresistance. Although such a correlation has not been reported previously in cancer, the expression of CD133 does influences the activity of several ABC transporters in anticancer agent induced cytotoxicity (Angelastro & Lame, 2010; Z. Zhu et al., 2010).

In summary, I-CCA and E-CCA cells demonstrated different patterns of MRP expression. Following exposure to gemcitabine, MRP5 and MRP6 expression were significantly upregulated in representative I-CCA and E-CCA cells. Inhibiting such upregulation rendered each cell population more sensitive to gemcitabine cytotoxicity. Thus, further research is warranted to determine whether inhibition of MRP6 expression in I-CCA and MRP5 in E-CCA are of value in the treatment of human CCA.

Table 4-1 Correlations between gemcitabine-induced cytotoxicity, MRP expression prior to and following exposure to gemcitabine, CSC prevalence, and SCSMs in CCA cells.

p-value of correlation	CD13	CD24	CD44	CD90	CD133	EpCAM
Chemoresistance	0.432754	0.574217	0.324501	0.760346	0.82405	0.367022
MRP1	0.972114	0.728055	0.891627	0.353785	0.367213	0.990237
MRP2	0.408656	0.524839	0.804751	0.898985	0.503605	0.371465
MRP3	0.523311	0.237033	0.807287	0.318077	0.540881	0.41205
MRP4	0.819711	0.437831	0.669287	0.312009	0.148367	0.695825
MRP5	0.679781	0.960724	0.926295	0.322911	0.938676	0.719079
MRP6	0.455975	0.694432	0.997063	0.308074	0.418386	0.710322
MRP1 24hr	0.703807	0.74401	0.769096	0.946902	0.308107	0.781416
MRP2 24hr	0.469996	0.587214	0.523536	0.798172	0.836446	0.431186
MRP3 24hr	0.152803	0.87688	0.434879	0.599214	0.208392	0.628749
MRP4 24hr	0.262065	0.159992	0.261609	0.711746	0.064869	0.17231
MRP5 24hr	0.816302	0.854366	0.731986	0.630588	0.568009	0.467792
MRP6 24hr	0.137589	0.398899	0.262388	0.604823	0.005352	0.359283
MRP1 48hr	0.440821	0.520283	0.538426	0.880631	0.217155	0.913288
MRP2 48hr	0.665157	0.794041	0.95724	0.267074	0.77647	0.909479
MRP3 48hr	0.120003	0.445361	0.254268	0.802433	0.241999	0.557311
MRP4 48hr	0.57568	0.238449	0.541036	0.737076	0.153325	0.042936
MRP5 48hr	0.717546	0.54922	0.71742	0.326117	0.088263	0.267501
MRP6 48hr	0.204847	0.341521	0.305177	0.539633	0.000941	0.289126

4.3 I-CCA and E-CCA Chemotaxis

CR is a superfamily found on cell surfaces that bind to chemokines. Beyond their functions of modulating immune trafficking and inflammation, CRs are also present on non-immune cells where they influence cell growth and migration (Charo & Ransohoff, 2006; Miyazaki et al., 2013). To determine whether CRs/chemokine interactions are involved in the features of CCA, a quantitative analysis of CR expression in representative I-CCA (HuCCT1) and E-CCA (KMBC) cells was performed.

Consistent with findings from other types of cancers, the CXCR family and CXCR4 in particular, were abundantly expressed in I-CCA and E-CCA cells. CXCR4 expression has been descried in a number of cell types, including lymphocytes, hematopoietic stem cells, normal tissues cells, and cancer cells (Guo et al., 2016). Recent studies have demonstrated that the CXCR4/CXCL12 axis is active in both human CCA tissues and cell lines (Leelawat et al., 2007). It has also been reported that inhibition of CXCR4 can successfully reduce CCA cell proliferation, metastasis, and neural invasion (Ohira et al., 2006; Tan et al., 2014; Y. Xie et al., 2016; S. Zhao et al., 2014), whereas overexpression of CXCR4 induces the capacity of cell invasion (Leelawat et al., 2013).

Regarding the CC motif of CCRs, there have been no previous reports documenting the complete CCR expression profile in human CCA tissues or cell lines. The current study revealed that CCA cells express CCRs at different levels. Of interest, the CCR expression profile detected in I-CCA

was similar to that described for HCC (C. M. Liang et al., 2015), which may reflect the common risk factors and/or origin of these tumors (Cardinale et al., 2012; Feng, 2015). Among the various CCRs, CCR5 were abundantly expressed in both I-CCA and E-CCA cells. This finding is in keeping with its high expression in chronic liver disease patients and tumor promotion properties in other tissues, where the mechanisms is thought to result from activation of mTOR and AKT pathways (Soria & Ben-Baruch, 2008; Weitzenfeld & Ben-Baruch, 2014).

The importance of CCR5 and/or its ligand CCL5 have previously been established in various malignancies, including breast, gastric and pancreatic cancers but not CCA (Gao et al., 2016; Mencarelli et al., 2013). To explore the function of CCR5 in CCAs, the current study employed both a CCR5 antagonist and agonist. Maraviroc is an FDA approved CCR5 antagonist that is used in the treatment of patients for HIV. As a treatment for cancer, Maraviroc has been described in pancreatic, gastric and HCC cancers (Mencarelli et al., 2013; Ochoa-Callejero et al., 2013; Singh et al., 2018). CCL5, also known as RANTES, is a ligand/agonist of CCR5. It has been suggested that CCL5 promotes tumor growth and metastasis by altering tumor associated macrophage populations, and enhancing angiogenesis (Azenshtein et al., 2002). Mesenchymal stem cell released CCL5 enhances breast cancer invasion and metastasis (Karnoub et al., 2007). In the current study, Maraviroc and RANTES altered tumor cell biology *in vitro* in a cell-specific manner. Specifically, Maraviroc inhibited cell proliferation, spheroid formation, and invasion in E-CCA cells but only migration and invasion in I-CCA cells.

A somewhat paradoxical finding was that I-CCA cell lines displayed a greater extent of cell proliferation and invasion compared to E-CCA cell lines, yet CR expression was more abundant in E-CCA cell lines and the effects of the CCR5 antagonist and agonist were more apparent in E-CCA cells. This might be explained by autocrine effects generated by the receptor and chemokine on the same cell, which may promote different behaviors of invasion and metastasis as has been described for the interaction between CCR5 and CCL5 in breast cancers (Khalid et al., 2015). Furthermore, metastatic tumor cell proliferation and spread depends in part on the release and response to autocrine and paracrine growth mechanisms. It is conceivable that an early stage of metastatic progression might be dominated by paracrine growth signals, while during later stages, metastasizing tumor cell spread and localization are influenced by autocrine growth signaling. Finally, at the end of the metastatic process, malignant cells might involve into an autonomous state without either paracrine or autocrine growth mechanisms being involved (Nicolson, 1993). Hence, the I-CCA and E-CCA cells employed in the current study may differ in their metastatic process and response patterns to CRs and other growth factors depending on their stage at the time of retrieval. Not to be overlooked is the effect of the tumor microenvironment on chemotaxis.

Somewhat surprisingly, RANTES did not eliminate KMBC cell invasion. This finding suggests the RANTES effect in this property may be CCR5-independent. It is also possible the results are concentration-dependent and higher concentrations of Maraviroc may have reversed the RANTES effect.

In terms of clinical relevance, the results of this research and those obtained with the commercially available CCR5 antagonist Maraviroc in particular, suggest that in CCA, therapeutic benefit might be derived from CCR5 inhibition. Such an approach has been applied to gastric cancers with some success (Mencarelli et al., 2013). The possibility is rendered more feasible by the fact the inhibitory concentration of Maraviroc (1000 nM) is well within the range reported in the blood of patients treated with this agent (Rosario et al., 2008). Also to be considered are recent findings that CCR5 antagonists may be of benefit in the treatment of primary sclerosing cholangitis, a condition associated with a significantly increased risk of CCA (Cheung, Lazaridis, LaRusso, & Gores, 2017).

Having demonstrated that HuCCT1 and KMBC cells possess different CCR expression profiles and respond differently to a CCR5 antagonist and agonist, the question arises as to why such differences exist. As indicated earlier, when analysed for differences in SCSM expression greater than 90% of HuCCT1 cells expressed SCSMs compared to less than 5% of KMBC cells. Given that the expression of certain SCSM has been associated with tumor cell biology, this could explain the differences observed. Clearly, further research is required to test this hypothesis.

There are a number of limitations to this aspect of the research that warrant emphasis. First, only one I-CCA and one E-CCA cell line were studied. Whether similar results would have been obtained with additional cell lines remains to be determined. Second, due to the lack of commercially available CCR antagonists other than Maraviroc, only the effects of CCR5 inhibition were documented. When available, results obtained with a CCR6 antagonist, the CCR subtype

expressed to the greatest extent in KMBC cells, will be of interest. Third, because CCR5 receptor inhibition and activation with Maraviroc and RANTES respectively have been documented in other cells studied to date (Velasco-Velazquez, Xolalpa, & Pestell, 2014), confirmation of the effects of these agents on receptor activity per se was not undertaken. Finally, the results reflect preliminary finding of an *in vitro* cell based system and additional studies in animal models of CCA are warranted.

In summary, the results of this research raise the possibility that differences in I-CCA and E-CCA behavior may reflect differences in CCR expression profiles. In general, exposure to a specific CCR5 antagonist inhibited while an agonist enhanced tumour cell growth. Additional studies are required to determine whether inhibition of CCR5 is effective in the treatment of CCA in humans.

5. GENERAL CONCLUSION AND SIGNIFICANCE

Overall, this study significantly extends our understanding of CCA and the distinction between I-CCA and E-CCA. I-CCA cell lines proliferated at a more rapid rate and demonstrated greater extents of invasiveness than E-CCA cells. Although I-CCA and E-CCA cells also expressed different SCSM profiles, no significant correlations were detected between tumor growth features and CSC prevalence or SCSMs. Upregulation of MRPs transporters occurred in both I-CCA and E-CCA cells following exposure to gemcitabine and knockdown of MRP5 and/or MRP6 enhanced gemcitabine induced cytotoxicity in I-CCA and E-CCA cells. The results also demonstrated that in addition to CXC motifs, CC motifs are also expressed on CCAs in a cell-specific manner and a commercially available CCR5 antagonist significantly inhibited CCA cell proliferation and invasion.

5.1 Knowledge Translation

CCA is characterized by aggressive growth as well as diagnostic and therapeutic challenges. Because CCA is an uncommon cancer, there are limited studies documenting the biological properties of CCA, specifically comparing tumor features of I-CCA to E-CCA. Therefore, an enhanced understanding of the tumor biology in I-CCA and E-CCA may uncover the pathological backgrounds and lead to the development of successful therapeutic approaches. By comparing tumor growth features, CSC prevalences and SCSM profiles in I-CCA and E-CCA cell lines, the findings indicate that intrinsic differences in cell biology exist but the tumor microenvironment also plays an important role in determining tumor growth. The importance of MRPs, particularly MRP5 and MRP6, in gemcitabine-induced resistance suggests that

employing MRP5 and/or MRP6 antagonists as adjuvant therapy may enhance the effect of gemcitabine-based regimens for both I-CCA and E-CCA patients in clinical practice. Finally, we described a functional role of CCR5/RANTES interaction in cell proliferation and invasion of CCA cells. This finding suggests that further studies with Maraviroc, an FDA approved CCR5 antagonist, should be considered for CCA patients.

6. REFERENCES

Adan, A., Kiraz, Y., & Baran, Y. (2016). Cell Proliferation and Cytotoxicity Assays. *Curr Pharm Biotechnol, 17*(14), 1213-1221. Retrieved from https://www.ncbi.nlm.nih.gov/pubmed/27604355

Agrawal, S., Kuvshinoff, B. W., Khoury, T., Yu, J., Javle, M. M., LeVea, C., . . . Gibbs, J. F. (2007). CD24 expression is an independent prognostic marker in cholangiocarcinoma. *J Gastrointest Surg, 11*(4), 445-451. doi:10.1007/s11605-007-0091-5

Aishima, S., & Oda, Y. (2015). Pathogenesis and classification of intrahepatic cholangiocarcinoma: different characters of perihilar large duct type versus peripheral small duct type. *J Hepatobiliary Pancreat Sci, 22*(2), 94-100. doi:10.1002/jhbp.154

Al-Hajj, M., Wicha, M. S., Benito-Hernandez, A., Morrison, S. J., & Clarke, M. F. (2003). Prospective identification of tumorigenic breast cancer cells. *Proc Natl Acad Sci U S A, 100*(7), 3983-3988. doi:10.1073/pnas.0530291100

Alpini, G., McGill, J. M., & Larusso, N. F. (2002). The pathobiology of biliary epithelia. *Hepatology, 35*(5), 1256-1268. doi:10.1053/jhep.2002.33541

Alvaro, D., Bragazzi, M. C., Benedetti, A., Fabris, L., Fava, G., Invernizzi, P., . . . committee, A. C. (2011). Cholangiocarcinoma in Italy: A national survey on clinical characteristics, diagnostic modalities and treatment. Results from the "Cholangiocarcinoma" committee of the Italian Association for the Study of Liver disease. *Dig Liver Dis, 43*(1), 60-65. doi:10.1016/j.dld.2010.05.002

Angelastro, J. M., & Lame, M. W. (2010). Overexpression of CD133 promotes drug resistance in C6 glioma cells. *Mol Cancer Res, 8*(8), 1105-1115. doi:10.1158/1541-7786.MCR-09-0383

Asghar, U., & Meyer, T. (2012). Are there opportunities for chemotherapy in the treatment of hepatocellular cancer? *J Hepatol, 56*(3), 686-695. doi:10.1016/j.jhep.2011.07.031

Autorino, R., Mattiucci, G. C., Ardito, F., Balducci, M., Deodato, F., Macchia, G., . . . Valentini, V. (2016). Radiochemotherapy with Gemcitabine in Unresectable Extrahepatic Cholangiocarcinoma: Long-term Results of a Phase II Study. *Anticancer Res, 36*(2), 737-740. Retrieved from https://www.ncbi.nlm.nih.gov/pubmed/26851032

Azenshtein, E., Luboshits, G., Shina, S., Neumark, E., Shahbazian, D., Weil, M., . . . Ben-Baruch, A. (2002). The CC chemokine RANTES in breast carcinoma progression: regulation of expression and potential mechanisms of promalignant activity. *Cancer Res, 62*(4), 1093-1102. Retrieved from https://www.ncbi.nlm.nih.gov/pubmed/11861388

Babu, V. P. K., Talwar, V., Raina, S., Goel, V., Dash, P. K., Bajaj, R., . . . Doval, D. C. (2018). Gemcitabine with carboplatin for advanced intrahepatic cholangiocarcinoma: A study from North India Cancer Centre. *Indian J Cancer, 55*(3), 222-225. doi:10.4103/ijc.IJC_622_17

Bai, H., Weng, Y., Bai, S., Jiang, Y., Li, B., He, F., . . . Shi, Q. (2014). CCL5 secreted from bone marrow stromal cells stimulates the migration and invasion of Huh7 hepatocellular carcinoma cells via the PI3K-Akt pathway. *Int J Oncol, 45*(1), 333-343. doi:10.3892/ijo.2014.2421

Balkwill, F. (2004a). Cancer and the chemokine network. *Nat Rev Cancer, 4*(7), 540-550. doi:10.1038/nrc1388

Balkwill, F. (2004b). The significance of cancer cell expression of the chemokine receptor CXCR4. *Semin Cancer Biol, 14*(3), 171-179. doi:10.1016/j.semcancer.2003.10.003

Banales, J. M., Cardinale, V., Carpino, G., Marzioni, M., Andersen, J. B., Invernizzi, P., . . . Alvaro, D. (2016). Expert consensus document: Cholangiocarcinoma: current knowledge and future perspectives consensus statement from the European Network for the Study of Cholangiocarcinoma (ENS-CCA). *Nat Rev Gastroenterol Hepatol, 13*(5), 261-280. doi:10.1038/nrgastro.2016.51

Banales, J. M., Huebert, R. C., Karlsen, T., Strazzabosco, M., LaRusso, N. F., & Gores, G. J. (2019). Cholangiocyte pathobiology. *Nat Rev Gastroenterol Hepatol, 16*(5), 269-281. doi:10.1038/s41575-019-0125-y

Barabe, F., Kennedy, J. A., Hope, K. J., & Dick, J. E. (2007). Modeling the initiation and progression of human acute leukemia in mice. *Science, 316*(5824), 600-604. doi:10.1126/science.1139851

Barashi, N., Weiss, I. D., Wald, O., Wald, H., Beider, K., Abraham, M., . . . Peled, A. (2013). Inflammation-induced hepatocellular carcinoma is dependent on CCR5 in mice. *Hepatology, 58*(3), 1021-1030. doi:10.1002/hep.26403

Batlle, E., & Clevers, H. (2017). Cancer stem cells revisited. *Nat Med, 23*(10), 1124-1134. doi:10.1038/nm.4409

Begicevic, R. R., & Falasca, M. (2017). ABC Transporters in Cancer Stem Cells: Beyond Chemoresistance. *Int J Mol Sci, 18*(11). doi:10.3390/ijms18112362

Ben-Josef, E., Guthrie, K. A., El-Khoueiry, A. B., Corless, C. L., Zalupski, M. M., Lowy, A. M., . . . Blanke, C. D. (2015). SWOG S0809: A Phase II Intergroup Trial of Adjuvant Capecitabine and Gemcitabine Followed by Radiotherapy and Concurrent Capecitabine in Extrahepatic Cholangiocarcinoma and Gallbladder Carcinoma. *J Clin Oncol, 33*(24), 2617-2622. doi:10.1200/JCO.2014.60.2219

Blechacz, B., Komuta, M., Roskams, T., & Gores, G. J. (2011). Clinical diagnosis and staging of cholangiocarcinoma. *Nat Rev Gastroenterol Hepatol, 8*(9), 512-522. doi:10.1038/nrgastro.2011.131

Borah, A., Raveendran, S., Rochani, A., Maekawa, T., & Kumar, D. S. (2015). Targeting self-renewal pathways in cancer stem cells: clinical implications for cancer therapy. *Oncogenesis, 4*, e177. doi:10.1038/oncsis.2015.35

Borovski, T., De Sousa, E. M. F., Vermeulen, L., & Medema, J. P. (2011). Cancer stem cell niche: the place to be. *Cancer Res, 71*(3), 634-639. doi:10.1158/0008-5472.CAN-10-3220

Borst, P., Evers, R., Kool, M., & Wijnholds, J. (2000). A family of drug transporters: the multidrug resistance-associated proteins. *J Natl Cancer Inst, 92*(16), 1295-1302. Retrieved from https://www.ncbi.nlm.nih.gov/pubmed/10944550

Bracken, C. P., Li, X., Wright, J. A., Lawrence, D. M., Pillman, K. A., Salmanidis, M., . . . Goodall, G. J. (2014). Genome-wide identification of miR-200 targets reveals a regulatory network controlling cell invasion. *EMBO J, 33*(18), 2040-2056. doi:10.15252/embj.201488641

Bragazzi, M. C., Ridola, L., Safarikia, S., Matteo, S. D., Costantini, D., Nevi, L., & Cardinale, V. (2018). New insights into cholangiocarcinoma: multiple stems and related cell lineages of origin. *Ann Gastroenterol, 31*(1), 42-55. doi:10.20524/aog.2017.0209

Braicu, C., Pileczki, V., Pop, L., Petric, R. C., Chira, S., Pointiere, E., . . . Berindan-Neagoe, I. (2015). Dual targeted therapy with p53 siRNA and Epigallocatechingallate in a triple negative breast cancer cell model. *PLoS One, 10*(4), e0120936. doi:10.1371/journal.pone.0120936

Brivio, S., Cadamuro, M., Fabris, L., & Strazzabosco, M. (2015). Epithelial-to-Mesenchymal Transition and Cancer Invasiveness: What Can We Learn from Cholangiocarcinoma? *J Clin Med, 4*(12), 2028-2041. doi:10.3390/jcm4121958

Buettner, S., van Vugt, J. L., JN, I. J., & Groot Koerkamp, B. (2017). Intrahepatic cholangiocarcinoma: current perspectives. *Onco Targets Ther, 10*, 1131-1142. doi:10.2147/OTT.S93629

Bupathi, M., Ahn, D. H., & Bekaii-Saab, T. (2017). Therapeutic options for intrahepatic cholangiocarcinoma. *Hepatobiliary Surg Nutr, 6*(2), 91-100. doi:10.21037/hbsn.2016.12.12

Burak, K., Angulo, P., Pasha, T. M., Egan, K., Petz, J., & Lindor, K. D. (2004). Incidence and risk factors for cholangiocarcinoma in primary sclerosing cholangitis. *Am J Gastroenterol, 99*(3), 523-526. doi:10.1111/j.1572-0241.2004.04067.x

Cai, X., Li, J., Yuan, X., Xiao, J., Dooley, S., Wan, X., . . . Lu, L. (2018). CD133 expression in cancer cells predicts poor prognosis of non-mucin producing intrahepatic cholangiocarcinoma. *J Transl Med, 16*(1), 50. doi:10.1186/s12967-018-1423-9

Cao, Z., Xu, X., Luo, X., Li, L., Huang, B., Li, X., . . . Gong, J. (2011). Role of RANTES and its receptor in gastric cancer metastasis. *J Huazhong Univ Sci Technolog Med Sci, 31*(3), 342-347. doi:10.1007/s11596-011-0378-3

Cardinale, V., Bragazzi, M. C., Carpino, G., Torrice, A., Fraveto, A., Gentile, R., . . . Alvaro, D. (2013). Cholangiocarcinoma: increasing burden of classifications. *Hepatobiliary Surg Nutr, 2*(5), 272-280. doi:10.3978/j.issn.2304-3881.2013.10.02

Cardinale, V., Carpino, G., Reid, L., Gaudio, E., & Alvaro, D. (2012). Multiple cells of origin in cholangiocarcinoma underlie biological, epidemiological and clinical heterogeneity. *World J Gastrointest Oncol, 4*(5), 94-102. doi:10.4251/wjgo.v4.i5.94

Cardinale, V., Renzi, A., Carpino, G., Torrice, A., Bragazzi, M. C., Giuliante, F., . . . Alvaro, D. (2015). Profiles of cancer stem cell subpopulations in cholangiocarcinomas. *Am J Pathol, 185*(6), 1724-1739. doi:10.1016/j.ajpath.2015.02.010

Cesarz, Z., & Tamama, K. (2016). Spheroid Culture of Mesenchymal Stem Cells. *Stem Cells Int, 2016*, 9176357. doi:10.1155/2016/9176357

Charo, I. F., & Ransohoff, R. M. (2006). The many roles of chemokines and chemokine receptors in inflammation. *N Engl J Med, 354*(6), 610-621. doi:10.1056/NEJMra052723

Chen, H. C. (2005). Boyden chamber assay. *Methods Mol Biol, 294*, 15-22. Retrieved from https://www.ncbi.nlm.nih.gov/pubmed/15576901

Chen, X. P., Wang, Q., Guan, J., Huang, Z. Y., Zhang, W. G., & Zhang, B. X. (2006). Reversing multidrug resistance by RNA interference through the suppression of MDR1 gene in human hepatoma cells. *World J Gastroenterol, 12*(21), 3332-3337. Retrieved from http://www.ncbi.nlm.nih.gov/pubmed/16733848

Chen, Z. S., & Tiwari, A. K. (2011). Multidrug resistance proteins (MRPs/ABCCs) in cancer chemotherapy and genetic diseases. *FEBS J, 278*(18), 3226-3245. doi:10.1111/j.1742-4658.2011.08235.x

Cheung, A. C., Lazaridis, K. N., LaRusso, N. F., & Gores, G. J. (2017). Emerging pharmacologic therapies for primary sclerosing cholangitis. *Curr Opin Gastroenterol, 33*(3), 149-157. doi:10.1097/MOG.0000000000000352

Chiba, T., Kita, K., Zheng, Y. W., Yokosuka, O., Saisho, H., Iwama, A., . . . Taniguchi, H. (2006). Side population purified from hepatocellular carcinoma cells harbors cancer stem cell-like properties. *Hepatology, 44*(1), 240-251. doi:10.1002/hep.21227

Chow, M. T., & Luster, A. D. (2014). Chemokines in cancer. *Cancer Immunol Res, 2*(12), 1125-1131. doi:10.1158/2326-6066.CIR-14-0160

Cirqueira, C. S., Felipe-Silva, A. S., Wakamatsu, A., Marins, L. V., Rocha, E. C., de Mello, E. S., & Alves, V. A. F. (2018). Immunohistochemical Assessment of the Expression of Biliary Transportation Proteins MRP2 and MRP3 in Hepatocellular Carcinoma and in Cholangiocarcinoma. *Pathol Oncol Res*. doi:10.1007/s12253-018-0386-8

Collins, A. T., Berry, P. A., Hyde, C., Stower, M. J., & Maitland, N. J. (2005). Prospective identification of tumorigenic prostate cancer stem cells. *Cancer Res, 65*(23), 10946-10951. doi:10.1158/0008-5472.CAN-05-2018

Cormier, N., Yeo, A., Fiorentino, E., & Paxson, J. (2015). Optimization of the Wound Scratch Assay to Detect Changes in Murine Mesenchymal Stromal Cell Migration After Damage by Soluble Cigarette Smoke Extract. *J Vis Exp*(106), e53414. doi:10.3791/53414

Costa, F. F. (2007). Non-coding RNAs: lost in translation? *Gene, 386*(1-2), 1-10. doi:10.1016/j.gene.2006.09.028

Couto, L. B., & High, K. A. (2010). Viral vector-mediated RNA interference. *Curr Opin Pharmacol, 10*(5), 534-542. doi:10.1016/j.coph.2010.06.007

Cox, J., & Weinman, S. (2016). Mechanisms of doxorubicin resistance in hepatocellular carcinoma. *Hepat Oncol, 3*(1), 57-59. doi:10.2217/hep.15.41

Cunha, C., Panseri, S., Villa, O., Silva, D., & Gelain, F. (2011). 3D culture of adult mouse neural stem cells within functionalized self-assembling peptide scaffolds. *Int J Nanomedicine, 6*, 943-955. doi:10.2147/IJN.S17292

Darwish Murad, S., Kim, W. R., Harnois, D. M., Douglas, D. D., Burton, J., Kulik, L. M., . . . Heimbach, J. K. (2012). Efficacy of neoadjuvant chemoradiation, followed by liver transplantation, for perihilar cholangiocarcinoma at 12 US centers. *Gastroenterology, 143*(1), 88-98 e83; quiz e14. doi:10.1053/j.gastro.2012.04.008

Daskalow, K., Rohwer, N., Raskopf, E., Dupuy, E., Kuhl, A., Loddenkemper, C., . . . Cramer, T. (2010). Role of hypoxia-inducible transcription factor 1alpha for progression and chemosensitivity of murine hepatocellular carcinoma. *J Mol Med (Berl), 88*(8), 817-827. doi:10.1007/s00109-010-0623-4

Davis, M. E., Zuckerman, J. E., Choi, C. H., Seligson, D., Tolcher, A., Alabi, C. A., . . . Ribas, A. (2010). Evidence of RNAi in humans from systemically administered siRNA via targeted nanoparticles. *Nature, 464*(7291), 1067-1070. doi:10.1038/nature08956

de Munnik, S. M., Smit, M. J., Leurs, R., & Vischer, H. F. (2015). Modulation of cellular signaling by herpesvirus-encoded G protein-coupled receptors. *Front Pharmacol, 6*, 40. doi:10.3389/fphar.2015.00040

Dean, M. (2009). ABC transporters, drug resistance, and cancer stem cells. *J Mammary Gland Biol Neoplasia, 14*(1), 3-9. doi:10.1007/s10911-009-9109-9

Doffou, M., Adams, G., Bowen, W. C., Paranjpe, S., Parihar, H. S., Nguyen, H., . . . Bhave, V. S. (2018). Oct4 Is Crucial for Transdifferentiation of Hepatocytes to Biliary Epithelial Cells in an In Vitro Organoid Culture Model. *Gene Expr, 18*(1), 51-62. doi:10.3727/105221617X15124876321401

Duda, D. G., Kozin, S. V., Kirkpatrick, N. D., Xu, L., Fukumura, D., & Jain, R. K. (2011). CXCL12 (SDF1alpha)-CXCR4/CXCR7 pathway inhibition: an emerging sensitizer for anticancer therapies? *Clin Cancer Res, 17*(8), 2074-2080. doi:10.1158/1078-0432.CCR-10-2636

Dykxhoorn, D. M., Wu, Y., Xie, H., Yu, F., Lal, A., Petrocca, F., . . . Lieberman, J. (2009). miR-200 enhances mouse breast cancer cell colonization to form distant metastases. *PLoS One, 4*(9), e7181. doi:10.1371/journal.pone.0007181

Evrard, A., Cuq, P., Ciccolini, J., Vian, L., & Cano, J. P. (1999). Increased cytotoxicity and bystander effect of 5-fluorouracil and 5-deoxy-5-fluorouridine in human colorectal

cancer cells transfected with thymidine phosphorylase. *Br J Cancer, 80*(11), 1726-1733. doi:10.1038/sj.bjc.6690589

Feng, D. F. P., G.; Li, W.; Xu, H.; Zhang, T.; Wang, N. (2015). Identification and Characterization of Tumorigenic Liver Cancer Stem Cells by CD133 and CD24. *Journal of Biomaterials and Tissue Engineering, 5*, 635-646. doi:10.1166/jbt.2015.1363

Fiebig, H. H., Maier, A., & Burger, A. M. (2004). Clonogenic assay with established human tumour xenografts: correlation of in vitro to in vivo activity as a basis for anticancer drug discovery. *Eur J Cancer, 40*(6), 802-820. doi:10.1016/j.ejca.2004.01.009

Friedl, P., & Alexander, S. (2011). Cancer invasion and the microenvironment: plasticity and reciprocity. *Cell, 147*(5), 992-1009. doi:10.1016/j.cell.2011.11.016

Fuchs, B. C., Fujii, T., Dorfman, J. D., Goodwin, J. M., Zhu, A. X., Lanuti, M., & Tanabe, K. K. (2008). Epithelial-to-mesenchymal transition and integrin-linked kinase mediate sensitivity to epidermal growth factor receptor inhibition in human hepatoma cells. *Cancer Res, 68*(7), 2391-2399. doi:10.1158/0008-5472.CAN-07-2460

Fujii, H., Itoh, Y., Yamaguchi, K., Yamauchi, N., Harano, Y., Nakajima, T., . . . Okanoue, T. (2004). Chemokine CCL20 enhances the growth of HuH7 cells via phosphorylation of p44/42 MAPK in vitro. *Biochem Biophys Res Commun, 322*(3), 1052-1058. doi:10.1016/j.bbrc.2004.07.207

Fujiwara, Y., Kobayashi, S., Nagano, H., Kanai, M., Hatano, E., Toyoda, M., . . . Ioka, T. (2015). Pharmacokinetic Study of Adjuvant Gemcitabine Therapy for Biliary Tract Cancer following Major Hepatectomy (KHBO1101). *PLoS One, 10*(12), e0143072. doi:10.1371/journal.pone.0143072

Gabriel, E., Gandhi, S., Attwood, K., Kuvshinoff, B., Hochwald, S., & Iyer, R. (2017). Gemcitabine and capecitabine for advanced biliary cancer. *J Gastrointest Oncol, 8*(4), 728-736. doi:10.21037/jgo.2017.01.24

Gao, D., Rahbar, R., & Fish, E. N. (2016). CCL5 activation of CCR5 regulates cell metabolism to enhance proliferation of breast cancer cells. *Open Biol, 6*(6). doi:10.1098/rsob.160122

Gaudio, E., Carpino, G., Cardinale, V., Franchitto, A., Onori, P., & Alvaro, D. (2009). New insights into liver stem cells. *Dig Liver Dis, 41*(7), 455-462. doi:10.1016/j.dld.2009.03.009

Ghanem, I., Riveiro, M. E., Paradis, V., Faivre, S., de Parga, P. M., & Raymond, E. (2014). Insights on the CXCL12-CXCR4 axis in hepatocellular carcinoma carcinogenesis. *Am J Transl Res, 6*(4), 340-352. Retrieved from https://www.ncbi.nlm.nih.gov/pubmed/25075251

Ghouri, Y. A., Mian, I., & Blechacz, B. (2015). Cancer review: Cholangiocarcinoma. *J Carcinog, 14*, 1. doi:10.4103/1477-3163.151940

Grubman, S. A., Perrone, R. D., Lee, D. W., Murray, S. L., Rogers, L. C., Wolkoff, L. I., . . . Jefferson, D. M. (1994). Regulation of intracellular pH by immortalized human

intrahepatic biliary epithelial cell lines. *Am J Physiol, 266*(6 Pt 1), G1060-1070. doi:10.1152/ajpgi.1994.266.6.G1060

Gu, M. J., & Choi, J. H. (2014). Epithelial-mesenchymal transition phenotypes are associated with patient survival in intrahepatic cholangiocarcinoma. *J Clin Pathol, 67*(3), 229-234. doi:10.1136/jclinpath-2013-201806

Guo, F., Wang, Y., Liu, J., Mok, S. C., Xue, F., & Zhang, W. (2016). CXCL12/CXCR4: a symbiotic bridge linking cancer cells and their stromal neighbors in oncogenic communication networks. *Oncogene, 35*(7), 816-826. doi:10.1038/onc.2015.139

Guzman, C., Bagga, M., Kaur, A., Westermarck, J., & Abankwa, D. (2014). ColonyArea: an ImageJ plugin to automatically quantify colony formation in clonogenic assays. *PLoS One, 9*(3), e92444. doi:10.1371/journal.pone.0092444

Hagmann, W., Jesnowski, R., & Lohr, J. M. (2010). Interdependence of gemcitabine treatment, transporter expression, and resistance in human pancreatic carcinoma cells. *Neoplasia, 12*(9), 740-747. Retrieved from https://www.ncbi.nlm.nih.gov/pubmed/20824050

Hahnvajanawong, C., Chaiyagool, J., Seubwai, W., Bhudhisawasdi, V., Namwat, N., Khuntikeo, N., . . . Tassaneeyakul, W. (2012). Orotate phosphoribosyl transferase mRNA expression and the response of cholangiocarcinoma to 5-fluorouracil. *World J Gastroenterol, 18*(30), 3955-3961. doi:10.3748/wjg.v18.i30.3955

Han, Y., Glaser, S., Meng, F., Francis, H., Marzioni, M., McDaniel, K., . . . Franchitto, A. (2013). Recent advances in the morphological and functional heterogeneity of the biliary epithelium. *Exp Biol Med (Maywood), 238*(5), 549-565. doi:10.1177/1535370213489926

Hanahan, D., & Weinberg, R. A. (2011). Hallmarks of cancer: the next generation. *Cell, 144*(5), 646-674. doi:10.1016/j.cell.2011.02.013

Haraguchi, N., Ishii, H., Mimori, K., Tanaka, F., Ohkuma, M., Kim, H. M., . . . Mori, M. (2010). CD13 is a therapeutic target in human liver cancer stem cells. *J Clin Invest, 120*(9), 3326-3339. doi:10.1172/JCI42550

Haraguchi, N., Utsunomiya, T., Inoue, H., Tanaka, F., Mimori, K., Barnard, G. F., & Mori, M. (2006). Characterization of a side population of cancer cells from human gastrointestinal system. *Stem Cells, 24*(3), 506-513. doi:10.1634/stemcells.2005-0282

Hirohashi, K., Uenishi, T., Kubo, S., Yamamoto, T., Tanaka, H., Shuto, T., & Kinoshita, H. (2002). Macroscopic types of intrahepatic cholangiocarcinoma: clinicopathologic features and surgical outcomes. *Hepatogastroenterology, 49*(44), 326-329. Retrieved from http://www.ncbi.nlm.nih.gov/pubmed/11995443

Hirschmann-Jax, C., Foster, A. E., Wulf, G. G., Nuchtern, J. G., Jax, T. W., Gobel, U., . . . Brenner, M. K. (2004). A distinct "side population" of cells with high drug efflux capacity in human tumor cells. *Proc Natl Acad Sci U S A, 101*(39), 14228-14233. doi:10.1073/pnas.0400067101

Horgan, A. M., Amir, E., Walter, T., & Knox, J. J. (2012). Adjuvant therapy in the treatment of biliary tract cancer: a systematic review and meta-analysis. *J Clin Oncol, 30*(16), 1934-1940. doi:10.1200/JCO.2011.40.5381

Hu, J., Li, J., Yue, X., Wang, J., Liu, J., Sun, L., & Kong, D. (2017). Expression of the cancer stem cell markers ABCG2 and OCT-4 in right-sided colon cancer predicts recurrence and poor outcomes. *Oncotarget, 8*(17), 28463-28470. doi:10.18632/oncotarget.15307

Huang, P., Chubb, S., Hertel, L. W., Grindey, G. B., & Plunkett, W. (1991). Action of 2',2'-difluorodeoxycytidine on DNA synthesis. *Cancer Res, 51*(22), 6110-6117. Retrieved from https://www.ncbi.nlm.nih.gov/pubmed/1718594

Humphries, B., & Yang, C. (2015). The microRNA-200 family: small molecules with novel roles in cancer development, progression and therapy. *Oncotarget, 6*(9), 6472-6498. doi:10.18632/oncotarget.3052

Iacopino, F., Angelucci, C., Piacentini, R., Biamonte, F., Mangiola, A., Maira, G., . . . Sica, G. (2014). Isolation of cancer stem cells from three human glioblastoma cell lines: characterization of two selected clones. *PLoS One, 9*(8), e105166. doi:10.1371/journal.pone.0105166

International classification of diseases for oncology (ICD-O-3.1). (2011). Geneva, Switzerland: World Health Organization

Ishimoto, U., Kondo, S., Ohba, A., Sasaki, M., Sakamoto, Y., Morizane, C., . . . Okusaka, T. (2018). Prognostic Factors for Survival in Patients with Advanced Intrahepatic Cholangiocarcinoma Treated with Gemcitabine plus Cisplatin as First-Line Treatment. *Oncology, 94*(2), 72-78. doi:10.1159/000480703

Jaggupilli, A., & Elkord, E. (2012). Significance of CD44 and CD24 as cancer stem cell markers: an enduring ambiguity. *Clin Dev Immunol, 2012*, 708036. doi:10.1155/2012/708036

Jang, J. Y., Kim, S. W., Park, D. J., Ahn, Y. J., Yoon, Y. S., Choi, M. G., . . . Park, Y. H. (2005). Actual long-term outcome of extrahepatic bile duct cancer after surgical resection. *Ann Surg, 241*(1), 77-84. Retrieved from http://www.ncbi.nlm.nih.gov/pubmed/15621994

Jedlitschky, G., Burchell, B., & Keppler, D. (2000). The multidrug resistance protein 5 functions as an ATP-dependent export pump for cyclic nucleotides. *J Biol Chem, 275*(39), 30069-30074. doi:10.1074/jbc.M005463200

Jonkman, J. E., Cathcart, J. A., Xu, F., Bartolini, M. E., Amon, J. E., Stevens, K. M., & Colarusso, P. (2014). An introduction to the wound healing assay using live-cell microscopy. *Cell Adh Migr, 8*(5), 440-451. doi:10.4161/cam.36224

Jung, H. R., Kang, H. M., Ryu, J. W., Kim, D. S., Noh, K. H., Kim, E. S., . . . Jung, C. R. (2017). Cell Spheroids with Enhanced Aggressiveness to Mimic Human Liver Cancer In Vitro and In Vivo. *Sci Rep, 7*(1), 10499. doi:10.1038/s41598-017-10828-7

Kaemmerer, D., Schindler, R., Mussbach, F., Dahmen, U., Altendorf-Hofmann, A., Dirsch, O., . . . Lupp, A. (2017). Somatostatin and CXCR4 chemokine receptor expression in hepatocellular and cholangiocellular carcinomas: tumor capillaries as promising targets. *BMC Cancer, 17*(1), 896. doi:10.1186/s12885-017-3911-3

Kang, M. H., Lee, W. S., Go, S. I., Kim, M. J., Lee, U. S., Choi, H. J., . . . Cho, J. M. (2014). Can thymidine phosphorylase be a predictive marker for gemcitabine and doxifluridine combination chemotherapy in cholangiocarcinoma?: case series. *Medicine (Baltimore), 93*(28), e305. doi:10.1097/MD.0000000000000305

Karnoub, A. E., Dash, A. B., Vo, A. P., Sullivan, A., Brooks, M. W., Bell, G. W., . . . Weinberg, R. A. (2007). Mesenchymal stem cells within tumour stroma promote breast cancer metastasis. *Nature, 449*(7162), 557-563. doi:10.1038/nature06188

Keeratichamroen, S., Leelawat, K., Thongtawee, T., Narong, S., Aegem, U., Tujinda, S., . . . Tohtong, R. (2011). Expression of CD24 in cholangiocarcinoma cells is associated with disease progression and reduced patient survival. *Int J Oncol, 39*(4), 873-881. doi:10.3892/ijo.2011.1088

Khalid, A., Wolfram, J., Ferrari, I., Mu, C., Mai, J., Yang, Z., . . . Shen, H. (2015). Recent Advances in Discovering the Role of CCL5 in Metastatic Breast Cancer. *Mini Rev Med Chem, 15*(13), 1063-1072. Retrieved from https://www.ncbi.nlm.nih.gov/pubmed/26420723

Khan, S. A., Davidson, B. R., Goldin, R. D., Heaton, N., Karani, J., Pereira, S. P., . . . British Society of, G. (2012). Guidelines for the diagnosis and treatment of cholangiocarcinoma: an update. *Gut, 61*(12), 1657-1669. doi:10.1136/gutjnl-2011-301748

Khvorova, A., Reynolds, A., & Jayasena, S. D. (2003). Functional siRNAs and miRNAs exhibit strand bias. *Cell, 115*(2), 209-216. Retrieved from http://www.ncbi.nlm.nih.gov/pubmed/14567918

Kim, H. J., Kim, J. S., Joo, M. K., Lee, B. J., Kim, J. H., Yeon, J. E., . . . Bak, Y. T. (2015). Hepatolithiasis and intrahepatic cholangiocarcinoma: A review. *World J Gastroenterol, 21*(48), 13418-13431. doi:10.3748/wjg.v21.i48.13418

Kim, J., & Orkin, S. H. (2011). Embryonic stem cell-specific signatures in cancer: insights into genomic regulatory networks and implications for medicine. *Genome Med, 3*(11), 75. doi:10.1186/gm291

Kim, J. W., Ye, Q., Forgues, M., Chen, Y., Budhu, A., Sime, J., . . . Wang, X. W. (2004). Cancer-associated molecular signature in the tissue samples of patients with cirrhosis. *Hepatology, 39*(2), 518-527. doi:10.1002/hep.20053

Kimlin, L. C., Casagrande, G., & Virador, V. M. (2013). In vitro three-dimensional (3D) models in cancer research: an update. *Mol Carcinog, 52*(3), 167-182. doi:10.1002/mc.21844

Kimura, O., Takahashi, T., Ishii, N., Inoue, Y., Ueno, Y., Kogure, T., . . . Sugamura, K. (2010). Characterization of the epithelial cell adhesion molecule (EpCAM)+ cell population in

hepatocellular carcinoma cell lines. *Cancer Sci, 101*(10), 2145-2155. doi:10.1111/j.1349-7006.2010.01661.x

Komuta, M., Govaere, O., Vandecaveye, V., Akiba, J., Van Steenbergen, W., Verslype, C., . . . Roskams, T. (2012). Histological diversity in cholangiocellular carcinoma reflects the different cholangiocyte phenotypes. *Hepatology, 55*(6), 1876-1888. doi:10.1002/hep.25595

Komuta, M., Spee, B., Vander Borght, S., De Vos, R., Verslype, C., Aerts, R., . . . Roskams, T. (2008). Clinicopathological study on cholangiolocellular carcinoma suggesting hepatic progenitor cell origin. *Hepatology, 47*(5), 1544-1556. doi:10.1002/hep.22238

Kunlabut, K., Vaeteewoottacharn, K., Wongkham, C., Khuntikeo, N., Waraasawapati, S., Pairojkul, C., & Wongkham, S. (2012). Aberrant expression of CD44 in bile duct cancer correlates with poor prognosis. *Asian Pac J Cancer Prev, 13 Suppl*, 95-99. Retrieved from http://www.ncbi.nlm.nih.gov/pubmed/23480770

Kusaka, Y., Tokiwa, T., & Sato, J. (1988). Establishment and characterization of a cell line from a human cholangiocellular carcinoma. *Res Exp Med (Berl), 188*(5), 367-375. Retrieved from https://www.ncbi.nlm.nih.gov/pubmed/2852388

Lage, H. (2009). Therapeutic potential of RNA interference in drug-resistant cancers. *Future Oncol, 5*(2), 169-185. doi:10.2217/14796694.5.2.169

Laing, K. J., & Secombes, C. J. (2004). Chemokines. *Dev Comp Immunol, 28*(5), 443-460. doi:10.1016/j.dci.2003.09.006

Lee, G. Y., Kenny, P. A., Lee, E. H., & Bissell, M. J. (2007). Three-dimensional culture models of normal and malignant breast epithelial cells. *Nat Methods, 4*(4), 359-365. doi:10.1038/nmeth1015

Leelawat, K., Keeratichamroen, S., Leelawat, S., & Tohtong, R. (2013). CD24 induces the invasion of cholangiocarcinoma cells by upregulating CXCR4 and increasing the phosphorylation of ERK1/2. *Oncol Lett, 6*(5), 1439-1446. doi:10.3892/ol.2013.1587

Leelawat, K., Leelawat, S., Narong, S., & Hongeng, S. (2007). Roles of the MEK1/2 and AKT pathways in CXCL12/CXCR4 induced cholangiocarcinoma cell invasion. *World J Gastroenterol, 13*(10), 1561-1568. Retrieved from http://www.ncbi.nlm.nih.gov/pubmed/17461449

Leelawat, K., Thongtawee, T., Narong, S., Subwongcharoen, S., & Treepongkaruna, S. A. (2011). Strong expression of CD133 is associated with increased cholangiocarcinoma progression. *World J Gastroenterol, 17*(9), 1192-1198. doi:10.3748/wjg.v17.i9.1192

Leyva-Illades, D., McMillin, M., Quinn, M., & Demorrow, S. (2012). Cholangiocarcinoma pathogenesis: Role of the tumor microenvironment. *Transl Gastrointest Cancer, 1*(1), 71-80. Retrieved from https://www.ncbi.nlm.nih.gov/pubmed/23002431

Li, B., Dorrell, C., Canaday, P. S., Pelz, C., Haft, A., Finegold, M., & Grompe, M. (2017). Adult Mouse Liver Contains Two Distinct Populations of Cholangiocytes. *Stem Cell Reports, 9*(2), 478-489. doi:10.1016/j.stemcr.2017.06.003

Li, M. J., & Rossi, J. J. (2007). Lentivirus transduction of hematopoietic cells. *CSH Protoc, 2007*, pdb prot4755. doi:10.1101/pdb.prot4755

Li, Z. (2013). CD133: a stem cell biomarker and beyond. *Exp Hematol Oncol, 2*(1), 17. doi:10.1186/2162-3619-2-17

Liang, C. C., Park, A. Y., & Guan, J. L. (2007). In vitro scratch assay: a convenient and inexpensive method for analysis of cell migration in vitro. *Nat Protoc, 2*(2), 329-333. doi:10.1038/nprot.2007.30

Liang, C. M., Chen, L., Hu, H., Ma, H. Y., Gao, L. L., Qin, J., & Zhong, C. P. (2015). Chemokines and their receptors play important roles in the development of hepatocellular carcinoma. *World J Hepatol, 7*(10), 1390-1402. doi:10.4254/wjh.v7.i10.1390

Liaskou, E., Wilson, D. V., & Oo, Y. H. (2012). Innate immune cells in liver inflammation. *Mediators Inflamm, 2012*, 949157. doi:10.1155/2012/949157

Liu, H., Pan, Z., Li, A., Fu, S., Lei, Y., Sun, H., . . . Zhou, W. (2008). Roles of chemokine receptor 4 (CXCR4) and chemokine ligand 12 (CXCL12) in metastasis of hepatocellular carcinoma cells. *Cell Mol Immunol, 5*(5), 373-378. doi:10.1038/cmi.2008.46

Liu, Z., Yang, L., Xu, J., Zhang, X., & Wang, B. (2011). Enhanced expression and clinical significance of chemokine receptor CXCR2 in hepatocellular carcinoma. *J Surg Res, 166*(2), 241-246. doi:10.1016/j.jss.2009.07.014

Livak, K. J., & Schmittgen, T. D. (2001). Analysis of relative gene expression data using real-time quantitative PCR and the 2(-Delta Delta C(T)) Method. *Methods, 25*(4), 402-408. doi:10.1006/meth.2001.1262

Lobo, N. A., Shimono, Y., Qian, D., & Clarke, M. F. (2007). The biology of cancer stem cells. *Annu Rev Cell Dev Biol, 23*, 675-699. doi:10.1146/annurev.cellbio.22.010305.104154

Lu, J. F., Pokharel, D., & Bebawy, M. (2015). MRP1 and its role in anticancer drug resistance. *Drug Metab Rev, 47*(4), 406-419. doi:10.3109/03602532.2015.1105253

Lu, P., Nakamoto, Y., Nemoto-Sasaki, Y., Fujii, C., Wang, H., Hashii, M., . . . Mukaida, N. (2003). Potential interaction between CCR1 and its ligand, CCL3, induced by endogenously produced interleukin-1 in human hepatomas. *Am J Pathol, 162*(4), 1249-1258. doi:10.1016/S0002-9440(10)63921-1

Makinoshima, H., & Dezawa, M. (2009). Pancreatic cancer cells activate CCL5 expression in mesenchymal stromal cells through the insulin-like growth factor-I pathway. *FEBS Lett, 583*(22), 3697-3703. doi:10.1016/j.febslet.2009.10.061

Manjunath, N., Wu, H., Subramanya, S., & Shankar, P. (2009). Lentiviral delivery of short hairpin RNAs. *Adv Drug Deliv Rev, 61*(9), 732-745. doi:10.1016/j.addr.2009.03.004

Marin, J. J. G., Lozano, E., Briz, O., Al-Abdulla, R., Serrano, M. A., & Macias, R. I. R. (2017). Molecular Bases of Chemoresistance in Cholangiocarcinoma. *Curr Drug Targets, 18*(8), 889-900. doi:10.2174/1389450116666150223121508

Marin, J. J. G., Lozano, E., Herraez, E., Asensio, M., Di Giacomo, S., Romero, M. R., . . . Macias, R. I. R. (2018). Chemoresistance and chemosensitization in cholangiocarcinoma. *Biochim Biophys Acta Mol Basis Dis, 1864*(4 Pt B), 1444-1453. doi:10.1016/j.bbadis.2017.06.005

Marra, F., & Tacke, F. (2014). Roles for chemokines in liver disease. *Gastroenterology, 147*(3), 577-594 e571. doi:10.1053/j.gastro.2014.06.043

Martinez-Becerra, P., Vaquero, J., Romero, M. R., Lozano, E., Anadon, C., Macias, R. I., . . . Marin, J. J. (2012). No correlation between the expression of FXR and genes involved in multidrug resistance phenotype of primary liver tumors. *Mol Pharm, 9*(6), 1693-1704. doi:10.1021/mp300028a

Mavros, M. N., Economopoulos, K. P., Alexiou, V. G., & Pawlik, T. M. (2014). Treatment and Prognosis for Patients With Intrahepatic Cholangiocarcinoma: Systematic Review and Meta-analysis. *JAMA Surg, 149*(6), 565-574. doi:10.1001/jamasurg.2013.5137

Mencarelli, A., Graziosi, L., Renga, B., Cipriani, S., D'Amore, C., Francisci, D., . . . Fiorucci, S. (2013). CCR5 Antagonism by Maraviroc Reduces the Potential for Gastric Cancer Cell Dissemination. *Transl Oncol, 6*(6), 784-793. Retrieved from https://www.ncbi.nlm.nih.gov/pubmed/24466382

Miraglia, S., Godfrey, W., Yin, A. H., Atkins, K., Warnke, R., Holden, J. T., . . . Buck, D. W. (1997). A novel five-transmembrane hematopoietic stem cell antigen: isolation, characterization, and molecular cloning. *Blood, 90*(12), 5013-5021. Retrieved from http://www.ncbi.nlm.nih.gov/pubmed/9389721

Mitra, P., Oskeritzian, C. A., Payne, S. G., Beaven, M. A., Milstien, S., & Spiegel, S. (2006). Role of ABCC1 in export of sphingosine-1-phosphate from mast cells. *Proc Natl Acad Sci U S A, 103*(44), 16394-16399. doi:10.1073/pnas.0603734103

Miyagiwa, M., Ichida, T., Tokiwa, T., Sato, J., & Sasaki, H. (1989). A new human cholangiocellular carcinoma cell line (HuCC-T1) producing carbohydrate antigen 19/9 in serum-free medium. *In Vitro Cell Dev Biol, 25*(6), 503-510. Retrieved from https://www.ncbi.nlm.nih.gov/pubmed/2544546

Miyazaki, H., Takabe, K., & Yeudall, W. A. (2013). Chemokines, chemokine receptors and the gastrointestinal system. *World J Gastroenterol, 19*(19), 2847-2863. doi:10.3748/wjg.v19.i19.2847

Mohs, A., Kuttkat, N., Reissing, J., Zimmermann, H. W., Sonntag, R., Proudfoot, A., . . . Trautwein, C. (2017). Functional role of CCL5/RANTES for HCC progression during chronic liver disease. *J Hepatol, 66*(4), 743-753. doi:10.1016/j.jhep.2016.12.011

Monnier, J., Boissan, M., L'Helgoualc'h, A., Lacombe, M. L., Turlin, B., Zucman-Rossi, J., . . . Samson, M. (2012). CXCR7 is up-regulated in human and murine hepatocellular carcinoma and is specifically expressed by endothelial cells. *Eur J Cancer, 48*(1), 138-148. doi:10.1016/j.ejca.2011.06.044

Morine, Y., Imura, S., Ikemoto, T., Iwahashi, S., Saito, Y. U., & Shimada, M. (2017). CD44 Expression Is a Prognostic Factor in Patients with Intrahepatic Cholangiocarcinoma After Surgical Resection. *Anticancer Res, 37*(10), 5701-5705. doi:10.21873/anticanres.12007

Morizane, C., Ueno, M., Ikeda, M., Okusaka, T., Ishii, H., & Furuse, J. (2018). New developments in systemic therapy for advanced biliary tract cancer. *Jpn J Clin Oncol, 48*(8), 703-711. doi:10.1093/jjco/hyy082

Munz, M., Baeuerle, P. A., & Gires, O. (2009). The emerging role of EpCAM in cancer and stem cell signaling. *Cancer Res, 69*(14), 5627-5629. doi:10.1158/0008-5472.CAN-09-0654

Murakami, S., Ajiki, T., Okazaki, T., Ueno, K., Kido, M., Matsumoto, I., . . . Ku, Y. (2014). Factors affecting survival after resection of intrahepatic cholangiocarcinoma. *Surg Today, 44*(10), 1847-1854. doi:10.1007/s00595-013-0825-9

Murphy, P. M. (2001). Viral exploitation and subversion of the immune system through chemokine mimicry. *Nat Immunol, 2*(2), 116-122. doi:10.1038/84214

Nagano, H., Ishii, H., Marubashi, S., Haraguchi, N., Eguchi, H., Doki, Y., & Mori, M. (2012). Novel therapeutic target for cancer stem cells in hepatocellular carcinoma. *J Hepatobiliary Pancreat Sci, 19*(6), 600-605. doi:10.1007/s00534-012-0543-5

Nakajima, T., Takayama, T., Miyanishi, K., Nobuoka, A., Hayashi, T., Abe, T., . . . Niitsu, Y. (2003). Reversal of multiple drug resistance in cholangiocarcinoma by the glutathione S-transferase-pi-specific inhibitor O1-hexadecyl-gamma-glutamyl-S-benzylcysteinyl-D-phenylglycine ethylester. *J Pharmacol Exp Ther, 306*(3), 861-869. doi:10.1124/jpet.103.052696

Nakanuma, Y., & Sato, Y. (2012). Cystic and papillary neoplasm involving peribiliary glands: a biliary counterpart of branch-type intraductal papillary mucinous [corrected] neoplasm? *Hepatology, 55*(6), 2040-2041. doi:10.1002/hep.25590

Nakanuma, Y., Sato, Y., Harada, K., Sasaki, M., Xu, J., & Ikeda, H. (2010). Pathological classification of intrahepatic cholangiocarcinoma based on a new concept. *World J Hepatol, 2*(12), 419-427. doi:10.4254/wjh.v2.i12.419

Nakeeb, A., & Pitt, H. A. (2005). Radiation therapy, chemotherapy and chemoradiation in hilar cholangiocarcinoma. *HPB (Oxford), 7*(4), 278-282. doi:10.1080/13651820500373028

Nakeeb, A., Pitt, H. A., Sohn, T. A., Coleman, J., Abrams, R. A., Piantadosi, S., . . . Cameron, J. L. (1996). Cholangiocarcinoma. A spectrum of intrahepatic, perihilar, and distal tumors. *Ann Surg, 224*(4), 463-473; discussion 473-465. Retrieved from http://www.ncbi.nlm.nih.gov/pubmed/8857851

Nicolson, G. L. (1993). Paracrine and autocrine growth mechanisms in tumor metastasis to specific sites with particular emphasis on brain and lung metastasis. *Cancer Metastasis Rev, 12*(3-4), 325-343. Retrieved from https://www.ncbi.nlm.nih.gov/pubmed/8281616

Nieth, C., Priebsch, A., Stege, A., & Lage, H. (2003). Modulation of the classical multidrug resistance (MDR) phenotype by RNA interference (RNAi). *FEBS Lett, 545*(2-3), 144-150. Retrieved from http://www.ncbi.nlm.nih.gov/pubmed/12804765

Nobili, V., Carpino, G., Alisi, A., Franchitto, A., Alpini, G., De Vito, R., . . . Gaudio, E. (2012). Hepatic progenitor cells activation, fibrosis, and adipokines production in pediatric nonalcoholic fatty liver disease. *Hepatology, 56*(6), 2142-2153. doi:10.1002/hep.25742

Nowell, P. C. (1976). The clonal evolution of tumor cell populations. *Science, 194*(4260), 23-28. Retrieved from http://www.ncbi.nlm.nih.gov/pubmed/959840

O'Brien, C. A., Pollett, A., Gallinger, S., & Dick, J. E. (2007). A human colon cancer cell capable of initiating tumour growth in immunodeficient mice. *Nature, 445*(7123), 106-110. doi:10.1038/nature05372

Ochoa-Callejero, L., Perez-Martinez, L., Rubio-Mediavilla, S., Oteo, J. A., Martinez, A., & Blanco, J. R. (2013). Maraviroc, a CCR5 antagonist, prevents development of hepatocellular carcinoma in a mouse model. *PLoS One, 8*(1), e53992. doi:10.1371/journal.pone.0053992

Ohira, S., Sasaki, M., Harada, K., Sato, Y., Zen, Y., Isse, K., . . . Nakanuma, Y. (2006). Possible regulation of migration of intrahepatic cholangiocarcinoma cells by interaction of CXCR4 expressed in carcinoma cells with tumor necrosis factor-alpha and stromal-derived factor-1 released in stroma. *Am J Pathol, 168*(4), 1155-1168. Retrieved from http://www.ncbi.nlm.nih.gov/pubmed/16565491

Park, J. O., Oh, D. Y., Hsu, C., Chen, J. S., Chen, L. T., Orlando, M., . . . Lim, H. Y. (2015). Gemcitabine Plus Cisplatin for Advanced Biliary Tract Cancer: A Systematic Review. *Cancer Res Treat, 47*(3), 343-361. doi:10.4143/crt.2014.308

Patel, T. (2011). Cholangiocarcinoma--controversies and challenges. *Nat Rev Gastroenterol Hepatol, 8*(4), 189-200. doi:10.1038/nrgastro.2011.20

Pipas, J. M. (2009). SV40: Cell transformation and tumorigenesis. *Virology, 384*(2), 294-303. doi:10.1016/j.virol.2008.11.024

Pratt, S., Shepard, R. L., Kandasamy, R. A., Johnston, P. A., Perry, W., 3rd, & Dantzig, A. H. (2005). The multidrug resistance protein 5 (ABCC5) confers resistance to 5-fluorouracil and transports its monophosphorylated metabolites. *Mol Cancer Ther, 4*(5), 855-863. doi:10.1158/1535-7163.MCT-04-0291

Rajakyla, K., Krishnan, R., & Tojkander, S. (2017). Analysis of Contractility and Invasion Potential of Two Canine Mammary Tumor Cell Lines. *Front Vet Sci, 4*, 149. doi:10.3389/fvets.2017.00149

Rao, D. D., Vorhies, J. S., Senzer, N., & Nemunaitis, J. (2009). siRNA vs. shRNA: similarities and differences. *Adv Drug Deliv Rev, 61*(9), 746-759. doi:10.1016/j.addr.2009.04.004

Rau, S., Autschbach, F., Riedel, H. D., Konig, J., Kulaksiz, H., Stiehl, A., . . . Rost, D. (2008). Expression of the multidrug resistance proteins MRP2 and MRP3 in human cholangiocellular carcinomas. *Eur J Clin Invest, 38*(2), 134-142. doi:10.1111/j.1365-2362.2007.01916.x

Reid, G., Wielinga, P., Zelcer, N., van der Heijden, I., Kuil, A., de Haas, M., . . . Borst, P. (2003). The human multidrug resistance protein MRP4 functions as a prostaglandin efflux transporter and is inhibited by nonsteroidal antiinflammatory drugs. *Proc Natl Acad Sci U S A, 100*(16), 9244-9249. doi:10.1073/pnas.1033060100

Ren, Y., Poon, R. T., Tsui, H. T., Chen, W. H., Li, Z., Lau, C., . . . Fan, S. T. (2003). Interleukin-8 serum levels in patients with hepatocellular carcinoma: correlations with clinicopathological features and prognosis. *Clin Cancer Res, 9*(16 Pt 1), 5996-6001. Retrieved from https://www.ncbi.nlm.nih.gov/pubmed/14676125

Reya, T., Morrison, S. J., Clarke, M. F., & Weissman, I. L. (2001). Stem cells, cancer, and cancer stem cells. *Nature, 414*(6859), 105-111. doi:10.1038/35102167

Ribatti, D., Mangialardi, G., & Vacca, A. (2006). Stephen Paget and the 'seed and soil' theory of metastatic dissemination. *Clin Exp Med, 6*(4), 145-149. doi:10.1007/s10238-006-0117-4

Rogers, J. E., Law, L., Nguyen, V. D., Qiao, W., Javle, M. M., Kaseb, A., & Shroff, R. T. (2014). Second-line systemic treatment for advanced cholangiocarcinoma. *J Gastrointest Oncol, 5*(6), 408-413. doi:10.3978/j.issn.2078-6891.2014.072

Rosario, M. C., Jacqmin, P., Dorr, P., James, I., Jenkins, T. M., Abel, S., & van der Ryst, E. (2008). Population pharmacokinetic/pharmacodynamic analysis of CCR5 receptor occupancy by maraviroc in healthy subjects and HIV-positive patients. *Br J Clin Pharmacol, 65 Suppl 1*, 86-94. doi:10.1111/j.1365-2125.2008.03140.x

Roskams, T. (2006). Liver stem cells and their implication in hepatocellular and cholangiocarcinoma. *Oncogene, 25*(27), 3818-3822. doi:10.1038/sj.onc.1209558

Ruban, E. L., Ferro, R., Arifin, S. A., & Falasca, M. (2014). Lysophosphatidylinositol: a novel link between ABC transporters and G-protein-coupled receptors. *Biochem Soc Trans, 42*(5), 1372-1377. doi:10.1042/BST20140151

Saijyo, S., Kudo, T., Suzuki, M., Katayose, Y., Shinoda, M., Muto, T., . . . Matsuno, S. (1995). Establishment of a new extrahepatic bile duct carcinoma cell line, TFK-1. *Tohoku J Exp Med, 177*(1), 61-71. Retrieved from https://www.ncbi.nlm.nih.gov/pubmed/8693487

Salvi, A., Arici, B., Portolani, N., Giulini, S. M., De Petro, G., & Barlati, S. (2007). In vitro c-met inhibition by antisense RNA and plasmid-based RNAi down-modulates migration and invasion of hepatocellular carcinoma cells. *Int J Oncol, 31*(2), 451-460. Retrieved from http://www.ncbi.nlm.nih.gov/pubmed/17611703

Sapisochin, G., Fernandez de Sevilla, E., Echeverri, J., & Charco, R. (2015). Liver transplantation for cholangiocarcinoma: Current status and new insights. *World J Hepatol, 7*(22), 2396-2403. doi:10.4254/wjh.v7.i22.2396

Schmelzer, E., & Reid, L. M. (2008). EpCAM expression in normal, non-pathological tissues. *Front Biosci, 13*, 3096-3100. Retrieved from http://www.ncbi.nlm.nih.gov/pubmed/17981779

Schrenk, D., Baus, P. R., Ermel, N., Klein, C., Vorderstemann, B., & Kauffmann, H. M. (2001). Up-regulation of transporters of the MRP family by drugs and toxins. *Toxicol Lett, 120*(1-3), 51-57. Retrieved from https://www.ncbi.nlm.nih.gov/pubmed/11323161

Shaikh, M. V., Kala, M., & Nivsarkar, M. (2016). CD90 a potential cancer stem cell marker and a therapeutic target. *Cancer Biomark, 16*(3), 301-307. doi:10.3233/CBM-160590

Shao, S. L., Cui, T. T., Zhao, W., Zhang, W. W., Xie, Z. L., Wang, C. H., . . . Liu, Q. (2014). RNAi-based knockdown of multidrug resistance-associated protein 1 is sufficient to reverse multidrug resistance of human lung cells. *Asian Pac J Cancer Prev, 15*(24), 10597-10601. Retrieved from http://www.ncbi.nlm.nih.gov/pubmed/25605145

Shi, G. M., Xu, Y., Fan, J., Zhou, J., Yang, X. R., Qiu, S. J., . . . Wu, Z. Q. (2008). Identification of side population cells in human hepatocellular carcinoma cell lines with stepwise metastatic potentials. *J Cancer Res Clin Oncol, 134*(11), 1155-1163. doi:10.1007/s00432-008-0407-1

Shimizu, Y., Demetris, A. J., Gollin, S. M., Storto, P. D., Bedford, H. M., Altarac, S., . . . Whiteside, T. L. (1992). Two new human cholangiocarcinoma cell lines and their cytogenetics and responses to growth factors, hormones, cytokines or immunologic effector cells. *Int J Cancer, 52*(2), 252-260. Retrieved from https://www.ncbi.nlm.nih.gov/pubmed/1355757

Shin, H. R., Lee, C. U., Park, H. J., Seol, S. Y., Chung, J. M., Choi, H. C., . . . Shigemastu, T. (1996). Hepatitis B and C virus, Clonorchis sinensis for the risk of liver cancer: a case-control study in Pusan, Korea. *Int J Epidemiol, 25*(5), 933-940. Retrieved from https://www.ncbi.nlm.nih.gov/pubmed/8921477

Singer, O., & Verma, I. M. (2008). Applications of lentiviral vectors for shRNA delivery and transgenesis. *Curr Gene Ther, 8*(6), 483-488. Retrieved from http://www.ncbi.nlm.nih.gov/pubmed/19075631

Singh, S. K., Hawkins, C., Clarke, I. D., Squire, J. A., Bayani, J., Hide, T., . . . Dirks, P. B. (2004). Identification of human brain tumour initiating cells. *Nature, 432*(7015), 396-401. doi:10.1038/nature03128

Singh, S. K., Mishra, M. K., Eltoum, I. A., Bae, S., Lillard, J. W., Jr., & Singh, R. (2018). CCR5/CCL5 axis interaction promotes migratory and invasiveness of pancreatic cancer cells. *Sci Rep, 8*(1), 1323. doi:10.1038/s41598-018-19643-0

Slot, A. J., Molinski, S. V., & Cole, S. P. (2011). Mammalian multidrug-resistance proteins (MRPs). *Essays Biochem, 50*(1), 179-207. doi:10.1042/bse0500179

Sombattheera, S., Proungvitaya, T., Limpaiboon, T., Wongkham, S., Wongkham, C., Luvira, V., & Proungvitaya, S. (2015). Total serum bile acid as a potential marker for the diagnosis of cholangiocarcinoma without jaundice. *Asian Pac J Cancer Prev, 16*(4), 1367-1370. Retrieved from https://www.ncbi.nlm.nih.gov/pubmed/25743800

Soria, G., & Ben-Baruch, A. (2008). The inflammatory chemokines CCL2 and CCL5 in breast cancer. *Cancer Lett, 267*(2), 271-285. doi:10.1016/j.canlet.2008.03.018

Spence, J. R., Lange, A. W., Lin, S. C., Kaestner, K. H., Lowy, A. M., Kim, I., . . . Wells, J. M. (2009). Sox17 regulates organ lineage segregation of ventral foregut progenitor cells. *Dev Cell, 17*(1), 62-74. doi:10.1016/j.devcel.2009.05.012

Sriamporn, S., Pisani, P., Pipitgool, V., Suwanrungruang, K., Kamsa-ard, S., & Parkin, D. M. (2004). Prevalence of Opisthorchis viverrini infection and incidence of cholangiocarcinoma in Khon Kaen, Northeast Thailand. *Trop Med Int Health, 9*(5), 588-594. doi:10.1111/j.1365-3156.2004.01234.x

Srimunta, U., Sawanyawisuth, K., Kraiklang, R., Pairojkul, C., Puapairoj, A., Titipungul, T., . . . Vaeteewoottacharn, K. (2012). High expression of ABCC1 indicates poor prognosis in intrahepatic cholangiocarcinoma. *Asian Pac J Cancer Prev, 13 Suppl*, 125-130. Retrieved from https://www.ncbi.nlm.nih.gov/pubmed/23480753

Sripa, B., Kaewkes, S., Sithithaworn, P., Mairiang, E., Laha, T., Smout, M., . . . Brindley, P. J. (2007). Liver fluke induces cholangiocarcinoma. *PLoS Med, 4*(7), e201. doi:10.1371/journal.pmed.0040201

Stoddart, M. J. (2011). Cell viability assays: introduction. *Methods Mol Biol, 740*, 1-6. doi:10.1007/978-1-61779-108-6_1

Storto, P. D., Saidman, S. L., Demetris, A. J., Letessier, E., Whiteside, T. L., & Gollin, S. M. (1990). Chromosomal breakpoints in cholangiocarcinoma cell lines. *Genes Chromosomes Cancer, 2*(4), 300-310. Retrieved from https://www.ncbi.nlm.nih.gov/pubmed/2176543

Su, M. C., Hsu, C., Kao, H. L., & Jeng, Y. M. (2006). CD24 expression is a prognostic factor in intrahepatic cholangiocarcinoma. *Cancer Lett, 235*(1), 34-39. doi:10.1016/j.canlet.2005.03.059

Sueoka, H., Hirano, T., Uda, Y., Iimuro, Y., Yamanaka, J., & Fujimoto, J. (2014). Blockage of CXCR2 suppresses tumor growth of intrahepatic cholangiocellular carcinoma. *Surgery, 155*(4), 640-649. doi:10.1016/j.surg.2013.12.037

Sugasawa, H., Ichikura, T., Tsujimoto, H., Kinoshita, M., Morita, D., Ono, S., . . . Mochizuki, H. (2008). Prognostic significance of expression of CCL5/RANTES receptors in patients with gastric cancer. *J Surg Oncol, 97*(5), 445-450. doi:10.1002/jso.20984

Sukowati, C. H., Anfuso, B., Torre, G., Francalanci, P., Croce, L. S., & Tiribelli, C. (2013). The expression of CD90/Thy-1 in hepatocellular carcinoma: an in vivo and in vitro study. *PLoS One, 8*(10), e76830. doi:10.1371/journal.pone.0076830

Sulpice, L., Rayar, M., Turlin, B., Boucher, E., Bellaud, P., Desille, M., . . . Coulouarn, C. (2014). Epithelial cell adhesion molecule is a prognosis marker for intrahepatic cholangiocarcinoma. *J Surg Res, 192*(1), 117-123. doi:10.1016/j.jss.2014.05.017

Sutton, A., Friand, V., Brule-Donneger, S., Chaigneau, T., Ziol, M., Sainte-Catherine, O., . . . Charnaux, N. (2007). Stromal cell-derived factor-1/chemokine (C-X-C motif) ligand 12 stimulates human hepatoma cell growth, migration, and invasion. *Mol Cancer Res, 5*(1), 21-33. doi:10.1158/1541-7786.MCR-06-0103

Suzuki, A., Sekiya, S., Onishi, M., Oshima, N., Kiyonari, H., Nakauchi, H., & Taniguchi, H. (2008). Flow cytometric isolation and clonal identification of self-renewing bipotent hepatic progenitor cells in adult mouse liver. *Hepatology, 48*(6), 1964-1978. doi:10.1002/hep.22558

Tabibian, J. H., Trussoni, C. E., O'Hara, S. P., Splinter, P. L., Heimbach, J. K., & LaRusso, N. F. (2014). Characterization of cultured cholangiocytes isolated from livers of patients with primary sclerosing cholangitis. *Lab Invest, 94*(10), 1126-1133. doi:10.1038/labinvest.2014.94

Tabrizian, P., Jibara, G., Hechtman, J. F., Franssen, B., Labow, D. M., Schwartz, M. E., . . . Sarpel, U. (2015). Outcomes following resection of intrahepatic cholangiocarcinoma. *HPB (Oxford), 17*(4), 344-351. doi:10.1111/hpb.12359

Tan, X. Y., Chang, S., Liu, W., & Tang, H. H. (2014). Silencing of CXCR4 inhibits tumor cell proliferation and neural invasion in human hilar cholangiocarcinoma. *Gut Liver, 8*(2), 196-204. doi:10.5009/gnl.2014.8.2.196

Tanaka, M., Itoh, T., Tanimizu, N., & Miyajima, A. (2011). Liver stem/progenitor cells: their characteristics and regulatory mechanisms. *J Biochem, 149*(3), 231-239. doi:10.1093/jb/mvr001

Tang, K. H., Ma, S., Lee, T. K., Chan, Y. P., Kwan, P. S., Tong, C. M., . . . Chan, K. W. (2012). CD133(+) liver tumor-initiating cells promote tumor angiogenesis, growth, and self-renewal through neurotensin/interleukin-8/CXCL1 signaling. *Hepatology, 55*(3), 807-820. doi:10.1002/hep.24739

Tatiparti, K., Sau, S., Kashaw, S. K., & Iyer, A. K. (2017). siRNA Delivery Strategies: A Comprehensive Review of Recent Developments. *Nanomaterials (Basel), 7*(4). doi:10.3390/nano7040077

Tepsiri, N., Chaturat, L., Sripa, B., Namwat, W., Wongkham, S., Bhudhisawasdi, V., & Tassaneeyakul, W. (2005). Drug sensitivity and drug resistance profiles of human intrahepatic cholangiocarcinoma cell lines. *World J Gastroenterol, 11*(18), 2748-2753. Retrieved from http://www.ncbi.nlm.nih.gov/pubmed/15884115

Thoma, C. R., Zimmermann, M., Agarkova, I., Kelm, J. M., & Krek, W. (2014). 3D cell culture systems modeling tumor growth determinants in cancer target discovery. *Adv Drug Deliv Rev, 69-70*, 29-41. doi:10.1016/j.addr.2014.03.001

Todoroki, T. (2000). Chemotherapy for bile duct carcinoma in the light of adjuvant chemotherapy to surgery. *Hepatogastroenterology, 47*(33), 644-649. Retrieved from https://www.ncbi.nlm.nih.gov/pubmed/10919004

Tsukishiro, S., Suzumori, N., Nishikawa, H., Arakawa, A., & Suzumori, K. (2006). Elevated serum RANTES levels in patients with ovarian cancer correlate with the extent of the disorder. *Gynecol Oncol, 102*(3), 542-545. doi:10.1016/j.ygyno.2006.01.029

Vaday, G. G., Peehl, D. M., Kadam, P. A., & Lawrence, D. M. (2006). Expression of CCL5 (RANTES) and CCR5 in prostate cancer. *Prostate, 66*(2), 124-134. doi:10.1002/pros.20306

Valle, J., Wasan, H., Palmer, D. H., Cunningham, D., Anthoney, A., Maraveyas, A., . . . Investigators, A. B. C. T. (2010). Cisplatin plus gemcitabine versus gemcitabine for biliary tract cancer. *N Engl J Med, 362*(14), 1273-1281. doi:10.1056/NEJMoa0908721

Valle, J. W., Borbath, I., Khan, S. A., Huguet, F., Gruenberger, T., Arnold, D., & Committee, E. G. (2016). Biliary cancer: ESMO Clinical Practice Guidelines for diagnosis, treatment and follow-up. *Ann Oncol, 27*(suppl 5), v28-v37. doi:10.1093/annonc/mdw324

Vander Borght, S., Komuta, M., Libbrecht, L., Katoonizadeh, A., Aerts, R., Dymarkowski, S., . . . Roskams, T. (2008). Expression of multidrug resistance-associated protein 1 in hepatocellular carcinoma is associated with a more aggressive tumour phenotype and may reflect a progenitor cell origin. *Liver Int, 28*(10), 1370-1380. doi:10.1111/j.1478-3231.2008.01889.x

Velasco-Velazquez, M., Xolalpa, W., & Pestell, R. G. (2014). The potential to target CCL5/CCR5 in breast cancer. *Expert Opin Ther Targets, 18*(11), 1265-1275. doi:10.1517/14728222.2014.949238

Vinci, M., Gowan, S., Boxall, F., Patterson, L., Zimmermann, M., Court, W., . . . Eccles, S. A. (2012). Advances in establishment and analysis of three-dimensional tumor spheroid-based functional assays for target validation and drug evaluation. *BMC Biol, 10*, 29. doi:10.1186/1741-7007-10-29

Wahid, F., Shehzad, A., Khan, T., & Kim, Y. Y. (2010). MicroRNAs: synthesis, mechanism, function, and recent clinical trials. *Biochim Biophys Acta, 1803*(11), 1231-1243. doi:10.1016/j.bbamcr.2010.06.013

Wang, J., Dong, M., Xu, Z., Song, X., Zhang, S., Qiao, Y., . . . Chen, X. (2018). Notch2 controls hepatocyte-derived cholangiocarcinoma formation in mice. *Oncogene, 37*(24), 3229-3242. doi:10.1038/s41388-018-0188-1

Wang, L., Zuo, X., Xie, K., & Wei, D. (2017). The role of CD44 and cancer stem cells. *Methods Mol Biol, 1692*.

Wang, X., Campos, C. R., Peart, J. C., Smith, L. K., Boni, J. L., Cannon, R. E., & Miller, D. S. (2014). Nrf2 upregulates ATP binding cassette transporter expression and activity at the blood-brain and blood-spinal cord barriers. *J Neurosci, 34*(25), 8585-8593. doi:10.1523/JNEUROSCI.2935-13.2014

Waseem, D., & Tushar, P. (2017). Intrahepatic, perihilar and distal cholangiocarcinoma: Management and outcomes. *Ann Hepatol, 16*(1), 133-139. doi:10.5604/16652681.1226927

Wee, B., Pietras, A., Ozawa, T., Bazzoli, E., Podlaha, O., Antczak, C., . . . Holland, E. C. (2016). ABCG2 regulates self-renewal and stem cell marker expression but not tumorigenicity or radiation resistance of glioma cells. *Sci Rep, 6*, 25956. doi:10.1038/srep25956

Wehr, A., Baeck, C., Heymann, F., Niemietz, P. M., Hammerich, L., Martin, C., . . . Tacke, F. (2013). Chemokine receptor CXCR6-dependent hepatic NK T Cell accumulation promotes inflammation and liver fibrosis. *J Immunol, 190*(10), 5226-5236. doi:10.4049/jimmunol.1202909

Weiswald, L. B., Bellet, D., & Dangles-Marie, V. (2015). Spherical cancer models in tumor biology. *Neoplasia, 17*(1), 1-15. doi:10.1016/j.neo.2014.12.004

Weitzenfeld, P., & Ben-Baruch, A. (2014). The chemokine system, and its CCR5 and CXCR4 receptors, as potential targets for personalized therapy in cancer. *Cancer Lett, 352*(1), 36-53. doi:10.1016/j.canlet.2013.10.006

Wielinga, P. R., van der Heijden, I., Reid, G., Beijnen, J. H., Wijnholds, J., & Borst, P. (2003). Characterization of the MRP4- and MRP5-mediated transport of cyclic nucleotides from intact cells. *J Biol Chem, 278*(20), 17664-17671. doi:10.1074/jbc.M212723200

Wijnholds, J., Evers, R., van Leusden, M. R., Mol, C. A., Zaman, G. J., Mayer, U., . . . Borst, P. (1997). Increased sensitivity to anticancer drugs and decreased inflammatory response in mice lacking the multidrug resistance-associated protein. *Nat Med, 3*(11), 1275-1279. Retrieved from https://www.ncbi.nlm.nih.gov/pubmed/9359705

Wilson, B. J., Schatton, T., Zhan, Q., Gasser, M., Ma, J., Saab, K. R., . . . Frank, N. Y. (2011). ABCB5 identifies a therapy-refractory tumor cell population in colorectal cancer patients. *Cancer Res, 71*(15), 5307-5316. doi:10.1158/0008-5472.CAN-11-0221

Wong, A., Soo, R. A., Yong, W. P., & Innocenti, F. (2009). Clinical pharmacology and pharmacogenetics of gemcitabine. *Drug Metab Rev, 41*(2), 77-88. doi:10.1080/03602530902741828

Xie, B., Xing, R., Chen, P., Gou, Y., Li, S., Xiao, J., & Dong, J. (2010). Down-regulation of c-Met expression inhibits human HCC cells growth and invasion by RNA interference. *J Surg Res, 162*(2), 231-238. doi:10.1016/j.jss.2009.04.030

Xie, Y., Wehrkamp, C. J., Li, J., Wang, Y., Wang, Y., Mott, J. L., & Oupicky, D. (2016). Delivery of miR-200c Mimic with Poly(amido amine) CXCR4 Antagonists for

Combined Inhibition of Cholangiocarcinoma Cell Invasiveness. *Mol Pharm, 13*(3), 1073-1080. doi:10.1021/acs.molpharmaceut.5b00894

Xu, J., Liang, J., Meng, Y. M., Yan, J., Yu, X. J., Liu, C. Q., . . . Zheng, L. (2017). Vascular CXCR4 Expression Promotes Vessel Sprouting and Sensitivity to Sorafenib Treatment in Hepatocellular Carcinoma. *Clin Cancer Res, 23*(15), 4482-4492. doi:10.1158/1078-0432.CCR-16-2131

Xue, T. C., Chen, R. X., Han, D., Chen, J., Xue, Q., Gao, D. M., . . . Ye, S. L. (2012). Down-regulation of CXCR7 inhibits the growth and lung metastasis of human hepatocellular carcinoma cells with highly metastatic potential. *Exp Ther Med, 3*(1), 117-123. doi:10.3892/etm.2011.358

Yaal-Hahoshen, N., Shina, S., Leider-Trejo, L., Barnea, I., Shabtai, E. L., Azenshtein, E., . . . Ben-Baruch, A. (2006). The chemokine CCL5 as a potential prognostic factor predicting disease progression in stage II breast cancer patients. *Clin Cancer Res, 12*(15), 4474-4480. doi:10.1158/1078-0432.CCR-06-0074

Yamada, D., Kobayashi, S., Wada, H., Kawamoto, K., Marubashi, S., Eguchi, H., . . . Mori, M. (2013). Role of crosstalk between interleukin-6 and transforming growth factor-beta 1 in epithelial-mesenchymal transition and chemoresistance in biliary tract cancer. *Eur J Cancer, 49*(7), 1725-1740. doi:10.1016/j.ejca.2012.12.002

Yamada, K. M., & Cukierman, E. (2007). Modeling tissue morphogenesis and cancer in 3D. *Cell, 130*(4), 601-610. doi:10.1016/j.cell.2007.08.006

Yamaoka, R., Ishii, T., Kawai, T., Yasuchika, K., Miyauchi, Y., Kojima, H., . . . Uemoto, S. (2018). CD90 expression in human intrahepatic cholangiocarcinoma is associated with lymph node metastasis and poor prognosis. *J Surg Oncol, 118*(4), 664-674. doi:10.1002/jso.25192

Yamashita, T., Honda, M., Nakamoto, Y., Baba, M., Nio, K., Hara, Y., . . . Kaneko, S. (2013). Discrete nature of EpCAM+ and CD90+ cancer stem cells in human hepatocellular carcinoma. *Hepatology, 57*(4), 1484-1497. doi:10.1002/hep.26168

Yamashita, T., Ji, J., Budhu, A., Forgues, M., Yang, W., Wang, H. Y., . . . Wang, X. W. (2009). EpCAM-positive hepatocellular carcinoma cells are tumor-initiating cells with stem/progenitor cell features. *Gastroenterology, 136*(3), 1012-1024. doi:10.1053/j.gastro.2008.12.004

Yamashita, T., & Wang, X. W. (2013). Cancer stem cells in the development of liver cancer. *J Clin Invest, 123*(5), 1911-1918. doi:10.1172/JCI66024

Yang, J., Gong, Y., Sontag, D. P., Corbin, I., & Minuk, G. Y. (2018). Effects of low-density lipoprotein docosahexaenoic acid nanoparticles on cancer stem cells isolated from human hepatoma cell lines. *Mol Biol Rep, 45*(5), 1023-1036. doi:10.1007/s11033-018-4252-2

Yang, X., Lu, P., Fujii, C., Nakamoto, Y., Gao, J. L., Kaneko, S., . . . Mukaida, N. (2006). Essential contribution of a chemokine, CCL3, and its receptor, CCR1, to hepatocellular carcinoma progression. *Int J Cancer, 118*(8), 1869-1876. doi:10.1002/ijc.21596

Yang, Z. F., Ho, D. W., Ng, M. N., Lau, C. K., Yu, W. C., Ngai, P., . . . Fan, S. T. (2008). Significance of CD90+ cancer stem cells in human liver cancer. *Cancer Cell, 13*(2), 153-166. doi:10.1016/j.ccr.2008.01.013

Yano, H., Maruiwa, M., Iemura, A., Mizoguchi, A., & Kojiro, M. (1992). Establishment and characterization of a new human extrahepatic bile duct carcinoma cell line (KMBC). *Cancer, 69*(7), 1664-1673. Retrieved from https://www.ncbi.nlm.nih.gov/pubmed/1312890

Yin, A. H., Miraglia, S., Zanjani, E. D., Almeida-Porada, G., Ogawa, M., Leary, A. G., . . . Buck, D. W. (1997). AC133, a novel marker for human hematopoietic stem and progenitor cells. *Blood, 90*(12), 5002-5012. Retrieved from http://www.ncbi.nlm.nih.gov/pubmed/9389720

http://www.bloodjournal.org/content/bloodjournal/90/12/5002.full.pdf

Zhang, L., Theise, N., Chua, M., & Reid, L. M. (2008). The stem cell niche of human livers: symmetry between development and regeneration. *Hepatology, 48*(5), 1598-1607. doi:10.1002/hep.22516

Zhang, R., Pan, X., Huang, Z., Weber, G. F., & Zhang, G. (2011). Osteopontin enhances the expression and activity of MMP-2 via the SDF-1/CXCR4 axis in hepatocellular carcinoma cell lines. *PLoS One, 6*(8), e23831. doi:10.1371/journal.pone.0023831

Zhang, S. Z., Pan, F. Y., Xu, J. F., Yuan, J., Guo, S. Y., Dai, G., . . . Li, C. J. (2005). Knockdown of c-Met by adenovirus-delivered small interfering RNA inhibits hepatocellular carcinoma growth in vitro and in vivo. *Mol Cancer Ther, 4*(10), 1577-1584. doi:10.1158/1535-7163.MCT-05-0106

Zhang, Y., Meng, F. Y., Li, W. L., Zhou, C. X., Guan, Z., & Fan, H. Y. (2013). Association of chemotactic factor receptor 5 gene with breast cancer. *Genet Mol Res, 12*(4), 5289-5300. doi:10.4238/2013.November.7.4

Zhang, Y., Yao, F., Yao, X., Yi, C., Tan, C., Wei, L., & Sun, S. (2009). Role of CCL5 in invasion, proliferation and proportion of CD44+/CD24- phenotype of MCF-7 cells and correlation of CCL5 and CCR5 expression with breast cancer progression. *Oncol Rep, 21*(4), 1113-1121. Retrieved from https://www.ncbi.nlm.nih.gov/pubmed/19288016

Zhao, J. (2016). Cancer stem cells and chemoresistance: The smartest survives the raid. *Pharmacol Ther, 160*, 145-158. doi:10.1016/j.pharmthera.2016.02.008

Zhao, S., Wang, J., & Qin, C. (2014). Blockade of CXCL12/CXCR4 signaling inhibits intrahepatic cholangiocarcinoma progression and metastasis via inactivation of canonical Wnt pathway. *J Exp Clin Cancer Res, 33*, 103. doi:10.1186/s13046-014-0103-8

Zheng, K., Li, H. Y., Su, X. L., Wang, X. Y., Tian, T., Li, F., & Ren, G. S. (2010). Chemokine receptor CXCR7 regulates the invasion, angiogenesis and tumor growth of human hepatocellular carcinoma cells. *J Exp Clin Cancer Res, 29*, 31. doi:10.1186/1756-9966-29-31

Zhong, W., Tong, Y., Li, Y., Yuan, J., Hu, S., Hu, T., & Song, G. (2017). Mesenchymal stem cells in inflammatory microenvironment potently promote metastatic growth of cholangiocarcinoma via activating Akt/NF-kappaB signaling by paracrine CCL5. *Oncotarget, 8*(43), 73693-73704. doi:10.18632/oncotarget.17793

Zhou, S. L., Dai, Z., Zhou, Z. J., Chen, Q., Wang, Z., Xiao, Y. S., . . . Zhou, J. (2014). CXCL5 contributes to tumor metastasis and recurrence of intrahepatic cholangiocarcinoma by recruiting infiltrative intratumoral neutrophils. *Carcinogenesis, 35*(3), 597-605. doi:10.1093/carcin/bgt397

Zhou, S. L., Dai, Z., Zhou, Z. J., Wang, X. Y., Yang, G. H., Wang, Z., . . . Zhou, J. (2012). Overexpression of CXCL5 mediates neutrophil infiltration and indicates poor prognosis for hepatocellular carcinoma. *Hepatology, 56*(6), 2242-2254. doi:10.1002/hep.25907

Zhu, W., Xu, H., Zhu, D., Zhi, H., Wang, T., Wang, J., . . . Liu, P. (2012). miR-200bc/429 cluster modulates multidrug resistance of human cancer cell lines by targeting BCL2 and XIAP. *Cancer Chemother Pharmacol, 69*(3), 723-731. doi:10.1007/s00280-011-1752-3

Zhu, Z., Hao, X., Yan, M., Yao, M., Ge, C., Gu, J., & Li, J. (2010). Cancer stem/progenitor cells are highly enriched in CD133+CD44+ population in hepatocellular carcinoma. *Int J Cancer, 126*(9), 2067-2078. doi:10.1002/ijc.24868

Zimmermann, H. W., & Tacke, F. (2011). Modification of chemokine pathways and immune cell infiltration as a novel therapeutic approach in liver inflammation and fibrosis. *Inflamm Allergy Drug Targets, 10*(6), 509-536. Retrieved from https://www.ncbi.nlm.nih.gov/pubmed/22150762

Zips, D., Thames, H. D., & Baumann, M. (2005). New anticancer agents: in vitro and in vivo evaluation. *In Vivo, 19*(1), 1-7. Retrieved from https://www.ncbi.nlm.nih.gov/pubmed/15796152

Zlotnik, A., Burkhardt, A. M., & Homey, B. (2011). Homeostatic chemokine receptors and organ-specific metastasis. *Nat Rev Immunol, 11*(9), 597-606. doi:10.1038/nri3049

Zucchini, A., Del Zotto, G., Brando, B., & Canonico, B. (2001). Cd90. *J Biol Regul Homeost Agents, 15*(1), 82-85. Retrieved from https://www.ncbi.nlm.nih.gov/pubmed/11388749